7. Site 1266[1]

Shipboard Scientific Party[2]

INTRODUCTION

Site 1266 (proposed Site WALV-10F) is located on the northwestern flank of Walvis Ridge. At a water depth of 3806 m, the site is ~20 m shallower than Deep Sea Drilling Project (DSDP) Site 528 to the north, where previous drilling recovered a 470-m-thick section of Neogene, Paleogene, and Maastrichtian sediment (Moore, Rabinowitz, et al., 1984). Sediment composition at Site 528 is relatively uniform, predominantly carbonate rich oozes and chalks with a few thin intervals of nannofossil clays. The Miocene–Pleistocene section consists of foraminiferal nannofossil oozes and extends from the seafloor to ~170 meters below seafloor (mbsf). The Oligocene section also consists of foraminiferal nannofossil ooze and extends to 225 mbsf. The Paleocene–Eocene sequence extends from 225 to 410 mbsf and consists of nannofossil oozes and chalks and clays. The Paleocene/Eocene (P/E) boundary was not recovered at this site, although an expanded Cretaceous/Paleogene (K/P) boundary was. A few thin disseminated layers of chert were encountered in the upper Paleocene between 330 and 400 mbsf. The sediments immediately above basement are of middle Maastrichtian age. Site 528 was rotary cored and, as a consequence, recovery was poor (63%) and much of the core suffered from severe drilling disturbance, particularly the unlithified Neogene and Paleogene oozes.

Our main objective for this site was the recovery of undisturbed sediments recording critical intervals in the early Cenozoic, specifically the Paleocene/Eocene Thermal Maximum, and the period of global cooling and growth of polar ice caps across the Eocene/Oligocene (E/O) boundary into the earliest Oligocene (early Oligocene Glacial Maximum). We planned to recover 100% of the sedimentary section in multiple holes to make it possible to establish a cyclostratigraphy and develop an astronomically tuned timescale. We aimed to fully document events

across the critical intervals as well as short episodes of climate fluctuation during the early Eocene Climatic Optimum.

Site 1266 is the approximate midpoint of the Leg 208 depth transect and is at a depth where fluctuations in depth of the calcite compensation depth are registered in the sediment. To optimize recovery of the P/E boundary, Site 1266 was located in an area where the Neogene sediments are thin. In this location, overall sediment thickness is ~400 m (common depth point 12,900 on line GeoB 01-030) (Figs. F1, p. 52, F2, p. 53, both in the "Leg 208 Summary" chapter; Fig. F1). The site sits along the edge of a north-south–trending channel. Seismic profiles show several packages of reflectors, which we describe as upper (0–105 ms two-way traveltime [TWT] below seafloor), middle (105–230 ms TWT below seafloor), and lower (230–430 ms TWT below seafloor) (Figs. F2, F3). The upper package, which is thinner than the upper package at Site 528, consists of middle Miocene–Pleistocene calcareous oozes; the middle package consists of Oligocene and lower Miocene calcareous oozes and clays; and the lower package consists of upper Maastrichtian to Eocene calcareous oozes and chalks. Reflectors in the upper and middle units are more chaotic than those at Site 528, indicating possible downslope transport and/or erosion. The lower package contains multiple sets of parallel reflectors that are essentially identical to Site 528 below 250 ms TWT below seafloor. The lowermost prominent reflector at 380 ms TWT below seafloor represents the K/P boundary contact at an estimated depth of ~371 mbsf (average velocity = 1.8 m/ms). Above this is a weaker reflector at 290 ms TWT below seafloor that we believe represents the P/E clay layer at an estimated depth of 276 mbsf. The reflectors above represent Eocene and Oligocene layers.

In short, coring in three holes at Site 1266 recovered a 333-m-thick section of upper Paleocene to Pleistocene calcareous-rich sediment. The advanced piston corer (APC) functioned to a depth of 250 mbsf, at which point the extended core barrel (XCB) was deployed. Significant condensed clay-rich intervals and unconformities are present in the middle and upper Eocene and the upper Miocene. Despite multiple holes, several short intervals were not recovered. Nevertheless, the P/E clay layer was recovered intact in one hole (~267 mbsf) where the XCB was used to a level just above the boundary, at which point the APC was redeployed.

OPERATIONS

Transit to Site 1266

The 22-nmi transit to Site 1266 (proposed Site WALV-10F) was accomplished in 2.3 hr at an average speed of 9.6 kt. The vessel was positioned over the site by 1405 hr on 15 April 2003. The corrected precision depth recorder depth estimate was 3819 meters below rig floor (mbrf).

Coring intervals, times, nominal recovery rates, core barrels that required drillover to be released from the sediment, and the deployments of the Advanced Piston Corer Temperature (APCT) tool, Tensor core orientation tool, and nonmagnetic core barrel are listed in Table T1.
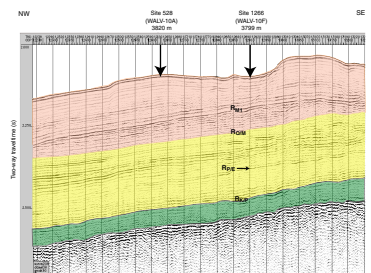
F1. Site 1266 and alternate sites, p. 27.
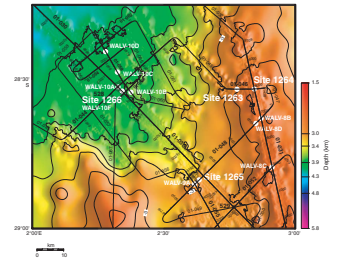
F2. Site 1266 and an alternate site on line GeoB 01-030, p. 28.
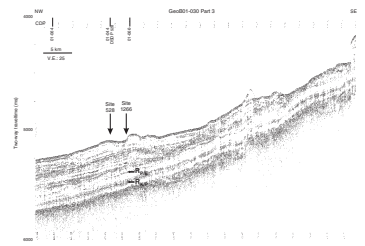
F3. Line GeoB 01-030 with reflector age estimates, p. 29.

T1. Coring summary, p. 62.

Hole 1266A

Hole 1266A was initiated at 2150 hr with the bit at 3811.0 mbrf. The seafloor depth, which was estimated by the recovery of a full core barrel, was provisionally established at 3811.0 mbrf. APC coring advanced to 217.1 mbsf, where the formation became too indurated to continue with the APC. The bit was advanced by recovery on the last two cores (208-1266A-24H and 25H) because of incomplete strokes. The hole was deepened with the XCB system to the target depth of 298.6 mbsf. Active heave compensation was used while coring the first XCB core (208-1266A-26X).

Hole 1266B

The bit was pulled clear of the seafloor at 1800 hr on 17 April, and the vessel was offset 20 m north. After a bottom water temperature was obtained with the APCT at 3806 mbrf, Hole 1266B was initiated with one piston core to establish a final water depth at this site. The seafloor depth calculated from the 7.65 m of recovery was 3807.9 mbrf, which was 3.1 m shallower than the provisional seafloor estimate from Hole 1266A. The center bit was lowered with the coring line, and the hole was drilled ahead without coring by 212.4 m to a depth of 220 mbsf. The hole was deepened from 220 to 248.5 mbsf with the XCB system before the piston corer was deployed in an effort to obtain an undisturbed sample of the P/E boundary. The two fully stroked cores (208-1266A-5H and 6H), spanning the interval 248.5–267.5 mbsf, contained the critical boundary interval in the bottom of Core 6H. XCB coring deepened the hole from 267.5 mbsf to the target depth of 321.0 mbsf. After the bit was pulled clear of the seafloor at 2050 hr on 18 April, the vessel was offset 20 m north.

Hole 1266C

The two objectives for Hole 1266C were to spot core and fill gaps in the sedimentary record and to obtain another sample of the critical P/E boundary. Hole 1266C was initiated after tagging the seafloor at 3807.9 mbrf. The hole was drilled with a center bit in place to 62.0 mbsf, where APC coring was initiated. APC coring advanced from 62.0 to 192.0 mbsf. The nonmagnetic core barrel was not used in this hole. The new Interstitial Water Sampler was deployed on the coring line to obtain a water sample and pore pressure and downhole temperature data at 192.0 mbsf. The data were compromised because of a leak. The center bit was lowered with the coring line, and the hole was drilled without coring from 192.0 to 245.0 mbsf (53.0 m interval). After the center bit was retrieved, one XCB core was obtained from 245.0 to 254.5 mbsf. The APC was then used to core from 254.5 to 282.7 mbsf. These three cores (208-1266C-16H, 17H, and 18H) spanned the critical P/E boundary interval and required drilling over to free the barrels from the sediment. XCB coring deepened the hole from 282.7 mbsf to the target depth of 334.2 mbsf. The 22.8-m interval from 292.2 to 315.0 mbsf was drilled without coring.

The total cored interval at Site 1266 was 604 m, and the recovered interval was 592 m (average nominal recovery = 98%). The total interval drilled without coring was 350 m.

Three downhole temperature measurements (Hole 1266A: 66–151 mbsf) and one bottom water temperature measurement (Hole 1266B)

with the APCT yielded an initial temperature gradient estimate of 4.7°C/100 m.

The drill string was recovered, the hydrophones and thrusters were secured, the beacon was recalled and recovered, and the vessel left for the next site at 0445 hr on 21 April.
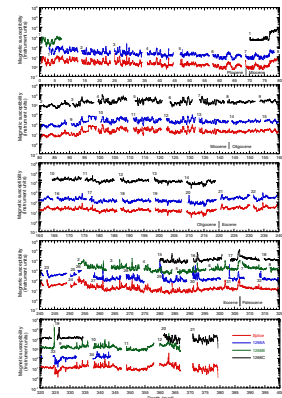
COMPOSITE DEPTH

Magnetic susceptibility (MS) data collected from Holes 1266A, 1266B, and 1266C at 2.5-cm intervals were used to correlate cores and to construct a composite section for Site 1266 (Fig. F4). The MS data indicate that Cores 208-1266A-7H through 20H and 208-1266C-1H through 14H were cored nearly in parallel, which limited efforts to build a complete composite section for the lower Miocene–Oligocene interval (see "Biostratigraphy," p. 9). The XCB cores taken from Holes 1266A, 1266B, and 1266C in the interval ~220–380 mbsf were significantly stretched, squeezed, or disturbed as a result of the coring process and therefore were not suitable for core-to-core correlation. Therefore, a composite depth section for Site 1266 was constructed by assuming a constant growth rate of 15% for Hole 1266A, based on the average growth rates of previous Leg 208 sites, and by adding a mudline offset of 3.14 m that was obtained from correlation with Core 208-1266B-1H (Fig. F5). Subsequently, Cores 208-1266C-1H through 14H were correlated to Cores 208-1266A-7H through 20H, respectively, and Cores 208-1266C-15X and 19X through 21X were extrapolated using, again, a 15% growth rate. Finally, all cores drilled from just below and above the P/E boundary were aligned as closely as possible.

Following construction of the composite depth section for Site 1266, a single spliced record was assembled (Table T2). The lack of overlap between most cores resulted in >30 gaps in the spliced record. The spliced record is complete for the ~297- to 315-meters composite depth (mcd) interval. The P/E boundary interval in the composite was taken from Core 208-1266C-17H. The Site 1266 splice (Table T3) was used to plot other data sets from this site.

LITHOSTRATIGRAPHY

Three holes were cored at Site 1266. Hole 1266A was cored continuously to a depth of 344 mcd (295.2 mbsf); the mudline was obtained in Hole 1266B, which was then washed to 253 mcd (220 mbsf) and cored to 367.3 mcd (318.9 mbsf); and Hole 1266C was washed to 57 mcd (62 mbsf) and then cored to 379.4 mcd (333.1 mbsf). The major lithologies recovered include nannofossil ooze, nannofossil chalk, foraminifer-bearing nannofossil ooze, and clay-bearing nannofossil ooze. Minor lithologies include clayey nannofossil ooze, nannofossil clay, and nanno-fossil-bearing clay. Zeolite-bearing clay and ash-bearing nannofossil clay were present in association with discrete volcanic ash horizons. We have divided this sequence into three units based on lithologic observations and physical property measurements (Table T4; Fig. F6). These observations and measurements are summarized in plots illustrating variation with depth: whole-core MS, natural gamma radiation (NGR), sediment density by gamma ray attenuation, and compressional wave (P-wave) velocity from the multisensor track (Fig. F7); sediment lightness (L*), carbonate content, and chromaticity (Fig. F8); smear slide
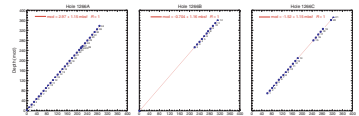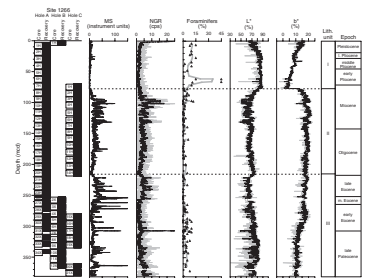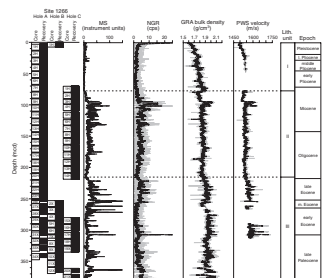
components (Fig. F9); split-core measurements of grain and bulk density, porosity, and Hamilton Frame *P*-wave velocity values (Figs. F10, F11, F12); and interstitial water Mn and Fe content (Fig. F13).

The succession of lithologies present at Site 1266 is quite similar to those observed at other Leg 208 sites. Unit I, a foraminifer-bearing nannofossil ooze, represents the upper Miocene through Holocene sequence. This is underlain by Units II and III, which share similar patterns of lithologic variation. Each of these two units comprises a lower nannofossil ooze–dominated facies that grades upward into clay-bearing nannofossil ooze and, periodically, to nannofossil clay. Unit III differs from Unit II in the presence of nannofossil chalk and diagenetic siliceous lithologies including chert and porcellanite in the lower part of the unit.

Description of Lithostratigraphic Units

Unit I

Interval: 208-1266A-1H-1, 0 cm, through 7H-6, 55 cm; 208-1266B-1H-1, 0 cm, through 1H-CC; 208-1266C-1H-1, 0 cm, through 1H-5, 57 cm

Depth: Hole 1266A: 0.0–65.1 mbsf (3.1–76.8 mcd); Hole 1266B: 0.0–7.7 mbsf (0.0–7.7 mcd); Hole 1266C: 62.0–68.6 mbsf (70.2–76.8 mcd)

Age: Pleistocene to Miocene

Lithology: foraminifer-bearing nannofossil ooze and nannofossil ooze

Unit I is a light gray and white to medium brown foraminifer-bearing nannofossil ooze that is differentiated from underlying units by a greater foraminiferal abundance, low clay concentration, and the common occurrence of size-graded sediment gravity flows (turbidites). The contact with underlying Unit II is distinct, marked by an abrupt transition to pale yellow or light brown nannofossil ooze and a significant decrease in foraminiferal abundance. This lower boundary is coincident with a downcore decrease in sediment L* and increases in chromaticity (b*), MS, and NGR values (Fig. F6). Bulk density and *P*-wave velocity also decrease, and sediment porosity increases for a short interval below this boundary (Figs. F10, F11A, F12A).

Unit I exhibits stratigraphic variation in color and sedimentary structures. The upper part of Unit I is a cyclic light gray to brown and medium brown foraminifer-bearing nannofossil ooze that alternates on a meter scale. Associated lithologic and sedimentologic features include extensive mottling of the upper part by blebs that appear to be bioturbational or diagenetic features. These 1- to 3-cm-sized pinkish to whitish blebs are distributed throughout the section and are similar to structures observed at other sites and in older units at this site.

The L* of Unit I increases downcore where nannofossil ooze and foraminifer-bearing nannofossil ooze oscillate from white to light gray on a decimeter to meter scale. The unit is marked by distinctive light brown layers of coarse-grained foraminiferal ooze that have sharp erosional bases and diffuse bioturbated upper boundaries (Fig. F14). These horizons range from 3 to 60 cm in thickness and are interpreted as turbidity or gravity flow deposits similar to those described at Site 1262. These occur primarily in the lower part of Unit I and compose <5% of the total unit thickness.
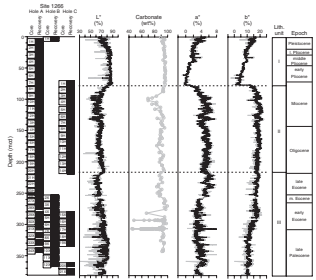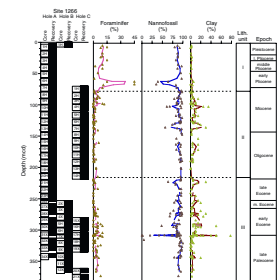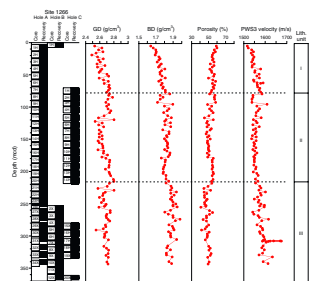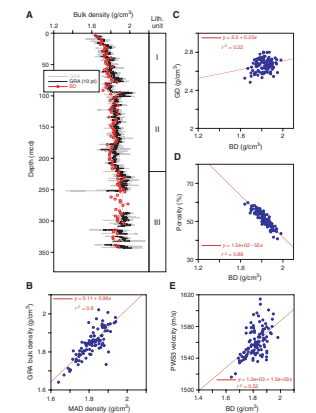
In Unit I, black and dark brown oxides are present as small dispersed granules, concentrated layers (Fig. F14), or discrete nodules. X-ray diffraction analyses of these oxides from Sites 1264 and 1265 (see Fig. F16, p. 37, in the "Site 1264" chapter and Fig. F13, p. 46, in the "Site 1265" chapter) identified lithophorite, a mineral composed primarily of Mn oxide. Precipitation of this mineral is controlled by diagenetic oxidation-reduction reactions within sediments that are mediated by variation in organic content and sediment porosity (i.e., burrow margins or discrete concentrations of organic matter). In this sequence, reduction of Mn likely occurs in the finer-grained sediment and oxidation occurs at the interface with sediment of higher porosity where oxidizing conditions exist. These sediments could represent coarser depositional laminae or margins of turbidite layers. Although Mn oxides are common throughout the cored sequence, in Unit I they are frequently present in discrete layers; lower in the Site 1266 sequence, these oxides are observed as dispersed micronodules and granules or as diffuse halos surrounding blebs.

Unit II

Interval: 208-1266A-7H-6, 55 cm, through 20H-4, 50 cm; 208-1266C-2H-1, 0 cm, through 14H-4, 95 cm
Depth: Hole 1266A: 65.1–184.6 mbsf (76.8–214.7 mcd); Hole 1266C: 71.5–188.0 mbsf (80.7–214.7 mcd)
Age: Miocene through Oligocene
Lithology: clay-bearing nannofossil ooze and nannofossil ooze

Unit II comprises two major lithologies, a light gray to light brown nannofossil ooze and a dark to medium brown clay-bearing nannofossil ooze. The upper boundary of Unit II is coincident with an abrupt downcore decrease in L* and an increase in both a* (red-green) and b* (blue-yellow) chromaticity (Figs. F8, F15). Magnetic susceptibility and NGR exhibit more gradual transitions from lower and stable values in Unit I to higher and more variable values in Unit II (Fig. F7), reflecting an increase in clay content.

Clay content in Unit II, although variable, generally decreases in abundance downcore. In the upper part of Unit II, the alternation of nannofossil ooze and clay-bearing nannofossil ooze on a decimeter to meter scale is expressed as oscillations in L*, a*, and b* and macroscopically as color cycles (Fig. F8). This alternation is also evident in MS and the NGR variation (Fig. F16). From the upper to lower part of Unit II, the relative abundance of clay-bearing nannofossil ooze progressively decreases as lighter-colored nannofossil ooze becomes the dominant lithology. This change is accompanied by a gradual decrease in MS and NGR and an increase in L* (Fig. F6). The lower boundary of Unit II exhibits a pattern of change in physical properties similar to that observed at the Unit I/II boundary: MS and NGR values increase and become more variable and L* decreases (Figs. F6, F7). Moreover, bulk density increases and is matched by a decrease in sediment porosity (Fig. F10); Mn concentration in interstitial water increases abruptly then decreases to a constant, low level (Fig. F13).

Sediments of Unit II were formed primarily by accumulation of pelagic clay and carbonate, with little sedimentologic evidence of downslope transport by gravity or turbidity flows. Paleontologic observations suggest a significant degree of reworking in both Units I and II. As discussed above, features diagnostic of transport and deposition by density

F12. *P*-wave velocity measurements, p. 38.
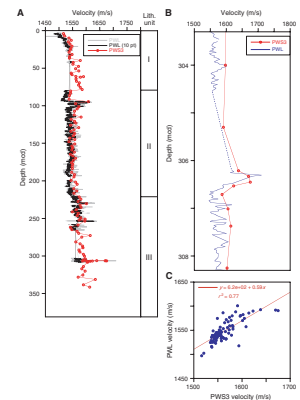
F13. Chromaticity, Mn and Fe, and grain density, p. 39.
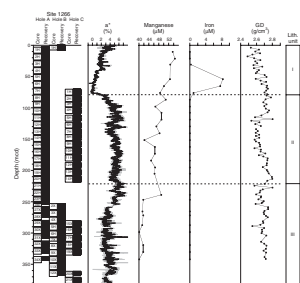
F14. Foraminiferal ooze turbidite horizon, p. 40.

F15. Chromaticity change at the Unit I/II boundary, p. 41
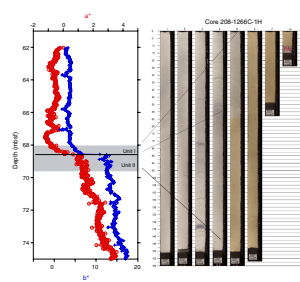
and gravity flows are present in the lower part of Unit I; however, little physical evidence is available in Unit II that demonstrates transport by such a mechanism. The paleontologic evidence for reworking may reflect a process of continuous, although volumetrically minor, transport of surface sediment downslope in response to bottom currents or small-scale gravity flows. It is possible that some of the decimeter- to meter-scale color alternations of upper Unit II could have formed by similar depositional processes. However, given the absence of size grading or other characteristic sedimentary structures, it is difficult to attribute this color and lithologic variation solely to gravity or turbidity flows. Rather, these differences are primarily due to variation in clay content, a feature that could be produced by numerous physical or chemical processes unrelated to downslope sediment transport.

Assuming a constant flux, pelagic clay could be segregated or concentrated by dissolution of carbonate components. In the case of clay-rich sediments of Unit II, carbonate dissolution is a plausible explanation given the nature of accessory phases associated with the clay-rich horizons. For example, volcanic glass is present in small amounts and various states of alteration in most of the lithologies at Site 1266, yet it is a minor to major component in the clayey horizons. These layers also contain abundant hematite and zeolites (primarily phillipsite; e.g., Sample 208-1266C-7H-1, 100 cm), which indicate in situ formation of these minerals from the alteration of volcanic glass. Concentration of clays by dissolution could explain the simultaneous segregation of fine-grained clays and coarser volcanic ash, an association difficult to produce by downslope transport. For these reasons, it is likely that the interbedding of clay-rich and clay-poor lithologies is the result of changes in oceanic carbonate saturation state, rather than some process of sediment transport.

Synsedimentary deformational features, such as inclined bedding and recumbently folded beds, are present in upper Unit II (Fig. F17). These features form through slumping and downslope creep and indicate deformation on a sloped depositional surface. Such observations are compatible with seismic interpretations of "chaotic reflections" in the Oligocene and Miocene and biostratigraphic observations suggesting sediment reworking.
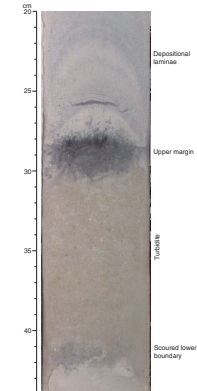
Unit III

Interval: 208-1266A-20H-4, 50 cm, through 34X-CC, 4 cm; 208-1266B-2X-1, 0 cm, through 12X-CC; 208-1266C-14H-4, 95 cm, through 21X-CC
Depth: Hole 1266A: 184.6–294.9 mbsf (214.7–343.7 mcd); Hole 1266B: 220.0–318.9 mbsf (253.0–367.3 mcd); Hole 1266C: 188.0–333.1 mbsf (214.7–379.4 mcd)
Age: Oligocene to late Paleocene
Lithology: clay-bearing nannofossil ooze, nannofossil ooze, and nannofossil chalk

Unit III is dominated by nannofossil ooze, clay-bearing nannofossil ooze, and nannofossil chalk. The boundary between Units II and III is coincident with an increase in MS and NGR, corresponding to an increase in clay content documented by smear slide analysis (Fig. F9). Moreover, sediment L* decreases (Figs. F6, F7), bulk density (BD) and P-wave velocity increase, and grain density and porosity decrease across the Unit II/III boundary (Fig. F10).

F16. Image and cyclic sedimentation patterns, p. 42.
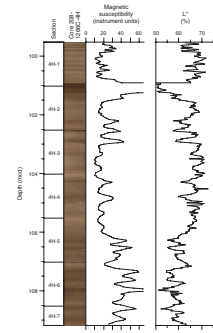
F17. Synsedimentary slump folding and inclined bedding, p. 43.

The stratigraphic variation in clay content is similar to that observed for Unit II. Clay-bearing nannofossil ooze is the predominant lithology in the upper part of Unit III and is progressively replaced downcore by clay-poor nannofossil ooze. Nannofossil ooze becomes increasingly indurated and grades into nannofossil chalk, which requires that most cores be sawed rather than split with a wire. Chalk abundance increases dramatically below the P/E boundary at 306.77 mcd, where as much as 50% of the sediment is highly indurated.

Minor lithologies of Unit III are clayey nannofossil ooze, nannofossil clay, ash-bearing nannofossil ooze, and ash-bearing clay. Volcanic ash is a minor component throughout the sequence and is locally concentrated as greenish brown clay-rich layers (e.g., Samples 208-1266A-27X-3, 118–121 cm, and 27X-CC, 12–14 cm) or intermixed within clay horizons where alteration of volcanic ash forms authigenic phillipsite, clinoptilolite, and hematite. These ash layers coincide with increases in MS and NGR and are responsible for much of the variability measured in these parameters in the lower part of Unit III.

The lower part of Unit III contains rare silicified horizons that formed by diagenetic replacement of carbonate by SiO_2. The bulk of material composing these layers is optically isotropic with the exception of rare nannofossils. These indurated layers are probably composed of opal-CT that has not yet stabilized to chert. As such, these horizons are more appropriately termed porcellanite, given their intermediate stage of lithification and mineral instability. Chert occurs rarely as isolated reddish to pink nodules in Unit III (e.g., Sample 208-1266C-19X-6, 105–110 cm).

The presence of nannofossil clay and clayey nannofossil ooze is likely controlled by carbonate dissolution that concentrates insoluble phases such as clay and volcanic glass. The most notable example of such dissolution events is the P/E boundary interval. This boundary was recovered in all three holes at Site 1266 with varying degrees of drilling disturbance (Fig. F18). The boundary was recovered at 306.77 mcd in Samples 208-1266A-31X-3, 37 cm (271.3 mbsf), 208-1266B-6H-CC, 25 cm (277.75 mbsf), and 208-1266C-17H-3, 112 cm (276.62 mbsf). Hole 1266C provides the most complete section with the least disruption by drilling. It is marked by a precipitous drop in carbonate from 90 wt% beneath the boundary to a ~20-cm-thick interval of clay that is virtually free of carbonate. The clay is a deep dusky red that is characteristic of Fe oxides (commonly hematite). Varying amounts of volcanic glass are associated with the boundary clay, giving rise to ash-bearing nannofossil clay and abundant zeolites derived from in situ alteration of ash. Carbonate content increases over an interval of 50–70 cm above the carbonate-free clay layer and consists dominantly of nannofossils. Bioturbation is nearly absent in the lowermost 20 cm of the boundary clay and then increases in the upper part where it contacts the overlying nannofossil ooze. Based on the overall thickness and MS record, it appears the P/E contact in Hole 1266A is not complete. The lower part of the clay layer was not recovered by XCB coring.

In addition to the P/E boundary sequence, reddish nannofossil clay is present in several intervals in Unit III. These clays are similar in appearance and lithologic structure to the Paleocene–Eocene dissolution interval, although much thinner. They are recognized by increases in MS and NGR (Fig. F7). One distinctly red clay horizon is present above the P/E boundary at ~293 mcd (Samples 208-1266A-30X-2, 53 cm, 208-1266B-5H-5, 87 cm, and 208-1266C-16H-2, 45 cm), is correlative among other Leg 208 sites, and is presently defined as the Chron C24n

F18. Image, MS, carbonate, and a* for the P/E boundary, p. 44.

clay layer. Initial analysis of carbonate content indicates that the degree of dissolution is not as extensive as that in the P/E boundary interval, with a minimum value of ~40 wt% carbonate (Fig. F19). As also illustrated in the records of MS and chromaticity, the basal contacts are gradational rather than sharp, as with the P/E boundary. This and other similar events probably represent shoaling in the depth of the lysocline during the Paleogene.

BIOSTRATIGRAPHY

At Site 1266, Pleistocene through upper Paleocene sediments were recovered. Nannofossils are present in all samples, showing generally moderate preservation with reworking and dissolution in the Miocene and reworking in the Pleistocene and in the lower Oligocene through upper Eocene (Fig. F20). Planktonic foraminifers are present, showing moderate to high abundance and variable preservation due to dissolution in the Miocene through the upper lower Eocene and reworking in the lower Pleistocene through upper Eocene (Fig. F20). Benthic foraminifers are rare and have good preservation in the upper (Pliocene–Pleistocene) and lower (lower Eocene–upper Paleocene) parts of the section. Between 33 and 267 mcd (middle Pliocene–upper lower Eocene), benthic foraminifers, large echinoid spines, and ostracodes are reworked and transported downslope from water depths no less than ~600–1500 m. Preservation of foraminifers deteriorates below 336 mcd, with specimens showing infill and some recrystallization.

Shipboard examination of calcareous nannofossils and planktonic foraminifers permitted preliminary zonal and stage assignments (Fig. F20; Tables T5, T6, T7, T8). Biochronological ages plotted against depth (mcd) delineate overall sedimentation rates (Fig. F21) ("Age Model and Mass Accumulation Rates," p. 24). Because of the extensive reworking and dissolution, the duration of unconformities is difficult to constrain, but two unconformities are recognized: one between 76 and 79 mcd corresponds to a time interval of at least 1.2 m.y. (upper Miocene), and a second one between 251 and 259 mcd corresponds to the time interval between ~37 and ~47 Ma (a large part of the middle Eocene).

Benthic foraminifers indicate lower abyssal depths (>3000 m) from the late Miocene through the Pleistocene. The paleodepth cannot be ascertained for the middle Miocene through the late Eocene (because of intensive downslope transport) or for the early Eocene. The paleodepth is transitional between upper and lower abyssal (~3000 m) in the latest Paleocene and upper abyssal (<3000 m) during the late Paleocene.

Calcareous Nannofossils

Calcareous nannofossil assemblages were examined in core catcher samples from all holes (Table T6) and in additional samples from Hole 1266A. Depths and age estimates of key biostratigraphic events are shown in Table T5. Nannofossils are abundant to common through the recovered section, and the preservation varies from good to moderate. From Cores 208-1266A-19H through 26H (199–254 mcd), the preservation deteriorates and the assemblages show variable degrees of dissolution and overgrowth. Reworking is present throughout the Miocene–lower Eocene.

F19. Image, MS, carbonate, and a* for early Eocene red clay, p. 45.

F20. Foraminifer and nannofossil biozonation, p. 46.

F21. Sedimentation rates, p. 47.

Pleistocene (0–19 mcd)

Pleistocene nannofossil assemblages are rich and well preserved and contain abundant helicoliths, placoliths of *Gephyrocapsa* and *Calcidiscus,* and *Rhabdosphaera.* Sample 208-1266A-1H-1, 110 cm, contains an upper Pleistocene assemblage of Zone CN14 (NN20). Middle and lower Pleistocene assemblages occur from Samples 208-1266A-1H-3, 110 cm, through 2H-3, 40 cm (7.2–18.9 mcd), and are characterized by the presence of different morphotypes of the genus *Gephyrocapsa.* The Pliocene/Pleistocene boundary is placed at 18.9 mcd, between the lowermost occurrence (bottom [B]) of medium *Gephyrocapsa* spp. and the uppermost occurrence (top [T]) of *Discoaster brouweri.*

Pliocene (19–71 mcd)

Pliocene nannofossils are well preserved, including a diverse *Discoaster* assemblage. *D. brouweri, Discoaster pentaradiatus, Discoaster surculus, Discoaster asymmetricus, Discoaster tamalis,* and *Discoaster variabilis* are common to abundant in the lower Pliocene, and *Reticulofenestra pseudoumbilicus,* helicoliths, and ceratolithids are common. Assemblages of Subzone CN10c have abundant *D. surculus* and *D. pentaradiatus,* common *Amaurolithus delicatus, Amaurolithus primus,* and rare *Ceratolithus rugosus.* Very rare ceratolithid specimens belonging to *Ceratolithus acutus* and *Ceratolithus larrymayeri* are present between Samples 208-1266A-7H-1, 30 cm, and 7H-2, 130 cm (69.0–71.5 mcd). Both species have short ranges that straddle the Miocene/Pliocene (M/P) boundary (Raffi et al., 1998); therefore, the M/P boundary is placed between Samples 208-1266A-7H-1, 130 cm, and 7H-2, 130 cm, at 70.7 mcd.

Miocene (71–139 mcd)

Oligocene, Eocene, and Paleocene reworked nannofossils are present throughout the Miocene except for the interval corresponding to upper Miocene Zones CN7 and CN6 (NN9 and NN8) (70.7–94.0 mcd). In the uppermost Miocene assemblages, *Discoaster berggrenii* and *Discoaster quinqueramus,* the Zone CN9/CN8 (NN11/NN10) boundary markers, and *Discoaster hamatus,* the marker for the CN8/CN7 (NN10/NN9) and CN7/CN6 (NN9/NN8) zonal boundaries, are missing. Biostratigraphic classification is based on the presence of secondary markers such as *Minylitha convallis* and *Discoaster bellus* gr. Specifically, the range of *M. convallis* corresponds to Subzone CN9a and Zone CN8, whereas *D. bellus* gr. appears concomitantly with *D. hamatus.* We use the presence of *M. convallis* to define Zone CN8 (NN10) within Core 208-1266A-8H. The Zone CN7/CN6 boundary is defined by the lowermost occurrence of *D. bellus* gr. between Samples 208-1266A-8H-5, 120 cm, and 8H-6, 120 cm (86.8–88.5 mcd).

The presence of a nannofossil assemblage of Subzone CN9bA (Sample 208-1266A-7H-6, 30 cm; 76.5 mcd), directly above sediments with abundant *M. convallis* placed in Zone CN8 (Sample 208-1266A-7H-6, 70 cm; 76.9 mcd), indicates that an unconformity is present in the lower part of Core 208-1266A-7H (76–79 mcd), corresponding to a time interval of at least 1.3 m.y. to at most 2.2 m.y. In the middle and lower Miocene, biostratigraphic inversions are associated with turbidites (e.g., in Sections 208-1266A-9H-3, 9H-4, and 9H-5 and within Core 208-1266A-11H [111–129 mcd]). Intense reworking has also hampered the recogni-

tion of the biostratigraphic sequence. Assemblages of Subzone CN5a and Zones CN3 and CN2 (NN6, NN4, and NN3) occur in scattered intervals between 93 and 121 mcd. Abundant specimens of *Discoaster druggii,* the lower Miocene marker for Subzone CN1c (Zone NN2), are present between Samples 208-1266A-11H-6, 60 cm, and 11H-7, 20 cm (119.5–120.6 mcd). The same nannofossil assemblage occurs reworked between Samples 208-1266A-11H-1, 30 cm, and 11H-5, 130 cm (111.4–118.7 mcd), in samples placed in Zone CN2 (NN3) based on the presence of common *Sphenolithus belemnos*. The presence of *Sphenolithus disbelemnos* in samples within Sections 208-1266A-13H-1 through 13H-3 (133–139 mcd) and the presence of *Sphenolithus delphix* and *Sphenolithus capricornutus* in Sections 208-1266A-13H-7 through 13H-CC (142.4–143.2 mcd) indicate that the Oligocene/Miocene (O/M) boundary is at ~139 mcd.

Oligocene (139–219 mcd)

Oligocene assemblages are present in Sections 208-1266A-13H-CC through 20H-CC (143–219 mcd). In this interval, nannofossils are abundant and preservation varies from good to poor. Reworked lower Eocene species are present in Core 208-1266A-18H. The upper Oligocene yields an assemblage mainly dominated by *Dictyococcites bisectus, Cyclicargolithus abisectus, Zygrhablithus bijugatus,* and the *Discoaster deflandrei* group. *Sphenolithus ciperoensis* and *Sphenolithus distentus* are rare, and the scarcity of *Sphenolithus predistentus* prevents the recognition of the base of Zone NP25.

The lower Oligocene zones and all the major nannofossil events that characterize the Eocene–Oligocene transition were recognized in Cores 208-1266A-17H through 19H (176.9–207.8 mcd). The zonal boundaries between Zone CP17 and Subzone CP16c and between Subzones CP16c and CP16b (NP23/NP22/NP21), defined by the uppermost occurrences of *Reticulofenestra umbilicus* and *Ericsonia formosa,* are recorded between Samples 208-1266A-19H-2, 30 cm, and 19H-2, 130 cm, and between Sample 19H-7, 75 cm, and Section 19H-CC (207.6–207.8 mcd), respectively. Rare specimens of *Isthmolithus recurvus* occur in Zones NP22 and NP21. The highest occurrence of *Discoaster saipanensis* is recorded between Samples 208-1266A-21H-1, 40 cm, and 21H-1, 120 cm (221.0–221.8 mcd) and defines the boundary between Subzone CP16a and Zone CP15 (NP21/NP20). The E/O boundary is thus placed between the bottom of Core 208-1266A-20H and top of Core 208-1266A-21H in a nonrecovered interval.

Eocene (219–307 mcd)

The uppermost Eocene assemblage consists mainly of *I. recurvus,* the marker species of Zone NP19, *Calcidiscus protoannulus, Bramletteius serraculoides, Discoaster barbadiensis, D. saipanensis, Dictyococcites* spp., and *Reticulofenestra* spp. Unconformities are present at the base of the upper Eocene and in the middle Eocene. A condensed interval in the lower part of Core 208-1266A-24H and the upper part of Core 25H spans part of Zone NP18, based on the closely spaced occurrences of the B of *I. recurvus* (36.6 Ma; between Sample 208-1266A-24H-1, 45 cm, and Section 24H-CC; 250.8–251.3 mcd) and the T of *Chiasmolithus grandis* (37.1 Ma; between Section 208-1266A-24H-CC and Sample 25H-1, 15 cm; 251.3–251.8 mcd). An unconformity, spanning ~7 m.y. of Zones CP14–CP13

(NP16–NP15), occurs between Section 208-1266A-26H-CC and Sample 27H-1, 128 cm (254.0–259.2 mcd).

All the lower Eocene zones can be identified (Fig. F20) in Cores 208-1266A-29H through 31X (280.0–306.8 mcd), with the exception of the Zone CP11/CP10 boundary. The marker species of this zonal boundary, *Toweius crassus,* is present in older sediments within Subzone CP9b and thus is not a reliable marker, as observed at other Leg 208 sites. Preservation is moderate, with partially dissolved and overgrown *Discoaster* and *Tribrachiatus orthostylus.* The B of *T. orthostylus* and *Sphenolithus radians* in Samples 208-1266A-30X-3, 99 cm, and 30X-4, 40 cm (295.0–295.9 mcd), are used to approximate the base of Subzone CP9b (Zone NP11). The B of *Discoaster diastypus* (between Samples 208-1266A-30X-4, 102 cm, and 30X-5, 50 cm; 296.5–297.5 mcd), marker of the base of Subzone CP9a, is used to approximate the zonal boundary between Zones NP10 and NP9. The P/E boundary interval occurs between Samples 208-1266A-31X-3, 36 cm, and 31X-3, 38 cm (306.86 mcd). The lowermost occurrences of *Rhomboaster cuspis* and *Rhomboaster calcitrapa* (306.49–306.51 mcd) are followed uphole by the decrease in abundance of *Fasciculithus* (between Samples 208-1266A-31X-3, 3 cm, and 31X-3, 13 cm; 306.16–306.26 mcd). The uppermost occurrences of *R. cuspis* and *R. calcitrapa* are observed between Samples 208-1266A-30X-7, 49 cm, and 31X-1, 10 cm (300.6–303.2 mcd).

Paleocene (307–379 mcd)

The upper Paleocene Zones NP9–NP5 (CP8–CP4) are represented in Sections 208-1266A-31X-3 through 34X-CC (306.8–343.9 mcd), 208-1266B-6H-CC through 11X-CC (306.9–358.3 mcd), and 208-1266C-16H-CC through 21X-CC (301.2–379.4 mcd). The nannofossil assemblages are generally diverse and moderately preserved. Common *Discoaster multiradiatus* and abundant *Fasciculithus* spp., *Toweius* spp., *Chiasmolithus* spp., and *Ericsonia* spp. characterize Zone NP9 (CP8). The lowermost occurrences of *Heliolithus riedelii* (Section 208-1266B-11X-CC and Sample 12X-1, 30 cm; 358.3–362.5 mcd), *Discoaster mohleri* (Samples 12X-2, 12 cm, and 12X-2, 115 cm; 361.5–362.5 mcd), and *Heliolithus kleinpellii* (Samples 208-1266C-21X-1, 19 cm, and 21X-1, 25 cm; 371.0–371.1 mcd) are recognized, allowing the identification of Zones NP8–NP6. The lowermost occurrence of *Sphenolithus anarrhopus* occurs in the upper part of Zone NP5 (CP4) between Samples 208-1266C-21X-2, 20 cm, and 21X-2, 25 cm (372.6–372.7 mcd). Reworked Cretaceous specimens occur in Core 208-1266B-11X, Section 12X-CC, Core 208-1266C-20X, and Section 21X-CC.

Planktonic Foraminifers

Planktonic foraminifers were examined in all core catcher samples from Holes 1266A and 1266B and in three additional samples per core in the upper 100 mcd (Tables T7, T8). Generally, planktonic foraminifers are abundant. Preservation varies from good to poor with severe dissolution from 83 mcd (Sample 208-1266A-8H-3, 32–34 cm) to 219 mcd (Section 26X-CC). Several turbidites disrupt the Pliocene and Miocene sequences. Turbidite Sample 208-1266A-3H-6, 49–50 cm (33.0 mcd), is dominated by *Globoconella conomiozea, Hirsutella scitula,* and rare specimens of *Pulleniatina primalis,* indicating lower Pliocene to Miocene sediments reworked into the upper Pliocene. Sample 208-1266A-6H-6, 22–23 cm (65.5 mcd), contains *Globoconella conoidea,*

Sphaeroidinellopsis seminulina, H. scitula, Hirsutella cibaoensis, Globigerinoides trilobus, Orbulina universa, and *Globoturborotalita nepenthes* reworked into sediments of similar age (M/P boundary interval). Reworking is common from 13 mcd (Section 208-1266A-1H-CC) through 245 mcd (Section 22H-CC).

Pleistocene (0–19 mcd)

Pleistocene samples show a mixture of well-preserved subtropical and temperate Pleistocene species. The fauna is dominated by *Globorotalia crassaformis, Globorotalia truncatulinoides, Globoconella inflata, Globigerina bulloides, Globigerinoides ruber, Globigerinoides sacculifer, Globigerinoides conglobatus, Globigerinella siphonifera, H. scitula,* and *O. universa.* The uppermost appearance of *Globorotalia tosaensis* is in Section 208-1266A-1H-CC (7.6 mcd). The Pliocene/Pleistocene boundary is between Sample 208-1266A-2H-3, 32–34 cm (uppermost appearance of *Globigerinoides extremus*), and Section 2H-CC (very rare *G. truncatulinoides*) (17.4–24.0 mcd). The Pliocene/Pleistocene boundary is placed at 19 mcd using calcareous nannofossil data.

Pliocene (19–71 mcd)

As reported at other sites, Pliocene tropical/subtropical age-diagnostic taxa are missing because the environmental conditions are temperate. *Globoconella crassaformis, G. conomiozea, G. conoidea, H. scitula,* and *G. inflata* dominate the assemblage. Although warm water species are generally rare, *G. ruber* and *G. sacculifer* are present. The absence of *Menardella miocenica* prevents the definition of the base of Zone PL6, which was approximated by the uppermost appearance of *Globoturborotalia woodi* between Samples 208-1266A-3H-1, 32–34 cm (25.3 mcd), and 3H-3, 32–34 cm (26.8 mcd). The middle to upper Pliocene boundary is placed between Samples 208-1266A-3H-1, 32–34 cm, and 3H-3, 32–34 cm (25.3–28.3 mcd), constrained by the uppermost appearances of *G. woodi* (2.3 Ma) and *Globigerina decoraperta* (2.7 Ma).

It is impossible to distinguish Zones PL4 and PL3 because the uppermost appearances of *S. seminulina* (base of Zone PL4) and *Neogloboquadrina acostaensis* (base of Zone PL3) are both present between Samples 208-1266A-4H-1, 32–34 cm (36.2 mcd), and 4H-3, 32–34 cm (39.2 mcd).

The lower to middle Pliocene boundary, as bracketed by the uppermost occurrences of *S. seminula* and *N. acostaensis,* is between Samples 208-1266A-4H-1, 32–34 cm, and 4H-3, 32–34 cm (36.2 and 39.2 mcd). The Miocene/Pliocene boundary is placed between Samples 208-1266A-6H-5, 32–34 cm (64.1 mcd), and 7H-3, 32–34 cm (72.0 mcd) (lowermost occurrences of *Sphaeroidinella dehiscens* and *G. conglobatus*).

Miocene (71–139 mcd)

G. conoidea, G. conomiozea, Globoconella miozea, Globigerina apertura, Hirsutella praescitula, and *G. nepenthes* are typical and frequent species in the Miocene. The preservation deteriorates downhole from Sample 208-1266A-8H-3, 32–34 cm (83 mcd). Fragmentation is severe so that dissolution-resistant species such as *G. nepenthes, Globoquadrina dehiscens, Dentoglobigerina altispira,* and *G. conoidea* dominate these assemblages. The close proximity of the lowermost occurrences of *G. conglobatus* (between Samples 208-1266A-7H-1, 32–34 cm, and 7H-3, 32–34 cm) and

Hirsutella juanai (between Sample 7H-5, 32–34 cm, and Section 7H-CC) to each other (i.e., <6.3 m) indicates an unconformity in this core as corroborated by the sharp boundary between lithostratigraphic Units I and II (76.85 mcd). The common uppermost appearance of *Globorotalia plesiotumida* (8.91 Ma) and *H. juanai* (9.75 Ma) in the same sample corroborate this observation.

The well-preserved planktonic foraminiferal shells in Sections 208-1266A-7H-CC and 208-1266C-1H-CC and 208-1266A-8H-CC and 208-1266C-2H-CC are assigned to Subzone M13a and Zones M11–M12, respectively. The age determination of this section in Holes 1266A and 1266C is tentative because of dissolution and reworking. The reworked material is mainly Oligocene and Eocene in origin (i.e., acarininids, *Pseudohastigerina* spp., and globigerinids). The presence of *D. altispira* and *Globoquadrina globularis* in Section 208-1266A-9H-CC (99.2 mcd) restricts the age to early Miocene, but strong reworking makes this age assignment unreliable, particularly because the moderately well preserved assemblage lacks the dissolution-resistant taxon *G. dehiscens,* which is usually common in the lower Miocene at the Walvis Ridge sites. Section 208-1266A-10H-CC (109.8 mcd) contains rare planktonic foraminifers because of poor preservation, and the assemblage appears to be associated with the O/M boundary interval. A more detailed determination of this boundary is impossible because of the severe dissolution in Sections 208-1266A-10H-CC (109.8 mcd) through 13H-CC (143.2 mcd) and 208-1266C-8H-CC and 9H-CC (152.2 to 162.5 mcd). The uppermost appearance of *Globigerina euapertura* between Sections 208-1266A-12H-CC and 13H-CC points to the presence of the O/M boundary in Core 208-1266A-13H.

Oligocene (139–219 mcd)

Dissolution and reworking of Eocene species are common in the interval, and planktonic foraminifers are rare in most samples. Upper Oligocene Sections 208-1266A-13H-CC through 16H-CC (143.2–176.0 mcd) are dominated by dissolution-resistant species such as *Globigerina venezuelana, Dentoglobigerina globularis, Globigerina tripartita,* and *Catapsydrax dissimilis.* The uppermost appearances of *Paragloborotalia opima* (141.9–164.8 mcd), *Chiloguembelina cubensis* (common) (176.0–186.2 mcd), and *"Globigerina" ampliapertura* (186.2–191.9 mcd) represent the few datums recognized in this sequence.

Section 208-1266A-17H-CC (186.2 mcd) is barren. Section 208-1266A-18H-CC (197.6 mcd) represents a massively reworked upper Eocene *"Globigerinatheka* sand" (*Globigerinatheka subconglobata* and *Globigerinatheka index*) with *Morozovella caucasica* (P10–P8) and Eocene acarininids. The uppermost common appearances of *Subbotina angioporoides* (30 Ma) and *Pseudohastigerina* spp. (32 Ma) in Section 208-1266A-20H-CC (219.3 mcd) indicate severe reworking in Zone P20 and the lower part of Zone P19 (lowermost Oligocene).

Eocene (219–307 mcd)

The uppermost clearly Eocene assemblage occurs in Section 208-1266A-21H-CC (230.6 mcd). The low-diversity assemblage, consisting mainly of *G. index* and *G. subconglobata,* is a product of dissolution and winnowing. Varying preservation and downhole contamination make age determination difficult in Sections 208-1266A-21H-CC to 26X-CC. Section 208-1266A-22H-CC (241.6 mcd) is assigned to Zones P12–P15

because *G. index* and *Morozovella spinulosa* are present. Section 208-1266A-23H-CC (249.4 mcd) is a *Globigerinatheka* sand.

Section 208-1266A-24H-CC (251.3 mcd) is tentatively assigned to Zone P12 because of the presence of *G. index, Globigerinatheka subconglobata luterbacheri, Turborotalia centralis, Turborotalia pomeroli, Turborotalia possagnoensis,* and the absence of acarininids and morozovellids. The co-occurrence of *Globigerinatheka* and *Acarinina primitiva* in Section 208-1266A-25H-CC (252.7 mcd) indicates an age range of Zones P12–P14 for this sample. The close proximity of the T of *Morozovella aragonensis* (43.6 Ma; base of Zone P12) and *Morozovella formosa* (50.8 Ma; base of Zone P8) within 12 m points toward an unconformity between 254.4 and 270.5 mcd (between Sections 208-1266A-26X-CC and 208-1266B-3X-CC).

Overall preservation improves from Sections 208-1266B-2X-CC and 208-1266A-27X-CC (262.6–267.3 mcd) downhole. Zone P8 through Subzone P6a are all represented. Sections 208-1266A-28X-CC (275.1 mcd) and 208-1266B-3X-CC (273.6 mcd) contain well-preserved lower Eocene assemblages with *A. primitiva, Acarinina spinuloinflata, Acarinina angulosa, Morozovella lensiformis, M. formosa,* and *Morozovella quetra.*

Section 208-1266A-30X-CC (300.6 mcd) contains a diverse, well-preserved assemblage that contains common biserial planktonic taxa and is assigned to Zone P5. Preservation is good within the lowermost Eocene but deteriorates downhole toward the P/E boundary. Samples 208-1266B-6H-7, 100 cm, through 6H-CC bracket the clay layer that marks the P/E boundary at ~306.84 mcd. Assemblages within this clay layer have suffered severe dissolution and contain mostly foraminiferal fragments and few whole specimens. Section 208-1266B-6H-CC (306.86 mcd), just below the clay layer, contains a well-preserved, diverse assemblage. This Zone P5 assemblage consists of *A. soldadoensis, Acarinina coalingensis, Morozovella velascoensis, M. acuta, Morozovella subbotinae, Morozovella aequa, Morozovella occlusa, Globanomalina planoconica,* and assorted subbotinid species. No "excursion taxa" were identified within the P/E boundary interval assemblages.

Paleocene (307–379 mcd)

The upper Paleocene is represented in Sections 208-1266A-31X-CC through 34X-CC (308.4–343.9 mcd), 208-1266B-6H-CC through 11X-CC (306.86–358.28), and 208-1266C-16H-CC through 21X-CC (301.2–379.4 mcd). As at the other Leg 208 sites, *M. velascoensis* is rare in Zone P5. Typical species are *A. soldadoensis, M. aequa, M. occlusa, Morozovella angulata, M. subbotinae, Subbotina triangularis,* and *Subbotina velascoensis.*

Sections 208-1266A-32X-CC (321.1 mcd) through 208-1266C-20X-CC (367.2 mcd) can be assigned to Zone P4. The assemblages are dominated by *M. acuta, M. angulata, A. aequa, M. occlusa, Igorina tadjikstanensis,* and *Globanomalina pseudomenardii.* The lowermost recovered subzone is P3b in Section 208-1266C-21X-CC (379.4 mcd). Primary faunal elements of Section 208-1266C-21X-CC include *Globanomalina ehrenbergi, Globanomalina chapmani, Morozovella acutispira, M. angulata, Morozovella conicotruncata, Acarinina nitida, I. tadjikstanensis,* and various species belonging to the spinose genera *Subbotina* and *Parasubbotina.*

Benthic Foraminifers

All core catcher samples from Holes 1266A and 1266B, Sections 208-1266C-15X-CC through 21X-CC, the mudline sample, and samples

across the P/E boundary in Hole 1266B were semiquantitatively investigated for benthic foraminifers (Table T9).

In samples above 33 mbsf and below 267 mcd, benthic foraminifers are rare compared to planktonic foraminifers and are generally well preserved, with the exception of a few samples from the lowermost Eocene (306–307 mcd), where assemblages have suffered strong dissolution and benthic foraminifers are more common relative to planktonic foraminifers. Benthic foraminifers are common and even abundant in many samples between 33 and 267 mcd (Sample 208-1266A-3H-6, 49–50 cm, and Section 27X-CC) (Table T9). In these samples, preservation is extremely variable (good to poor). Delicate thin-walled specimens have good preservation, whereas very large thick-walled specimens are broken and/or abraded. Benthic faunas indicate downslope transport from depths that are not shallower than middle to lower bathyal (~600–1500 m).

Typical indicators of downslope transport in benthic foraminiferal assemblages throughout this interval are abundant large siphonodosariid species (e.g., *Siphonodosaria pomuligera*), large nodosariids, and large specimens of *Oridorsalis umbonatus, Globocassidulina subglobosa,* and *Vulvulina spinosa.* Large and broken abraded specimens of *Cibicidoides* species, which were not otherwise observed or rare at Leg 208 sites (e.g., *Cibicidoides havanensis, Cibicidoides grimsdalei,* and *Cibicidoides eocaenus*), are common in samples between 99 and 267 mcd (Sections 208-1266A-9H-CC and 208-1266B-2X-CC). *Plectofrondicularia paucicostata* (Table T9), recorded as *Plectofrondicularia lirata* in the upper Eocene at several South Atlantic DSDP sites to the east and west of the Mid-Atlantic Ridge (Tjalsma, 1983; Clark and Wright, 1984), occurs in samples between 198 and 242 mcd (Sections 208-1266A-18H-CC and 22H-CC) and is abundant in the latter sample.

Benthic foraminiferal assemblages between 0 and 109 mcd (Sample 208-1266B-1H-1, 0–2 cm, through Section 208-1266C-4H-CC) indicate deposition at lower abyssal depths (>3000 m). Paleodepths cannot be determined for samples between 121 and 267 mcd (Sections 208-1266A-11H-CC through 208-1266B-2X-CC) because of extensive downslope transport. Paleodepths cannot be estimated for samples between 274 and 307 mcd (Section 208-1266B-3X-CC through Sample 6H-CC, 6–7 cm) because benthic foraminifers are not reliable depth indicators in the lower Eocene (Müller-Merz and Oberhänsli, 1991). Sample 208-1266B-6H-CC, 22–23 cm (306.82 mcd), is barren. Samples from 307 through 348 mcd (Sample 208-1266B-6H-CC, 26–27 cm, through Section 10X-CC; upper Paleocene) were deposited at depths transitional between upper and lower abyssal (~3000 m), and samples between 358 mcd and the bottom of the hole (379 mcd) were deposited at upper abyssal depths (2000–3000 m).

Benthic foraminiferal assemblages between 0 and 3 mcd (Samples 208-1266B-1H-1, 0–2 cm, and 1H-3, 148–150 cm) contain assemblages with common *Epistominella exigua, Alabaminella weddellensis, G. subglobosa, Cibicidoides wuellerstorfi, Cibicidoides mundulus, O. umbonatus,* and *Pyrgo* spp., along with the *Uvigerina peregrina* group, *Pullenia* spp., and *Nuttallides umbonifera.* These samples do not contain pleurostomellid and siphonodosariid species and were probably deposited after the "*Stilostomella* extinction" at 0.65 Ma (Hayward, 2002). At present, similar assemblages occur along Walvis Ridge between ~2000 and 3800 m (Schmiedl et al., 1997). The common occurrence of *E. exigua* indicates seasonally fluctuating primary productivity in the overlying waters.

Samples between 7 and 89 mcd (Sections 208-1266B-1H-CC through 208-1266A-8H-CC) resemble those in the upper samples but lack com-

mon *E. exigua* and contain pleurostomellid and siphonodosariid species in addition to those listed above (Table T9). In these samples, the relative abundances of *N. umbonifera, Uvigerina* spp., and *Melonis* spp. fluctuate strongly, possibly indicating fluctuations in surface productivity and bottom water mass characteristics. These faunas resemble those living at depths between 2600 and 4000 m presently in the Walvis Ridge area (Schmiedl et al., 1997). *C. wuellerstorfi* and *Pyrgo* spp. have their joint lowest occurrences in Section 208-1266A-8H-CC (89 mcd).

Between 99 and 219 mcd, in situ components of the assemblages include long-lived species such as *Gyroidinoides* spp., *O. umbonatus, G. subglobosa, Bolivinoides huneri, Pullenia* spp., *N. umbonifera,* and common *Siphonodosaria* spp. and pleurostomellid and unilocular taxa. The transition between *Cibicidoides praemundulus* and *C. mundulus* occurs in this interval, and *Anomalinoides spissiformis* and *Nonion havanense* have their highest occurrence. *Bigenerina nodosaria* and *Astronion pusillum* have their lowest occurrence in Section 208-1266A-20H-CC (219 mcd) at the base of this interval. Reworked components include *S. pomuligera, Siphonodosaria hispidula,* various large nodosariid and orthomorphinid species, *Clavulinoides* spp., *V. spinosa, C. havanensis,* and *C. grimsdalei.*

Nuttallides truempyi has its uppermost, nonreworked occurrence in Section 208-1266A-21H-CC (231 mcd). Samples between 231 and 267 mcd (Sections 208-1266A-21H-CC through 27H-CC) contain typical species-rich abyssal middle–upper Eocene assemblages, with abundant *N. truempyi, C. praemundulus, C. grimsdalei, O. umbonatus, Gyroidinoides* spp., *A. spissiformis, N. havanense,* and common *Siphonodosaria* spp., as well as unilocular, laevidentalinid, and pleurostomellid taxa. Reworked components are as in the interval described above (Table T9).

Section 208-1266B-3X-CC through Sample 6H-CC, 6–7 cm (274–307 mcd), contain assemblages that are less species rich, as is typical for the lower Eocene in the South Atlantic over a large depth range (Clark and Wright, 1984; Müller-Merz and Oberhänsli, 1991; Thomas and Shackleton, 1996). These assemblages are characterized by the presence of *Aragonia aragonensis* and common to abundant small smooth-walled species of *Abyssamina* and *Clinapertina,* small smooth-walled buliminid species (e.g., *Bulimina kugleri* and *Bulimina simplex*), and small specimens of *N. truempyi, O. umbonatus, A. spissiformis,* and *N. havanense. Tappanina selmensis* and *Siphogenerinoides brevispinosa* vary strongly in relative abundance, and unilocular, laevidentalinid, and pleurostomellid taxa are present. A sample in a relatively clay rich interval at 293 mcd (Sample 208-1266A-30X-2, 56–57 cm) contains an assemblage with a relatively low species richness and common to abundant *Clinapertina* and *Abyssamina* spp.

In the lowermost part of this interval (306.10–306.66 mcd; Samples 208-1266B-6H-7, 100–101 cm, through 6H-CC, 6–7 cm), species richness is extremely low and long-lived unilocular and laevidentalinid taxa are absent. Similar assemblages have been described from immediately after the P/E benthic foraminiferal extinction event (BEE) (Müller-Merz and Oberhänsli, 1991; Thomas and Shackleton, 1996) and occur at other Leg 208 sites. Minute specimens of *Abyssamina quadrata, B. kugleri, Clinapertina inflata, Quadrimorphina profunda,* and small specimens of *O. umbonatus* and *N. truempyi* are common to abundant. The latter two species dominate most samples, but the lowermost sample is dominated by *A. quadrata* and *B. kugleri.*

The BEE occurs between Samples 208-1266B-6H-CC, 22–23 cm, and 6H-CC, 26–27 cm (306.82 and 306.86 mcd), Sample 208-1266A-31X-3, 0–2 cm, and Section 1X-CC (306.13 and 308.39 mcd), and Sections 208-

1266C-16H-CC and 17H-CC (301.24 and 313.54 mcd). One sample (208-1266B-6H-CC, 22–23 cm; 306.82 mcd), immediately above the lithologic contact of clay-rich material over carbonate-rich material, is barren.

Samples below the BEE through Section 208-1266B-10X-CC (307–348 mbsf) contain species-rich Paleocene assemblages with *Stensioeina beccariiformis, Paralabamina lunata, Paralabamina hillebrandti, Pullenia coryelli,* large thick-walled species of *Gyroidinoides* such as *Gyroidinoides beisseli* and *Gyroidinoides globosa,* and large agglutinant taxa (e.g., *Clavulinoides* spp., *Marssonella oxycona,* and *Gaudryina pyramidata*), as well as relatively common *Aragonia velascoensis.* As at Site 1262, but not at Sites 1263 and 1265, these assemblages are characterized by strongly fluctuating relative abundances of *S. brevispinosa, Bulimina thanetensis,* and *Rectobulimina carpentierae.*

Several species commonly thought to be lower bathyal indicators (e.g., *Alabamina creta, Bolivinoides delicatulus,* and *Coryphostoma midwayensis*) have rare and scattered occurrences in this interval, but the relative abundances of various agglutinated taxa, *Abyssamina* spp., and *A. velascoensis* indicate a paleodepth transitional between upper and lower abyssal (~3000 m).

Assemblages between 358 mcd and the bottom of the hole (Sections 208-1266B-11X-CC through 208-1266C-21X-CC) resemble those between the BEE and 348 mcd but have much more even species distributions. These samples have less common *Abyssamina* spp. and more common *S. beccariiformis, Bulimina velascoensis,* large *Gyroidinoides* spp., and *A. velascoensis,* indicating deposition at upper abyssal depths (between 2000 and 3000 m).

PALEOMAGNETISM

Drilling and Core Orientation

Every other core from Site 1266 was recovered with a nonmagnetic core barrel until the first core barrel had to be drilled over (see Table **T1;** **"Operations,"** p. 2). As at other sites, no obvious difference was noted in the magnetic data between sediments recovered with the nonmagnetic barrel and those with a standard core barrel. All APC cores in Holes 1266A and 1266C were successfully oriented with the Tensor tool with the exception of Cores 208-1266A-1H, 2H, and 9H and 208-1266C-6H.

Archive-Half Measurements

The archive halves of 67 cores from Holes 1266A, 1266B, and 1266C were measured in the pass-through magnetometer. Natural remanent magnetization (NRM) was measured on all cores. Most cores were demagnetized at 10 and 15 mT. As at other sites, a strong vertical overprint was largely removed by demagnetization to 10 mT.

After reviewing data from previous sites, questions were raised regarding the quality of the data obtained from the archive halves. It was thought that the relatively soft and weakly magnetized carbonate sediments may have suffered from additional deformation and overprinting during splitting, resulting in a biased or poorly resolved polarity record. In an attempt to determine if core splitting significantly affected the pass-through data, a comparison test between measurements made

on archive-half split cores and measurements made on whole-round sections was performed at Site 1266. All measurements from Hole 1266A were performed on the archive-half split cores, whereas those from Hole 1266C were made on whole rounds prior to splitting. This resulted in the demagnetization (up to 15 mT) of the working-half section (see "Paleomagnetism," p. 20, in the "Explanatory Notes" chapter) (Table T10). Following splitting, a sampling of sections from Hole 1266C was also measured as archive halves, following demagnetization to 15 mT.

The results are somewhat ambiguous, but they suggest that at Site 1266 the effects of splitting were generally not significant enough to justify the demagnetization of the working half. The soft component of magnetization (i.e., measured before demagnetization and largely corresponding to the overprint) is generally stronger and more stable in the whole-round cores, suggesting that this soft component may provide a proxy for postcoring deformation. The characteristic remanence, however, does not appear to be significantly better resolved for Hole 1266C whole rounds. We should point out, though, that the inclination record from the Hole 1266A split cores is relatively clean and stable compared to those of Sites 1263 and 1264; a similar comparison experiment for one of these sites has shown different results.

A more direct comparison of the effects of splitting can be made by comparing sections that were measured both as whole rounds and as archive halves. Data from these sections suggest that splitting can affect both directional and intensity data. Of the twelve sections measured as both whole round and archive halves, only two showed significant differences in the inclination data (Fig. F22A, F22B). Section 208-1266C-18H-3 in particular showed significant inclination shallowing following splitting (Fig F22B). These sections did not appear to be any less firm or lithified than the remainder of the sections, which showed no significant change in inclination following splitting (e.g., Fig. F22C). The intensity data from the split vs. whole-round sections generally parallel each other, although often with an offset in absolute value. Even in cases where the inclination records are identical, this offset between intensity records is sometimes observed. This may be at least partially attributed to uneven core splitting. Cores are often not split evenly in half, meaning that the volume of the archive half is not exactly half that of the whole round. This could lead to an incorrect calculation of magnetization (a volume-normalized quantity) in the archive half, where a constant volume is assumed.

Remanent Magnetization Intensity

Intensities of initial NRM, including the vertical overprint component, are mostly on the order of 10^{-3} to 10^{-2} A/m (Fig. F23). After demagnetization to 15 mT, intensities are about an order of magnitude lower (Fig. F23) and exhibit similar downhole trends to initial MS values (Fig. F24).

The uppermost 75 mcd (lithostratigraphic Unit I) is characterized by low depositional remanent magentization (DRM) intensities (less than ~5×10^{-3} A/m at 15 mT), lower susceptibility, and higher DRM normalized by susceptibility ($nDRM_{15\ mT}$) (Figs. F23, F24, F25) when compared to the interval below. These higher values of $nDRM_{15\ mT}$ suggest a change in ferromagnetic mineral properties, if we assume no change in geomagnetic field intensity. As discussed in "Paleomagnetism," p. 12,
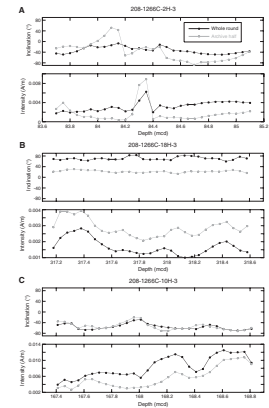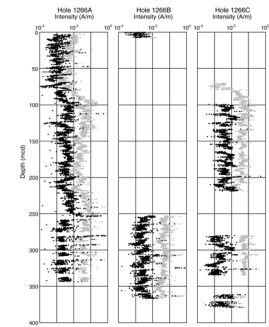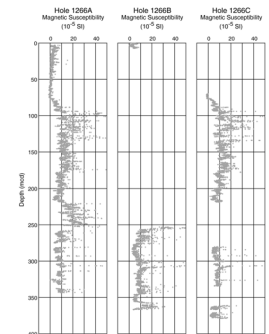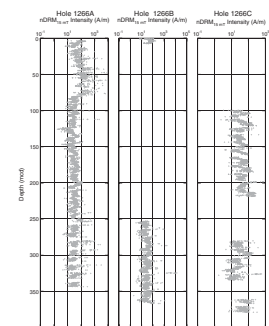
in the "Site 1264" chapter, long-term trends or offsets in average $nDRM_{15\ mT}$ may be useful as an indicator of diagenetic changes. These elevated $nDRM_{15\ mT}$ values are also observed at all other Leg 208 sites (with an onset in the upper Miocene), although they are largely obscured by a hiatus at Site 1263. The increase in the derived nDRM parameter is reflected in relatively lower susceptibility and magnetic intensity and in some cases is additionally characterized by a decrease in the low-coercivity (0–15 mT) component. These observations may be explained by diagenetic dissolution of magnetite, but further measurements will be necessary to confirm this interpretation.

Magnetostratigraphy

Magnetostratigraphic age-depth tie points are given in Table T10. The Pliocene was only cored in Hole 1266A, but we believe that all the major polarity boundaries are identifiable, although some appear to fall in core breaks (base of Chron C2An and the base of Chron C3n) or are not well resolved (top of Chron C2An).

Much of the upper Miocene is either condensed or missing. The placement of Chron C5n (Fig. F26B) was chosen to agree with the bottoms of biostratigraphic datums *Discoaster bellus* gr. (10.48 Ma) and *Catinaster coalitus* (10.79 Ma). The remainder of the Miocene is poorly resolved, and the placement of Chron C6Cn was chosen to correspond to the biostratigraphic placement of the O/M boundary.

The entire Oligocene polarity sequence appears to be reasonably well resolved in both Holes 1266A and 1266C (Fig. F26C), but some ambiguities remain in the preliminary interpretation. The lack of overlap between cores from the two holes leaves some boundaries unclear, and the biostratigraphic datums from this interval suffer from significant reworking. Chron C7n through the top of C8n is placed with some confidence, and the placement of Chron C13n is constrained with the tops of nannofossil datums *E. formosa* at 207.7 mcd and *D. saipanensis* at 221.4 mcd, as at all other sites. Between these two intervals, however, several interpretations are possible. If the age and placement of the top of nannofossil datum *R. umbilicus* (31.7 Ma) at ~200 mcd is correct, then Chron C12n should correspond to the short normal which is observed in both holes at ~194 mcd. This interpretation results in a normal polarity interval between ~205 and 208 mcd in both Holes 1266A and 1266C that does not correspond to the geomagnetic polarity timescale. Alternative interpretations would assign this normal polarity interval to Chron C12n or to part of Chron C13n but would result in dramatic changes in sedimentation rates throughout the lower Oligocene. Detailed shore-based sampling may help resolve some of these ambiguities.

Tentative identification of a few chrons in the upper Eocene was possible, but most of the Eocene is either condensed, missing, or poorly resolved. The lower part of Chron C24n appears to be resolved for Holes 1266B and 1266C. The transition from Chron C24n to C24r was placed between 319.6 and 320.4 mcd. If this placement is correct, it implies that the portion of Chron C24r above the P/E boundary is considerably condensed compared to the portion below the boundary. Below ~325 mcd, the inclination record from all holes is based solely on data from XCB cores and is not well resolved. However, a reversed to normal transition is observed in sediments from Holes 1266B and 1266C at ~364.5 mcd. Based on the biostratigraphy, this reversal was assigned to the base of Chron C26n.

F26. Magnetostratigraphic interpretation, p. 52.
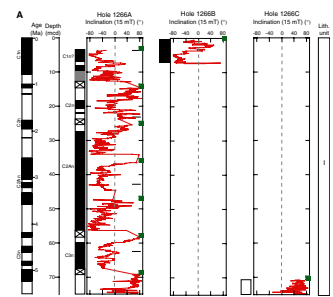
GEOCHEMISTRY

Volatile Hydrocarbons

The concentration of CH_4 (C_1) in 28 headspace samples analyzed from Site 1266 was at an atmospheric background level (range = 1.6–2.0 µL/L); no hydrocarbon gases higher than C_1 were detected.

Interstitial Water Chemistry

Interstitial water from 27 samples was collected from Hole 1266A, extending from 10.5 to 342.1 mcd. Chemical constituents were determined according to the procedures outlined in "Geochemistry," p. 23, in the "Explanatory Notes" chapter. Results of the chemical analyses are presented in Table T11.

pH, Salinity, Alkalinity, Chloride, and Sodium

The pH of pore waters from Site 1266 ranges from 7.1 to 7.5 (average = 7.3 ± 0.1) (Table T11). All values are lower than the average seawater value of 8.1 and generally decrease with depth. Salinity values range from 35.0 to 35.5 g/kg.

Alkalinity decreases slightly from 3.3 mM in the shallowest sample at 10.5 mcd to 1.9 mM at 330.2 mcd (Fig. F27A). One sample had an anomalously high value of 4.9 mM at 151.5 mcd.

The pore water chloride concentration increases slightly with depth from a minimum value of 561 mM (10.5 mcd) to 569 mM (330.2 mcd) (Fig. F27B). Three samples contain lower chloride values of 503 mM (107.8 mcd), 513 mM (129.7 mcd), and 510 mM (173.4 mcd). Excluding these values, the mean pore water chloride value is 565 mM (standard deviation = 6 mM).

Sodium concentrations average 480 mM (standard deviation = 10.2 mM) over the entire pore water profile, with no distinct trend aside from an initial increase from 452 to 497 mM from 10.54 to 21.47 mcd (Fig. F27C).

Potassium, Calcium, Magnesium, Strontium, and Lithium

Site 1266 downhole trends in potassium, calcium, and magnesium are consistent with those resulting from exchange with basaltic basement at depth (Gieskes, 1981), with potassium and magnesium decreasing and calcium increasing slightly downhole (Fig. F27D, F27E, F27F). Pore water potassium concentrations decrease slightly from 9.9 mM (10.54 mcd) to 6.8 mM (342.1 mcd) (Fig. F27D). Calcium values increase from 10.4 mM (10.54 mcd) to 26.9 mM (319.2 mcd) (Fig. F27E). The magnesium profile (Fig. F27F) is characterized by a general decrease with depth from 53.6 mM in the shallowest sample (10.54 mcd) to 40.1 mM at the base of the section (342.1 mcd). Superimposed upon this trend is an increase from 42.4 mM (151.5 mcd) to 49.0 mM (238.9 mcd).

Strontium concentrations increase from 165 µM (10.54 mcd) to 452 µM (319.2 mcd). Below this depth, strontium values remain high (>420 µM) to the base of the analyzed record (342.1 mcd) (Fig. F27G). These high pore water concentrations may be related to carbonate diagenesis, where the dissolution of biogenic calcite and subsequent reprecipita-

T11. Pore water analyses, p. 74.

F27. Chemical constituents in interstitial waters, p. 57.
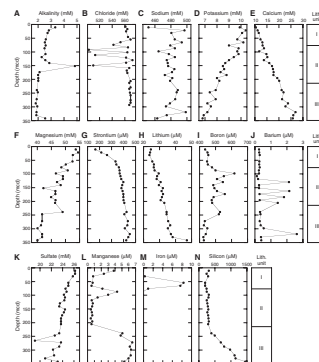
tion of inorganic diagenetic calcite supplies dissolved strontium to the interstitial waters (e.g., Baker et al., 1982).

The lithium concentration profile exhibits a slight decrease from 24.6 to 23.7 µM over the interval from 10.54 to 30.89 mcd then increases gradually to 47.0 µM at the base of the section (342.1 mcd) (Fig. F27H). This trend suggests a minor shallow subsurface sink for dissolved lithium and a deeper source of lithium from the sediment into the pore waters.

Boron and Barium

Boron values increase with depth from 435 µM (10.54 mcd) to 618 µM (97.94 mcd), remain relatively high (>485 µM) to 246.9 mcd, then decrease to 426 µM at the base of the profile (342.1 mcd) (Fig. F27I). Pore water barium concentrations range between background values of <0.5 and 2.6 µM (Fig. F27J). Elevated barium concentrations do not correlate with any decrease in pore water sulfate concentrations that might suggest enhanced barite solubility.

Sulfate, Manganese, and Iron

The pore water profile from Site 1266 is characterized by a general decrease in sulfate from 26.2 mM (10.5 mcd) to 20.9 mM (330.2 mcd) (Fig. F27K). One sample had a relatively low sulfate concentration of 19.1 mM (265.4 mcd). The relatively high concentrations of sulfate (mean = 23.8 ± 1.5 mM) reflect the very low organic matter content of the sedimentary section recovered at Site 1266 (see "Carbonate and Organic Carbon," p. 23).

Pore water manganese values decrease from 3.82 µM at the top of the profile (10.5 mcd) to values <1.0 µM in the interval from 30.9 to 65.2 mcd. Below this depth, values increase to a local maximum value of 4.32 µM (87.0 mcd) and then decrease again to 0.47 µM (151.5 mcd). Manganese values remain low (<1.0 µM) to 205.3 mcd then increase to >5.0 µM (271.8 mcd) (Fig. F27L).

Pore water concentrations of dissolved iron are below detection limit throughout much of the interval analyzed (Fig. F27M). However, concentrations rise from 0.26 to 8.34 µM at 54.2 mcd. Dissolved iron concentrations then decrease to 0 at 87.0 mcd. Maximum iron concentrations correspond to a decrease in sediment chromaticity (a*), suggesting a source of reduced iron from the sediments to pore waters in the interval from ~8 to 55 mcd (see Fig. F13; "Lithostratigraphy," p. 4).

Silicon

Pore water silicon concentrations (Fig. F27N) average 269 µM over the interval from 10.5 to 205.3 mcd then increase to 1446 µM at the base of the profile (342.1 mcd). This increase coincides with the increase in pore water manganese concentrations at ~239 mcd.

Summary of Interstitial Water Chemistry

The Site 1266 pore water profiles of potassium, calcium, and magnesium reflect the diffusional gradient between seawater and basalt. In contrast, the profiles of strontium, lithium, boron, silicon, and part of the manganese and iron records are dominated by sedimentary contributions of dissolved ions to the pore waters. Little evidence of microbial

influence exists in these profiles as reflected in the sulfate, manganese, and iron profiles.

Sediment Geochemistry

Carbonate and Organic Carbon

Carbonate determinations by coulometry were made for a total of 257 samples from Site 1266 (Table T12). Low-resolution samples were selected to provide a measure of the carbonate content within different units, and two sets of high-resolution samples were taken to assess the magnitude of carbonate decrease within the P/E boundary interval (305.0–307.6 mcd) and clay horizon (292.0–293.0 mcd). The carbonate values in lithostratigraphic Unit I average 94.7 wt%. In Unit II, carbonate values decrease to 69.6 wt% (97.9 mcd) then increase to 93.9 wt% (129.0 mcd). From 129.0 to 274.9 mcd, carbonate values average 90.0 wt% (Table T12; Fig. F28).

The interval spanning 281.2 to 306.8 mcd contains two notable clay-rich horizons (intervals of low carbonate): the P/E boundary interval (305.0 to 307.5 mcd) and another clay horizon spanning 292 to 293 mcd (Fig. F28). Description of these detailed records will proceed from the base of the interval upward. A composite record of the P/E clay interval (Fig. F28B) constructed from all three holes (Sections 208-1266A-31X-3, 208-1266B-6H-7, and 208-1266C-17H-3) indicates that carbonate contents drop from 92.6 wt% below the base (Sample 208-1266A-31X-3, 70 cm; 306.8 mcd) to 0.5 wt% (Sample 208-1266C-17H-3, 110 cm; 302.8 mcd) at the base of the P/E clay interval. Carbonate values remain below 1.0 wt% for 6 cm (306.69 mcd) and then gradually increase upsection to ~90 wt% at 306.18 mcd.

High-resolution sampling of an additional clay-rich interval (Fig. F28) indicates that carbonate values decrease from 91.9 wt% (Sample 208-1266B-5H-5, 100 cm; 292.78 mcd) to 47.7 wt% (Sample 5H-5, 88 cm; 292.66 mcd). Above this minimum, carbonate values gradually increase to 94.1 wt% (Sample 208-1266B-5H-5, 75 cm; 292.53 mcd).

Extractable Hydrocarbons

Four samples were selected for organic matter extraction: squeeze cake Samples 208-1266A-2H-5, 140–150 cm (21.5 mcd), and 13H-5, 140–150 cm (140.6 mcd), and core catcher Samples 208-1266C-11H-CC, 0–1 cm (185.2 mcd), and 12H-CC, 0–1 cm (196.7 mcd).

Mass chromatograms (m/z 85) for all samples analyzed were dominated by n-C_{14} through n-C_{18} alkanes (Fig. F29), with minor occurrences of branched isoprenoids in each aliphatic hydrocarbon fraction (except for pristane and phytane). This feature is generally observed in the sediments of the Miocene interval and above from the previous sites of Leg 208. Samples 208-1266C-11H-CC, 0–1 cm, and 12H-CC, 0–1 cm (Fig. F29), indicate that this character of aliphatic hydrocarbons extends down to at least the upper lower Oligocene but no deeper than the middle Eocene as shown by an analysis of Sample 208-1263A-17H-5, 140–150 cm. The Site 1266 results support findings from other Leg 208 sites that a turnover of the major primary producer occurred between the middle Eocene and late early Oligocene.

Pristane and phytane were also abundant in the aliphatic hydrocarbon fraction of all samples (Figs. F29, F30). This character is particularly distinct in Sample 208-1266A-13H-5, 140–150 cm (Fig. F30), in which

T12. Sedimentary calcium carbonate and total and organic carbon concentrations, p. 75.

F28. Sedimentary carbonate vs. composite depth, p. 58.
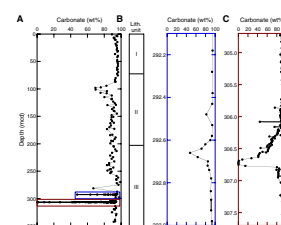
F29. Mass chromatograms of aliphatic hydrocarbons, p. 59.
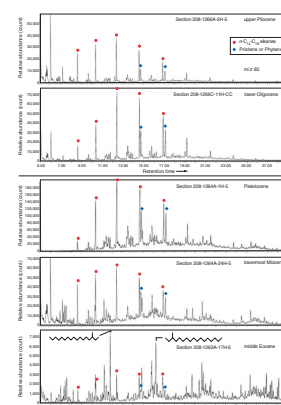
F30. Examples of mass chromatograms, p. 60.
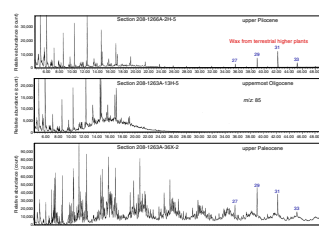
pristane and phytane showed comparable abundances of n-C_{17} and n-C_{18}, respectively.

The aliphatic hydrocarbon fraction from Sample 208-1266C-2H-5, 140–150 cm, contained the long-chain alkanes n-C_{27} through n-C_{33}, with a strong predominance of the odd carbon number indicating a contribution of terrestrial higher plants (Fig. F30). Leaf wax of terrestrial higher plants is believed to be the sole source of long-chain n-alkanes with a strong odd carbon preference in thermally immature sediments (e.g., Tissot and Welte, 1984). The largest abundance among the n-$C_{27–33}$ in Sample 208-1266C-2H-5, 140–150 cm, is characteristically marked by n-C_{31} instead of n-C_{29}, suggesting a specific origin among a variety of terrestrial plants. A similar distribution of long-chain n-alkanes was observed in Sample 208-1262B-1H-3, 140–150 cm.

AGE MODEL AND MASS ACCUMULATION RATES

A 379.4-mcd-thick (333.1 mbsf) upper Paleocene (~59 Ma) to Pleistocene pelagic sediment sequence was recovered at Site 1266. Ninety-three biostratigraphic datums and twenty-five magnetostratigraphic datums (Table T13) were used to construct an age-depth model for this site (Table T14; Fig. F31). Linear sedimentation rates (LSRs), total mass accumulation rates (MARs), and carbonate MARs were calculated at 1-m.y. intervals (see **"Age Model and Mass Accumulation Rates,"** p. 33, in the "Explanatory Notes" chapter).

Age-Depth Model

The main objective of Site 1266 was to recover a complete and well-resolved upper Paleocene to lower Eocene section, and the site was chosen to yield this critical stratigraphic interval at a relatively shallow burial depth. The sediment section from Site 1266 is therefore characterized by significant condensed intervals and unconformities in the younger section, particularly the middle Eocene interval (47–37 Ma; 259–251 mcd) and the upper Miocene (9.9–8.7 Ma; 79–76 mcd). Biostratigraphic and magnetic reversal datums are generally in good agreement, the exception being a lower to upper Oligocene interval where magnetic tie points agree better with planktonic foraminifers than with calcareous nannoplankton datums.

Linear Sedimentation and Mass Accumulation Rates

LSRs range between <1 and 26 m/m.y., and total MARs range from <0.1 to 3.4 g/cm²/k.y. Total MAR fluctuations essentially represent variations in carbonate MAR. LSRs and carbonate MARs were highest from 57 to 52 Ma (late Paleocene–early Eocene). The interval corresponding to 51–37 Ma has very low accumulation rates and comprises a major condensed interval/unconformity. It is followed by the upper Eocene to lower Miocene section with moderately high LSRs and MARs. Distinctly low accumulation rates are indicated for the middle Miocene (18–11 Ma) and for the upper Miocene interval that comprises an unconformity (10–6 Ma). The Pliocene–Pleistocene rates are of moderate magnitude (~1 g/cm²/k.y.).

Noncarbonate MARs averaged over 1-m.y. intervals are generally low (<0.3 g/cm²/k.y.), and the small fluctuations are probably within the an-

alytical uncertainty of the data. The highest values in the interval from 57 to 52 Ma are an exception and might be related to the occurrence of carbonate-poor intervals of a few centimeters to several decimeters in length (see "Lithostratigraphy," p. 4, and "Geochemistry," p. 21). These short-term carbonate dissolution events are smoothed out in the MAR record as a result of our 1-m.y. sampling of the age-depth model, dictated by the limited resolution of the shipboard age-depth control points and density and carbonate data.
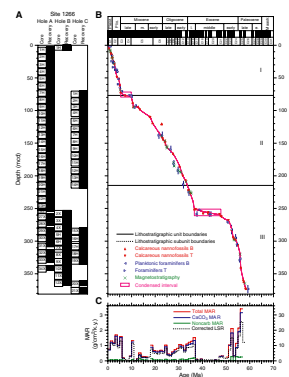
REFERENCES

Baker, P.A., Gieskes, J.M., and Elderfield, H., 1982. Diagenesis of carbonates in deep-sea sediments—evidence from Sr^{2+}/Ca^{2+} ratios and interstitial dissolved Sr^{2+} data. *J. Sediment. Petrol.,* 52:71–82.

Cande, S.C., and Kent, D.V., 1995. Revised calibration of the geomagnetic polarity timescale for the Late Cretaceous and Cenozoic. *J. Geophys. Res.,* 100:6093–6095.

Clark, M.W., and Wright, R.C., 1984. Paleogene abyssal foraminifers from the Cape and Angola Basins, South Atlantic Ocean: DSDP 73. *In* Hsü, K.J., LaBrecque, J.L., et al., *Init. Repts. DSDP,* 73: Washington (U.S. Govt. Printing Office), 459–480.

Gieskes, J.M., 1981. Deep-sea drilling interstitial water studies: implications for chemical alteration of the oceanic crust, layers I and II. *In* Warme, J.E., Douglas, R.G., and Winterer, E.L. (Eds.), *The Deep Sea Drilling Project: A Decade of Progress.* Spec. Publ.—Soc. Econ. Paleontol. Mineral., 32:149–167.

Hayward, B.W., 2002. Late Pliocene to middle Pleistocene extinctions of deep-sea benthic foraminifera ("*Stilostomella* extinction") in the southwest Pacific. *J. Foraminiferal Res.,* 32:274–307.

Lourens, L.J., Hilgen, F.J., Laskar, J., Shackleton, N.J., and Wilson, D., in press. The Neogene period. *In* Gradstein, F.M., Ogg, J., and Smith, A.G. (Eds.), *A Geological Time Scale 2004:* Cambridge (Cambridge Univ. Press).

Moore, T.C., Jr., Rabinowitz, P.D., et al., 1984. *Init. Repts. DSDP,* 74: Washington (U.S. Govt. Printing Office).

Müller-Merz, E., and Oberhänsli, H., 1991. Eocene bathyal and abyssal benthic foraminifera from a South Atlantic transect at 20–30°S. *Palaeogeogr., Palaeoclimatol., Palaeoecol.,* 83:117–171.

Raffi, I., Backman, J., and Rio, D., 1998. Evolutionary trends of calcareous nannofossils in the late Neogene. *Mar. Micropaleontol.,* 35:17–41.

Schmiedl, G., Mackensen, A., and Müller, P.J., 1997. Recent benthic foraminifera from the eastern South Atlantic Ocean: dependence on food supply and water masses. *Mar. Micropaleontol.,* 32:249–287.

Thomas, E., and Shackleton, N., 1996. The Palaeocene–Eocene benthic foraminiferal extinction and stable isotope anomalies. *In* Knox, R.W.O'B., Corfield, R.M., and Dunay, R.E. (Eds.), *Correlation of the Early Paleogene in Northwest Europe.* Geol. Soc. Spec. Publ., 101:401–441.

Tissot, B.P., and Welte, D.H., 1984. *Petroleum Formation and Occurrence* (2nd ed.): Heidelberg (Springer-Verlag).

Tjalsma, R.C., 1983. Eocene to Miocene benthic foraminifers from DSDP Site 516, Rio Grande Rise, South Atlantic. *In* Barker, P.F., Carlson, R.L., Johnson, D.A., et al., *Init. Repts. DSDP,* 72: Washington (U.S. Govt. Printing Office), 731–756.

Figure F1. *Meteor* cruise M49/1 track chart showing the locations of Leg 208 sites, including Site 1266 (proposed Site WALV-10F) and alternate sites (WALV-8B–D, WALV-9A, and WALV-10A–D) along lines GeoB 01-030, GeoB 01-044, GeoB 01-066, and GeoB 01-059.

Figure F2. Line GeoB 01-030 (Part 3) with Site 1266 and alternate site WALV-10A (DSDP Site 528). CDP = common depth point. V.E. = vertical exaggeration. $R_{P/E}$ = Paleocene/Eocene boundary reflector, $R_{K/P}$ = Cretaceous/Paleogene boundary reflector.
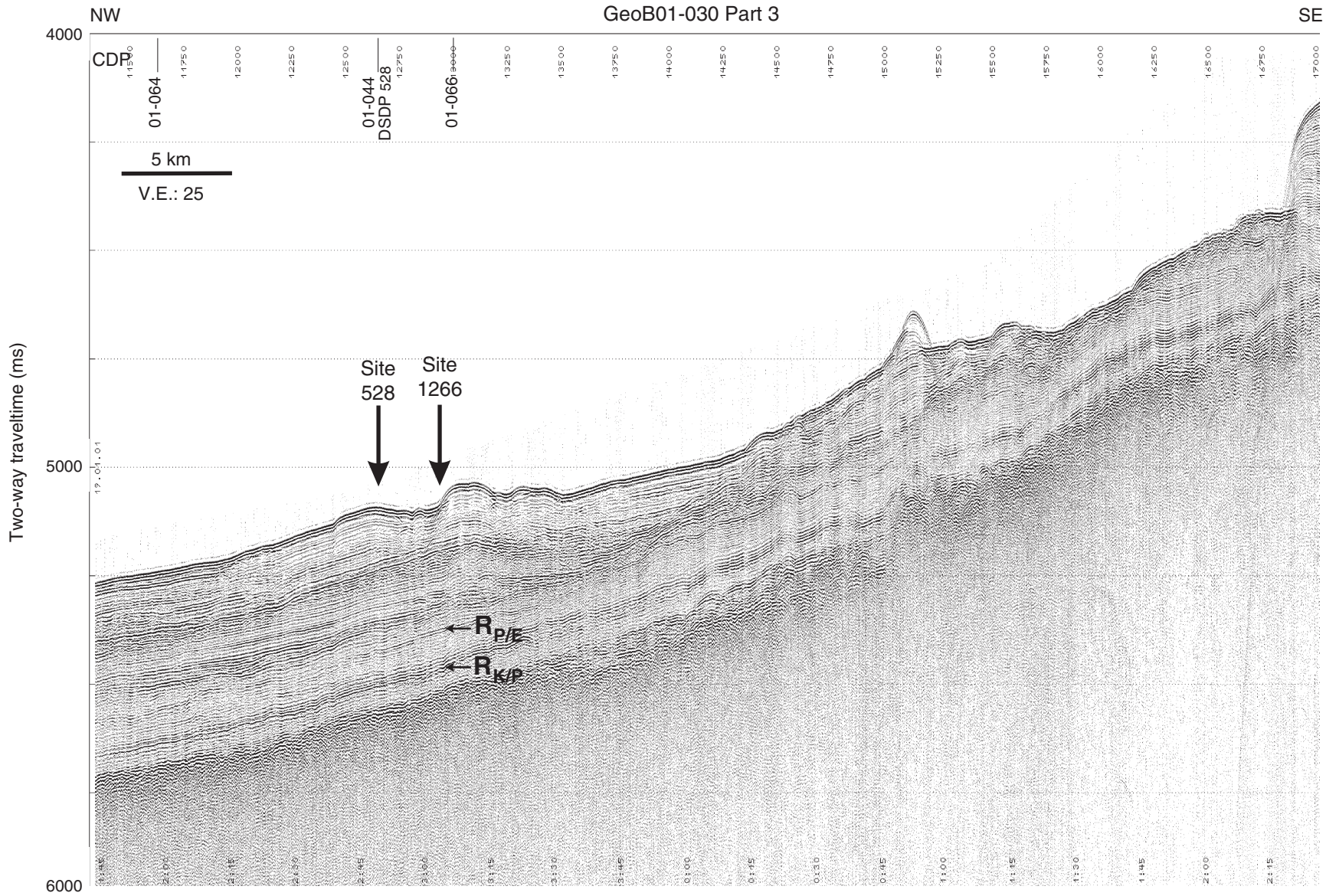
Figure F3. Line GeoB 01-030 with the locations of Site 1266 and DSDP Site 528 (proposed Site WALV-10A) and age estimates of prominent reflectors. A middle–upper Miocene reflector (R_{M1}) is estimated to be at 105 mbsf, the Oligocene/Miocene boundary reflector ($R_{O/M}$,) is estimated to be at 140 mbsf, the Paleocene/Eocene boundary reflector ($R_{P/E}$) is estimated to be at 275 mbsf, and the Cretaceous/Paleogene boundary ($R_{K/P}$) is estimated to be at 350 mbsf. All reflectors can be identified over most of the surveyed area. CDP = common depth point.
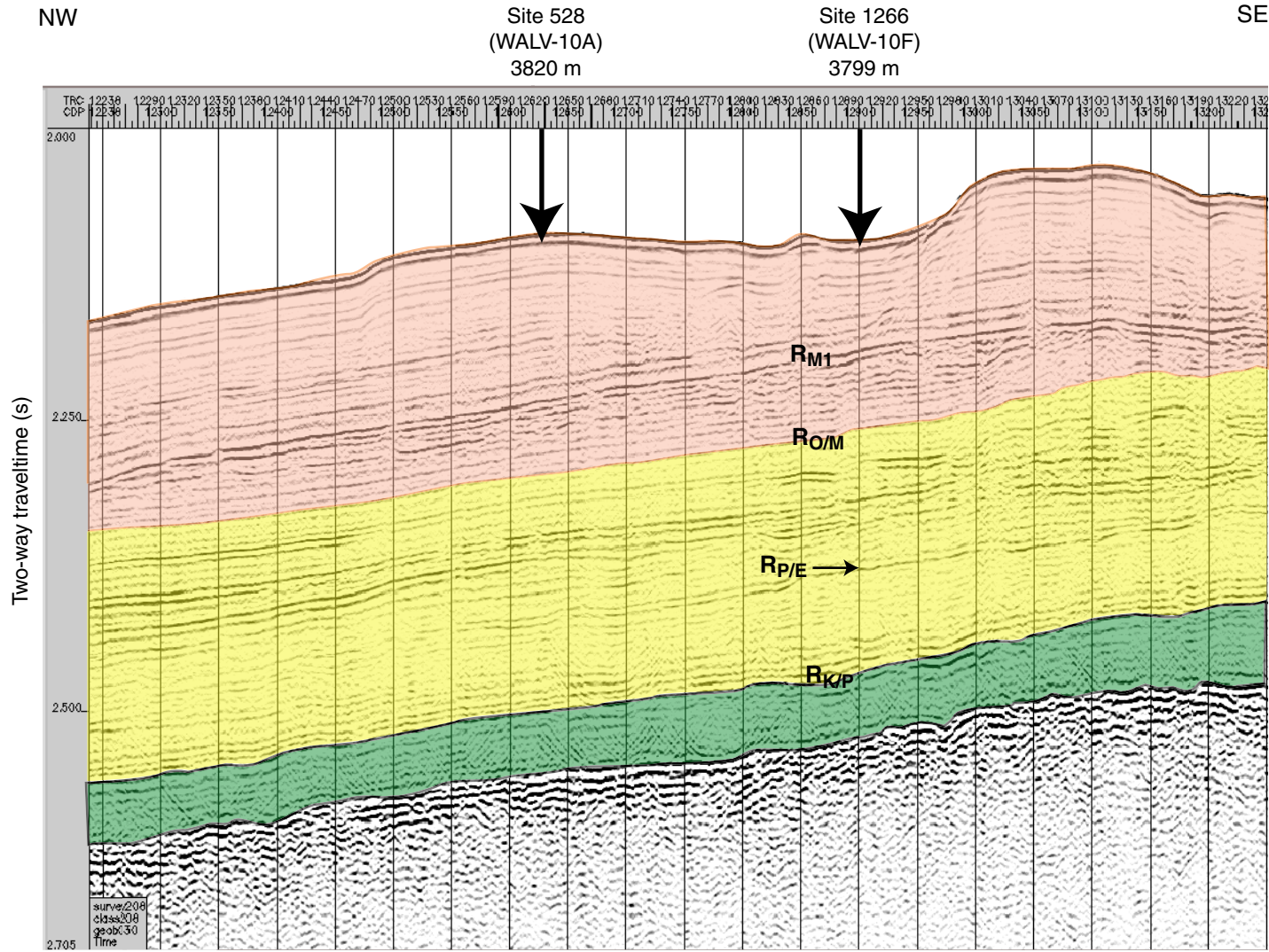
Figure F4. Magnetic susceptibility data from 0 to 380 mcd of Site 1266. Data from Holes 1266A, 1266B, and 1266C are offset from the spliced record by 10, 100, and 1000 times their values, respectively. Magnetic susceptibility values less than –1 instrument units were cut off at –1, and all values lower than 2 were multiplied by 0.5 and incremented by 1. Numbers near the tops of the individual core records refer to the core numbers.
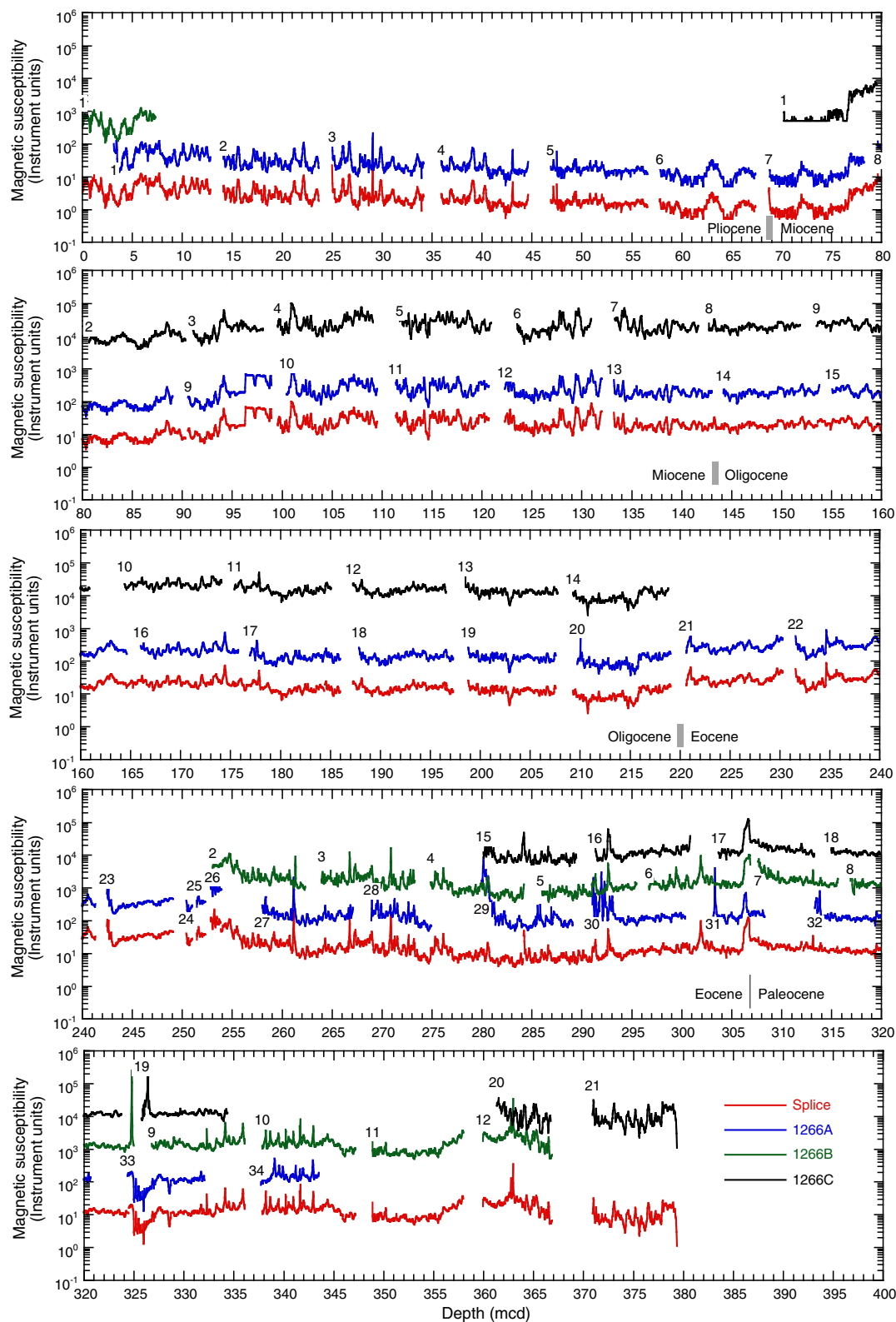
Figure F5. Mcd growth rates for Holes 1266A, 1266B, and 1266C.
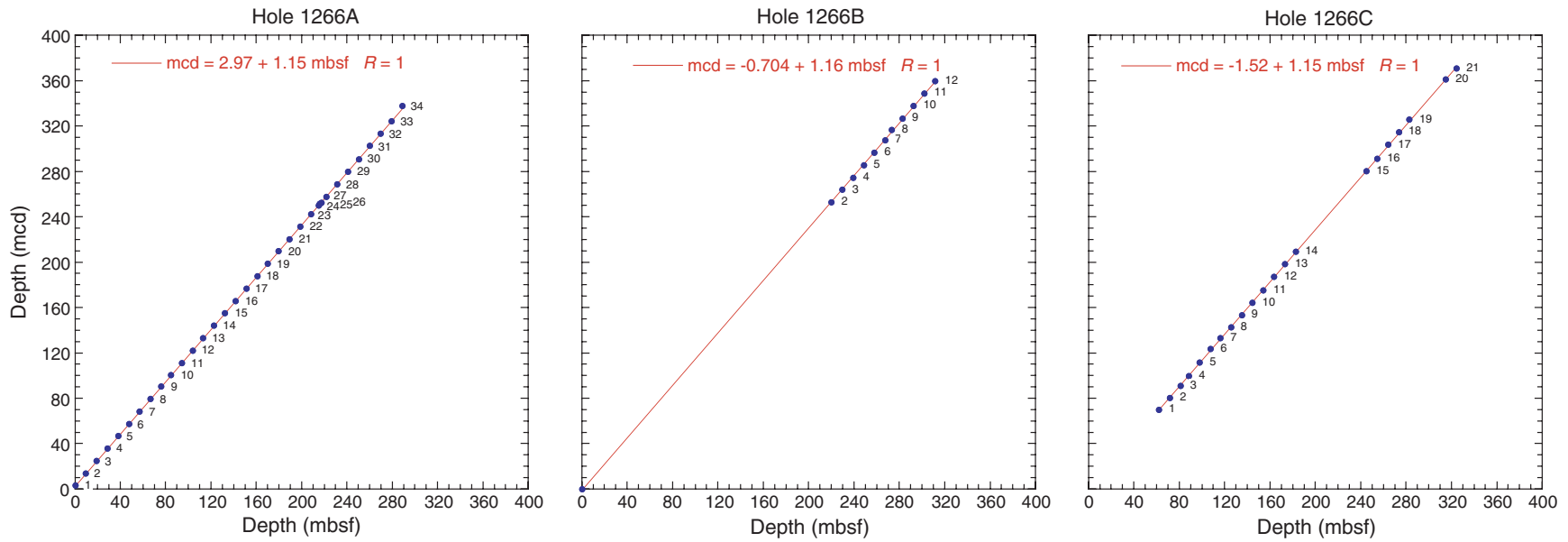
Figure F6. Site 1266 lithostratigraphic composite illustrating stratigraphic variation in parameters used to define lithostratigraphic units. The Unit I/II boundary was chosen at an abrupt step change in chromaticity value b*, lightness (L*), inflection in magnetic susceptibility (MS), and decrease in foraminiferal abundance. The Unit II/III boundary was chosen at a decrease in L* and increase in MS and natural gamma radiation (NGR). All data are smoothed with a 5-point moving average with the exception of NGR and smear slide components, which were smoothed with a 10-point and 3-point moving average, respectively.
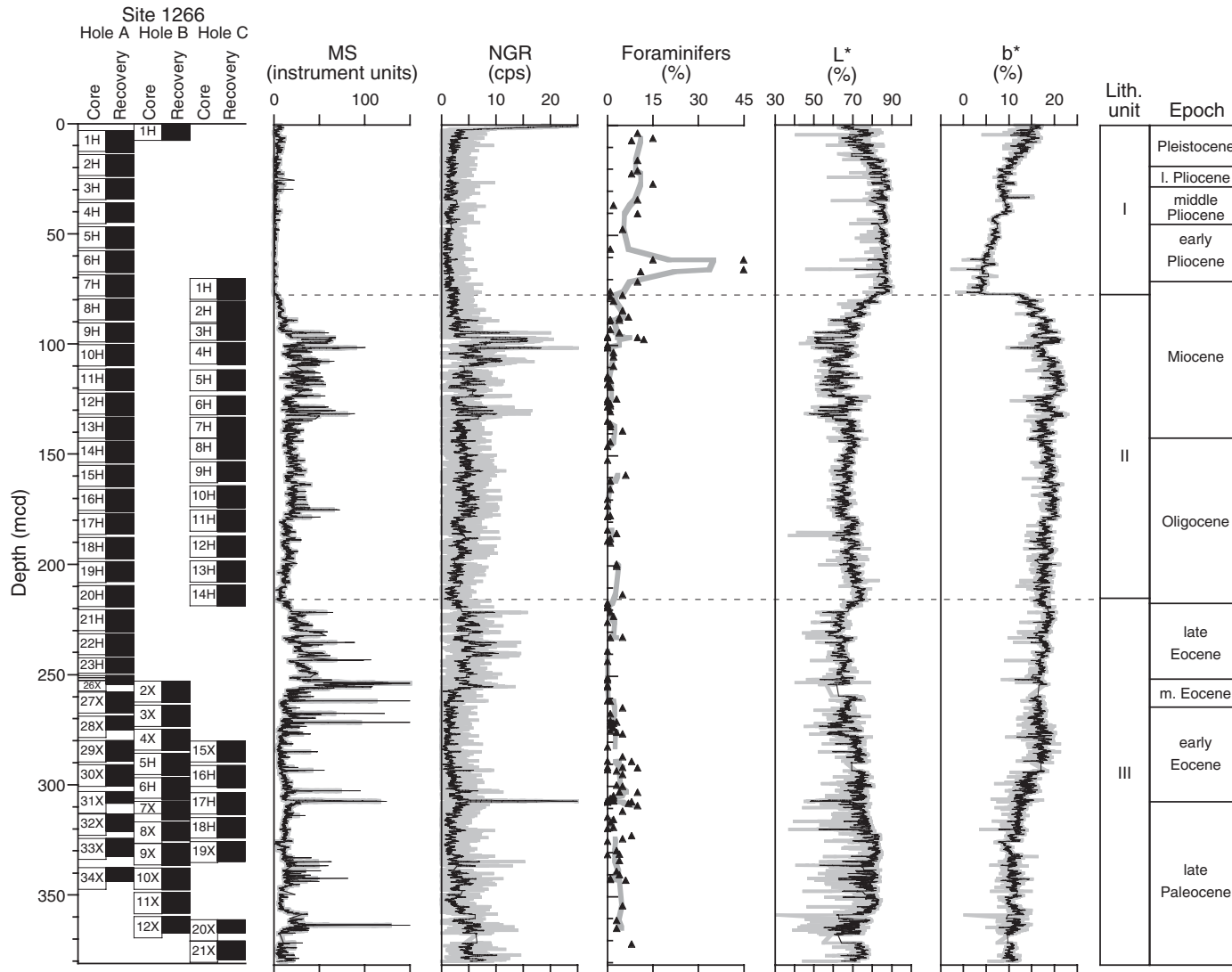
Figure F7. Site 1266 lithostratigraphic composite illustrating stratigraphic variation in whole-core multi-sensor track measurements of magnetic susceptibility (MS), natural gamma radiation (NGR), gamma ray attenuation (GRA) bulk density, and *P*-wave velocity sensor (PWS) measurements. NGR data are smoothed with a 10-point moving average; all other data are smoothed with a 5-point moving average.
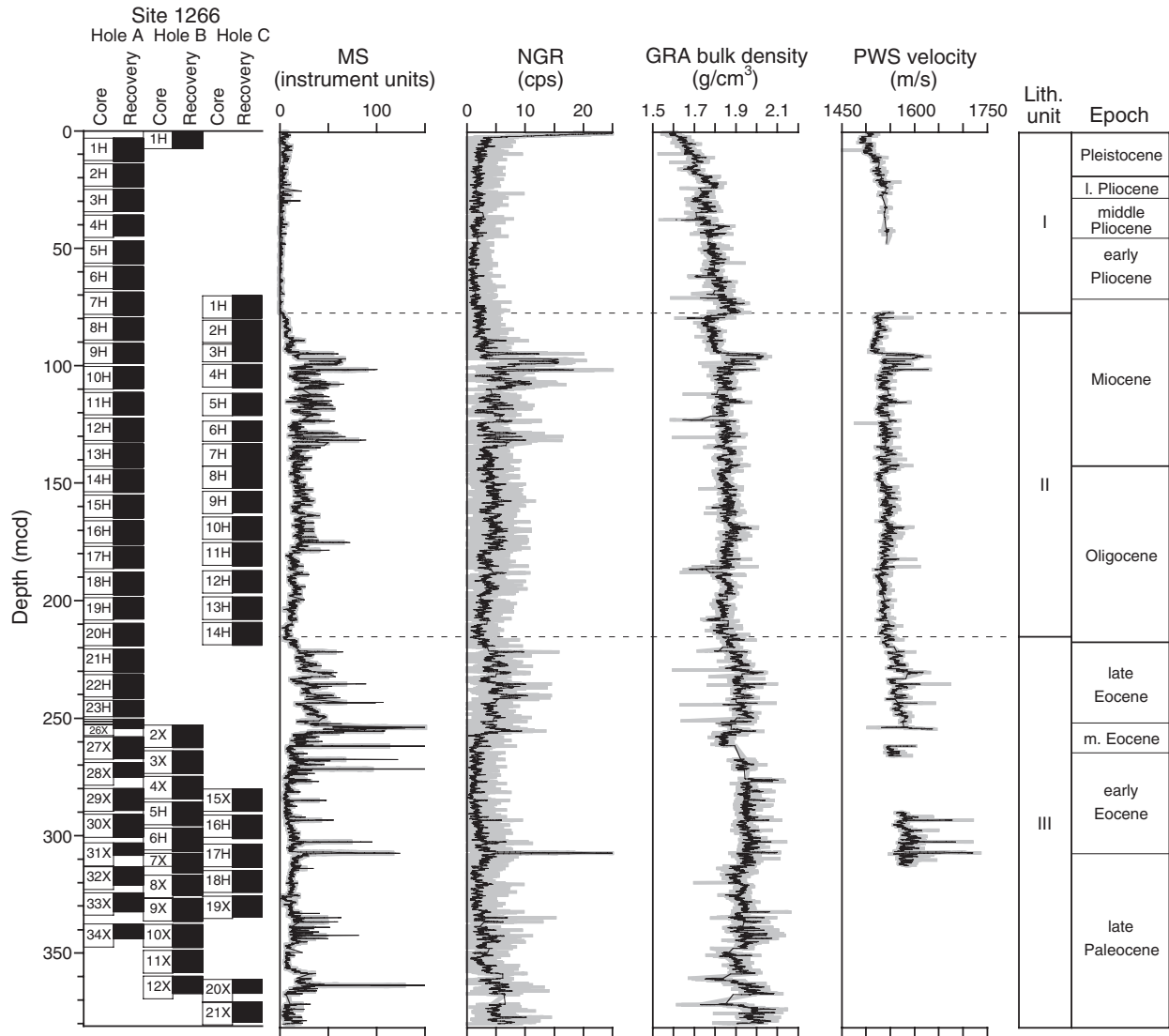
Figure F8. Site 1266 lithostratigraphic composite illustrating stratigraphic variation in lightness (L*), carbonate content, and chromaticity (a* and b*). All data except carbonate were smoothed with a 5-point moving average.

Figure F9. Site 1266 (single points) lithostratigraphic composite illustrating stratigraphic variation in predominant and accessory smear slide components, smoothed with a 3-point moving average (solid lines).
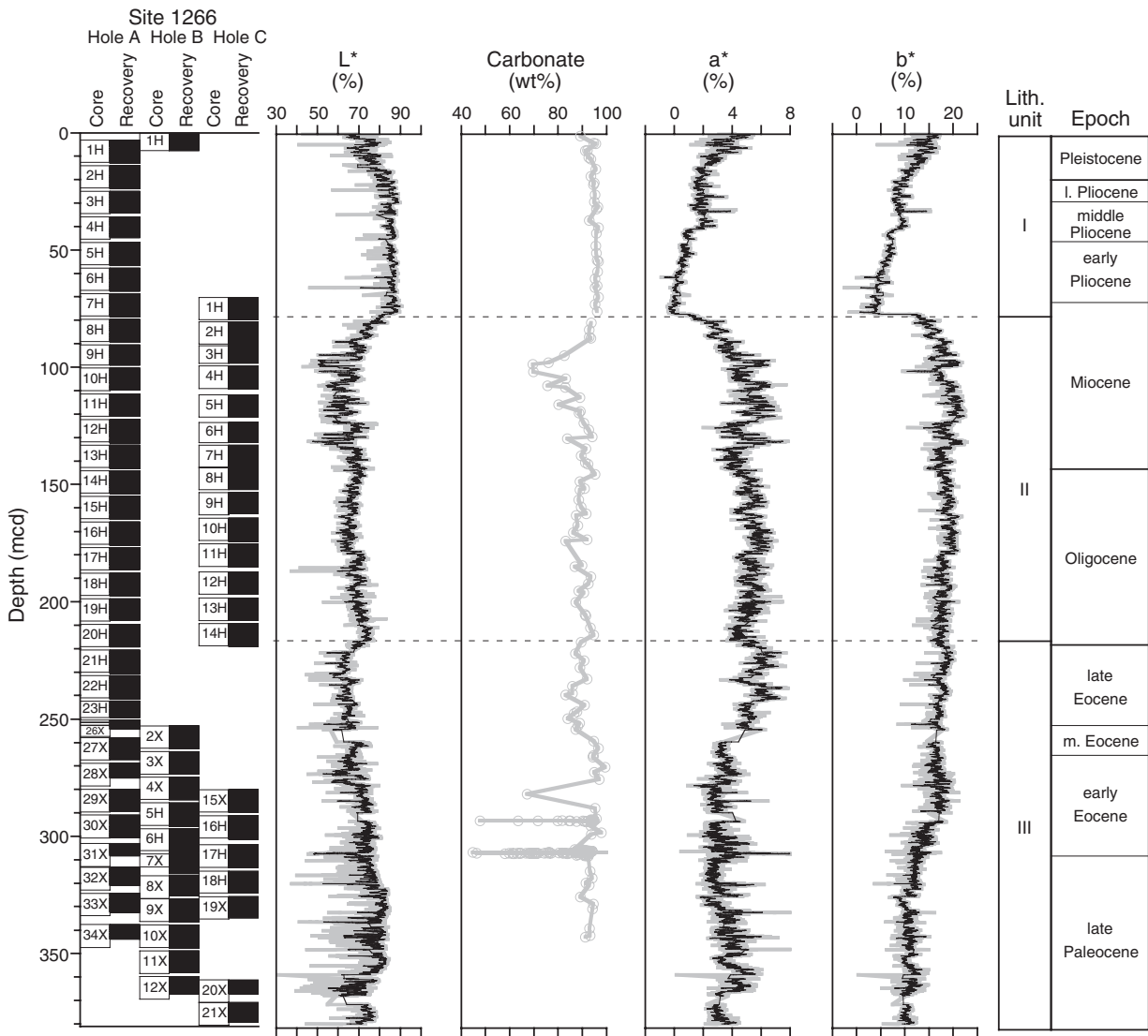
Figure F10. Site 1266 lithostratigraphic composite illustrating stratigraphic variation in physical properties of grain density (GD), bulk density (BD; MAD method), porosity, and *P*-wave velocity sensor (PWS3) measurements.
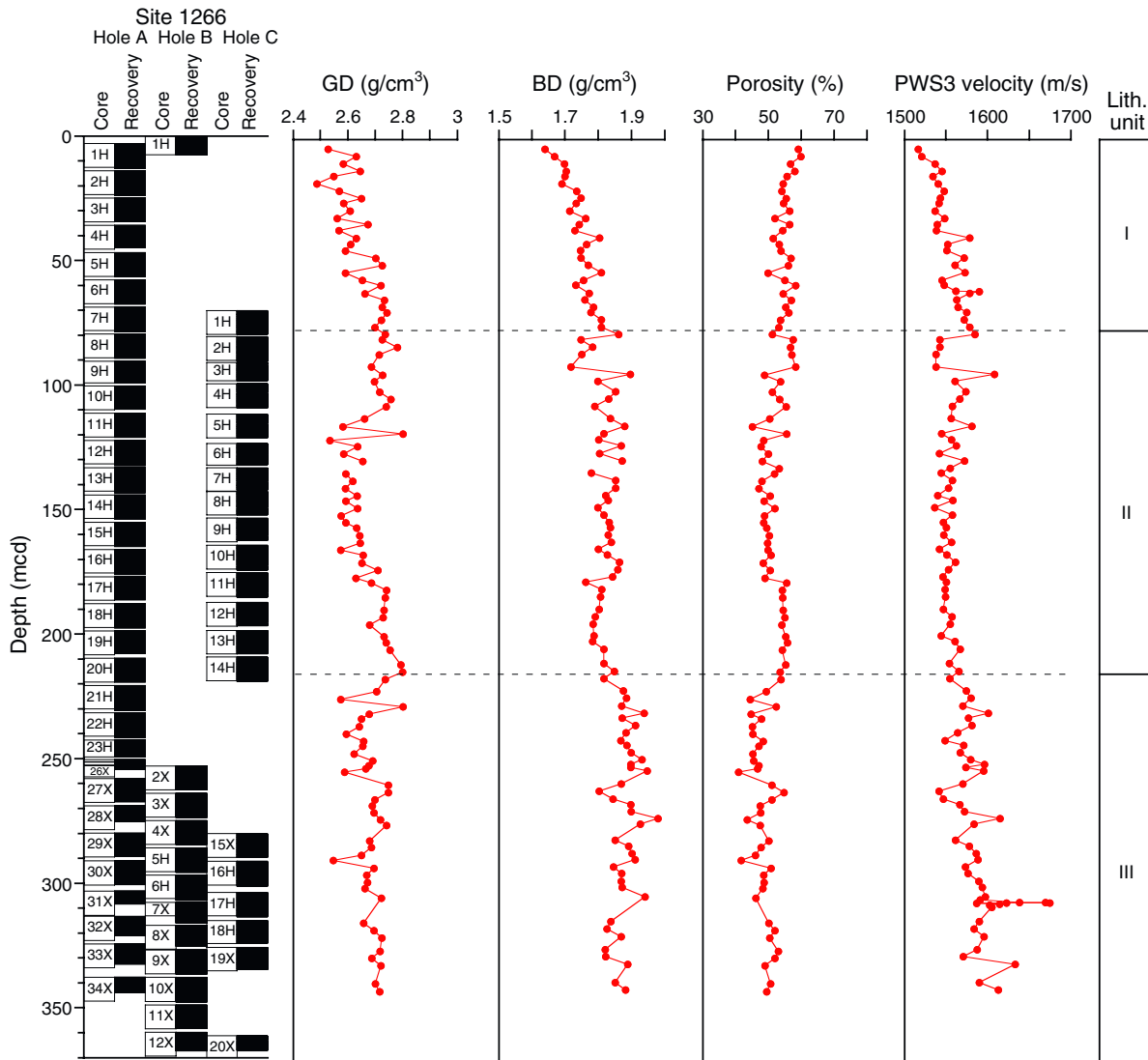
Figure F11. A, B. Comparison between bulk density measured by gamma ray attenuation (GRA) and moisture and density (MAD) methods. **C.** Correlation of grain density (GD) and bulk density (BD; MAD method). **D.** Correlation of porosity and BD (MAD method). **E.** Correlation of *P*-wave velocity sensor (PWS3) and BD (MAD method) measurements.
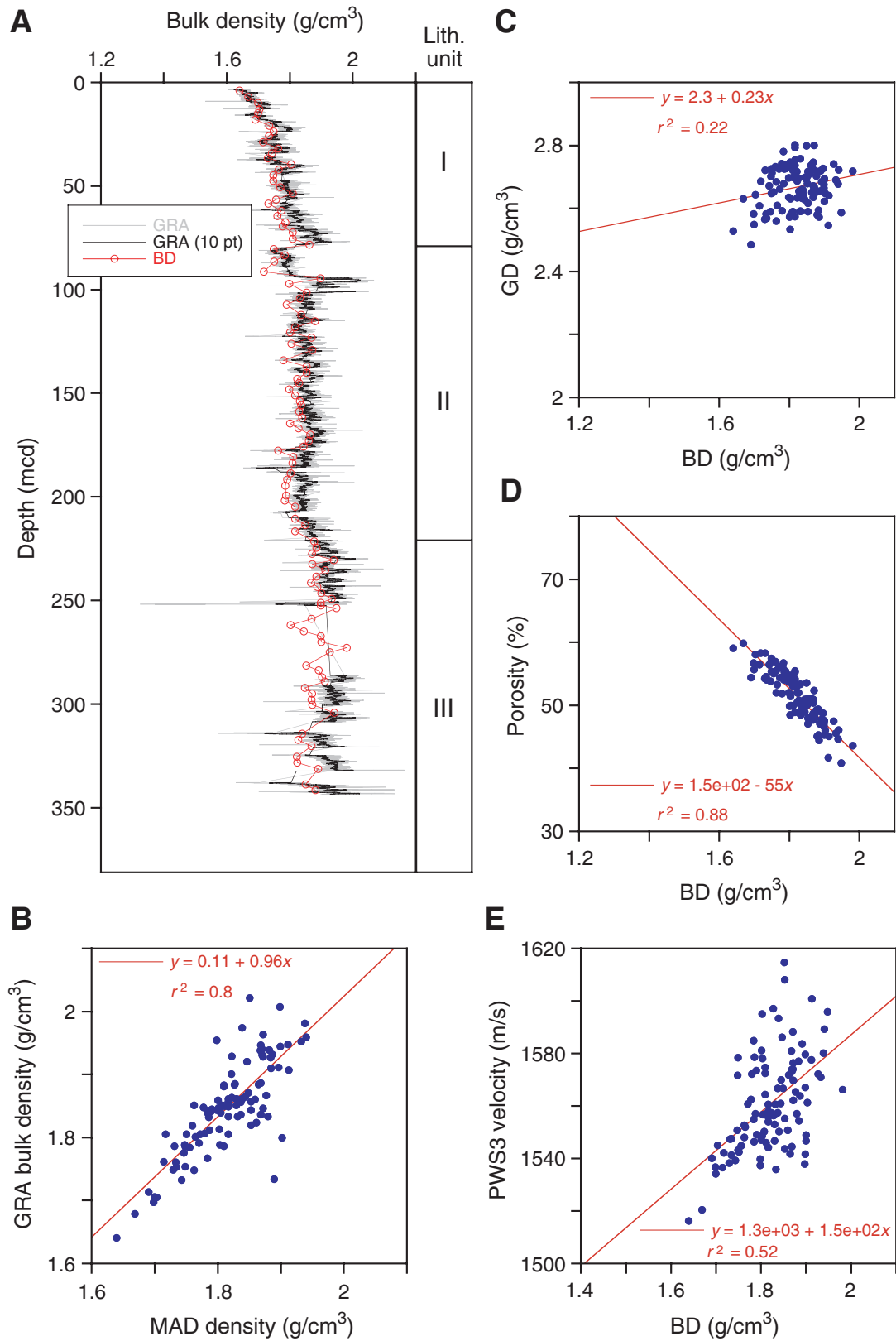
Figure F12. A. Comparison of *P*-wave logger velocities measured on the whole-core multisensor track *P*-wave logger (PWL) and the split-core *P*-wave sensor 3 transducer (PWS3). **B.** Scatterplot of PWL vs. PWS3 measurements. **C.** Close-up of *P*-wave velocities at the P/E boundary.
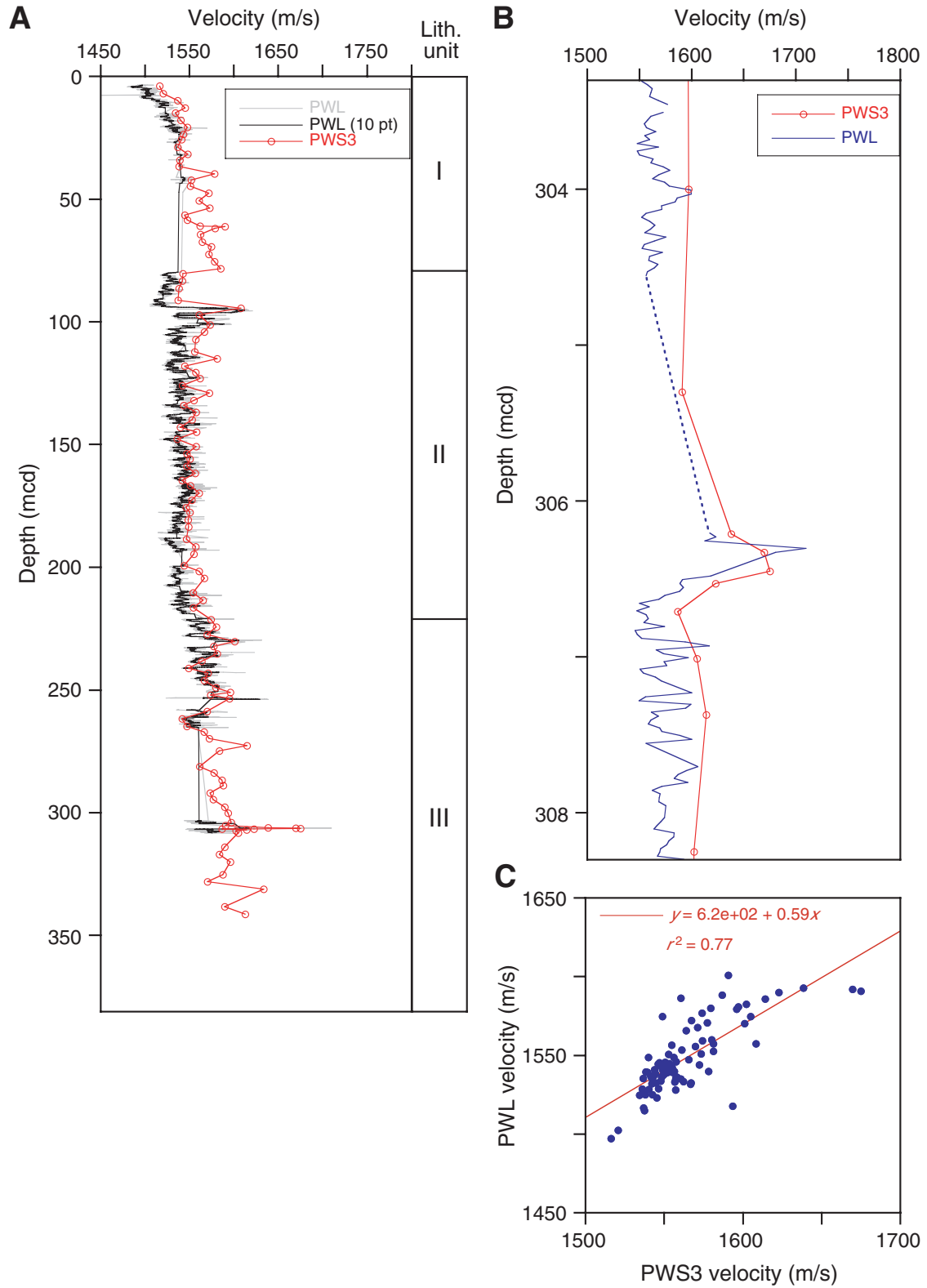
Figure F13. Site 1266 lithostratigraphic composite illustrating chromaticity (a*), manganese and iron concentrations in the interstitial waters, and grain density (GD) in lithostratigraphic units in Hole 1266A.
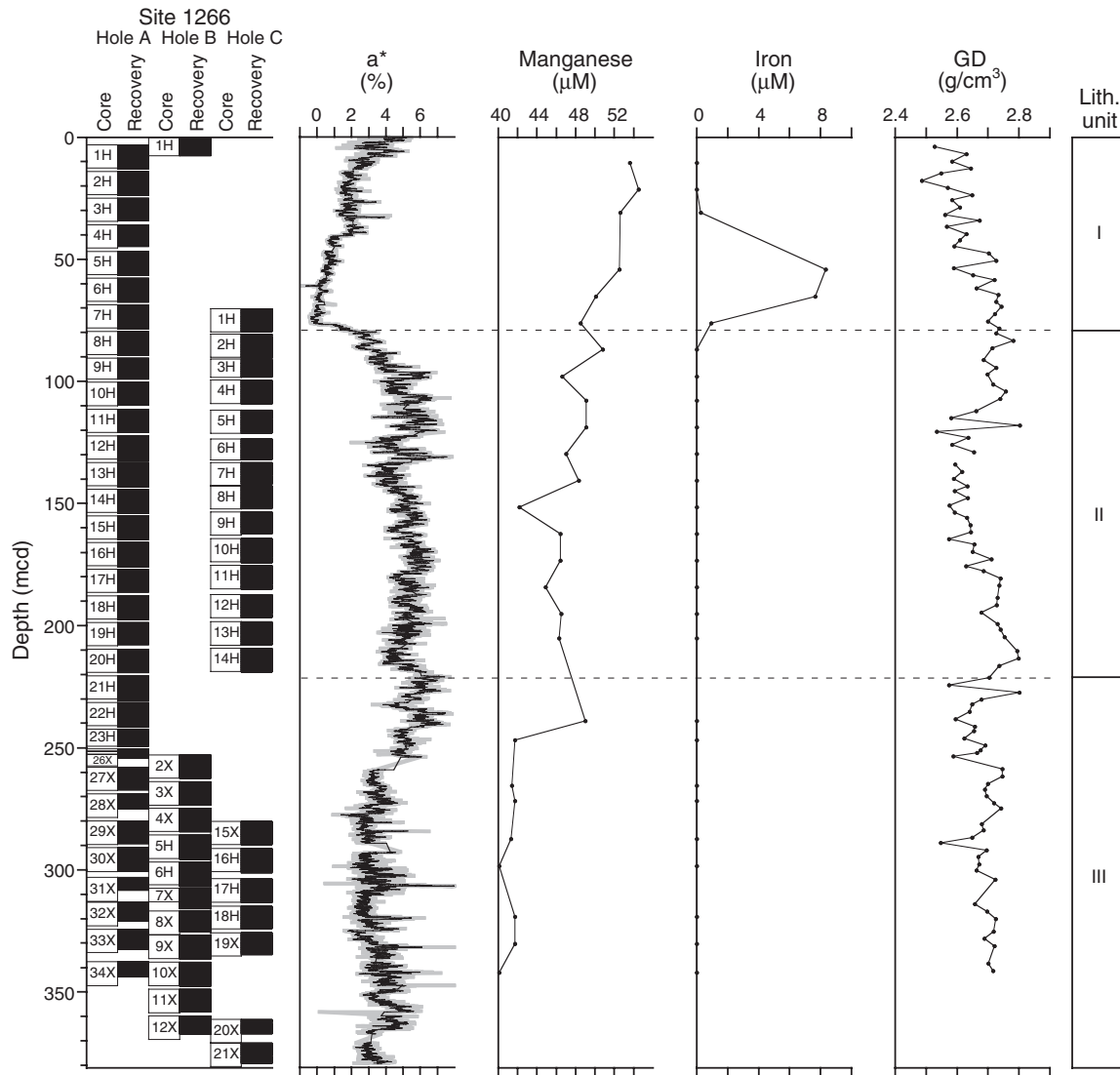
Figure F14. Digital image of a coarse-grained foraminiferal ooze turbidite horizon (interval 208-1266A-6H-3, 25–44 cm) showing a scoured basal boundary with minor oxides along this surface. The upper boundary of the turbidite layer is highly mineralized with black micronodules of Mn oxides concentrated along the interface of the coarse turbidite and fine enclosing sediments. Oxides also concentrate along depositional laminae, as in alternating thin bands above the turbidite horizon.
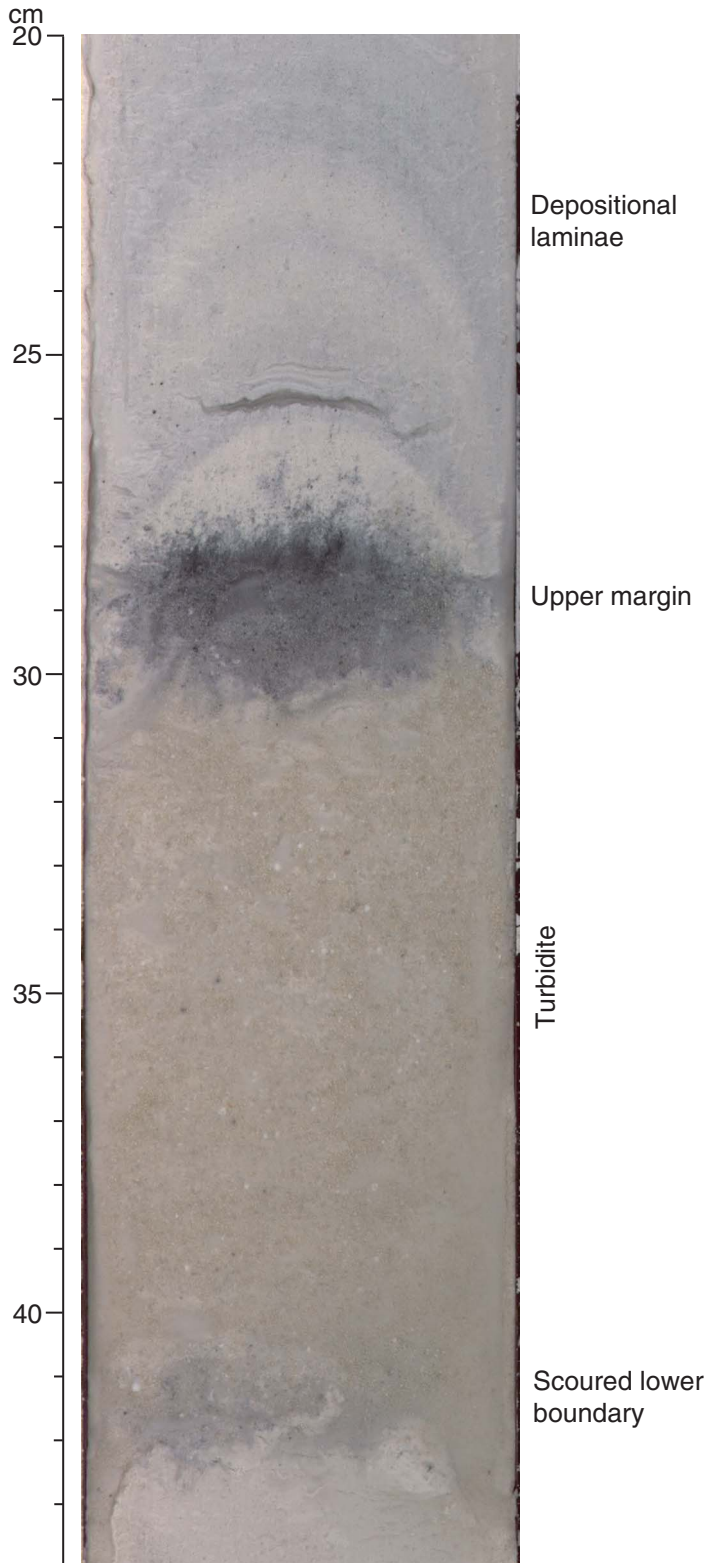
Figure F15. Chromaticity change at the Unit I/II boundary and corresponding digital image of Core 208-1266C-1H.
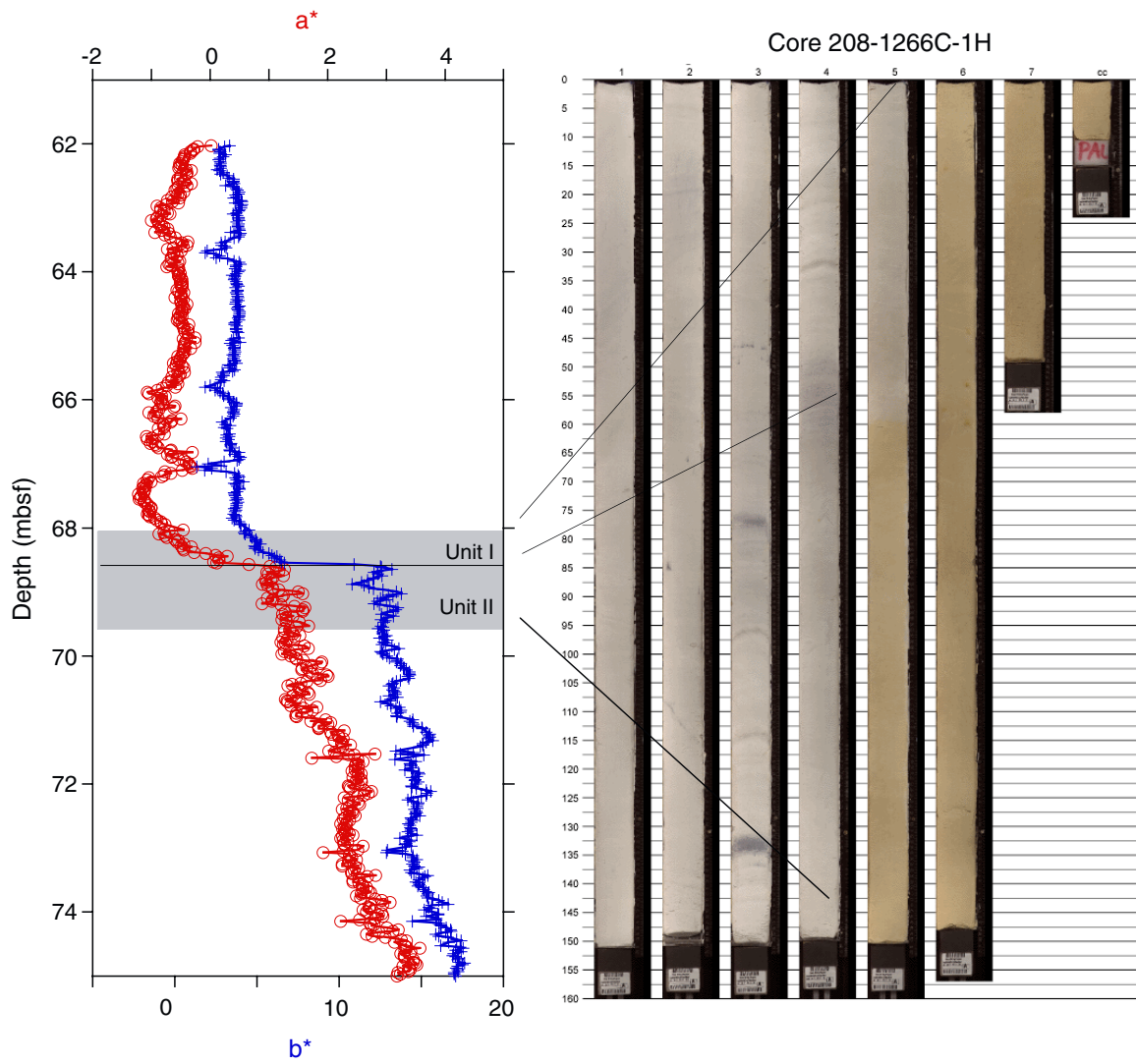
Figure F16. Composite digital image and cyclic patterns of sedimentation recorded in magnetic suscepti-
bility and sediment lightness (L*).
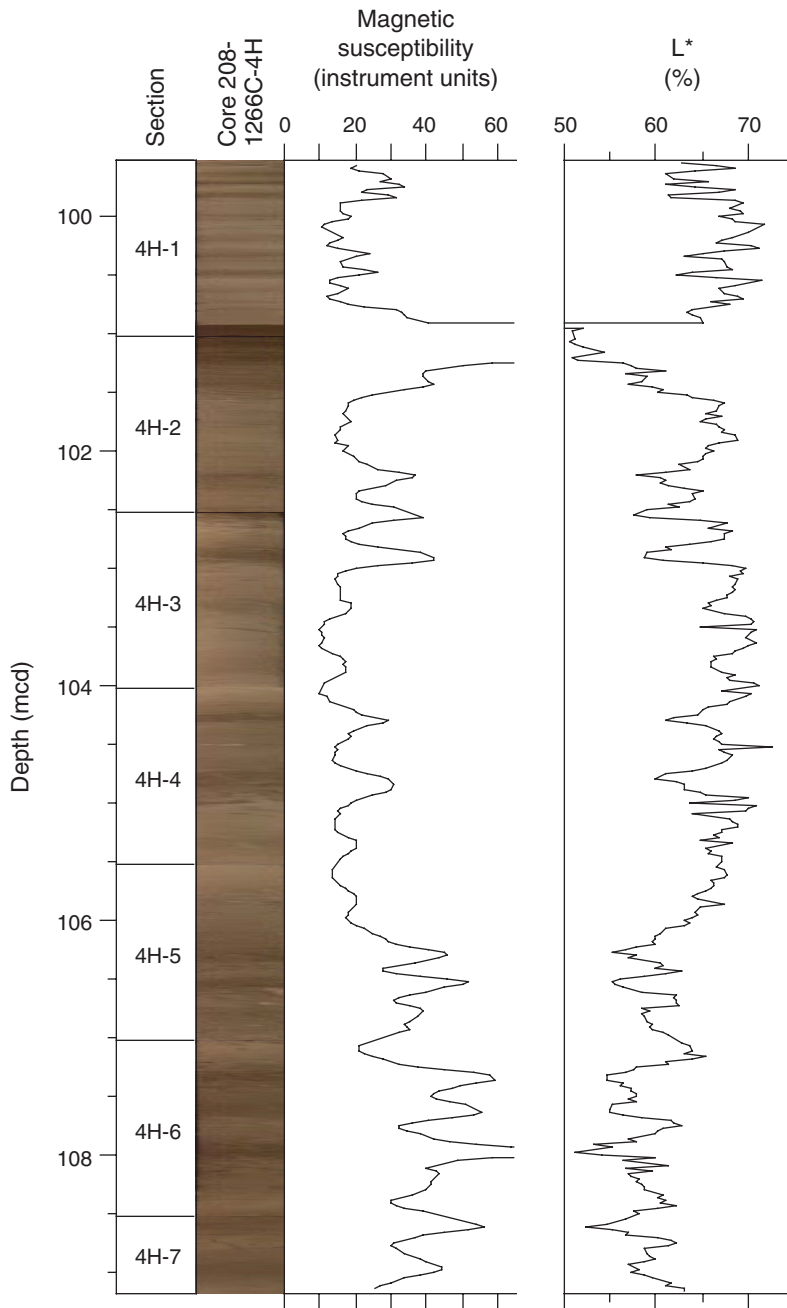
Figure F17. Digital images of (**A**) synsedimentary slump folding (interval 208-1266C-6H-2, 118–149 cm) and (**B**) inclined bedding (interval 208-1266A-10H-1, 95–140 cm), which suggests sedimentation on a depositional slope. Deposits formed in such a setting could result in mixing and duplication of the sequence through downslope creep or slides. The uppermost couplet of dark ash in A is overlain by white ooze and is in the correct orientation. Folding of this interval has overturned this sequence as an anticline with an axial plane that dips to the left, resulting in an inverted sequence. The lower ash-ooze couplet is again correctly oriented.

Figure F18. Composite digital images, carbonate content (blue), magnetic susceptibility (black), and red-green chromaticity (a*; red) for sections spanning the P/E boundary.
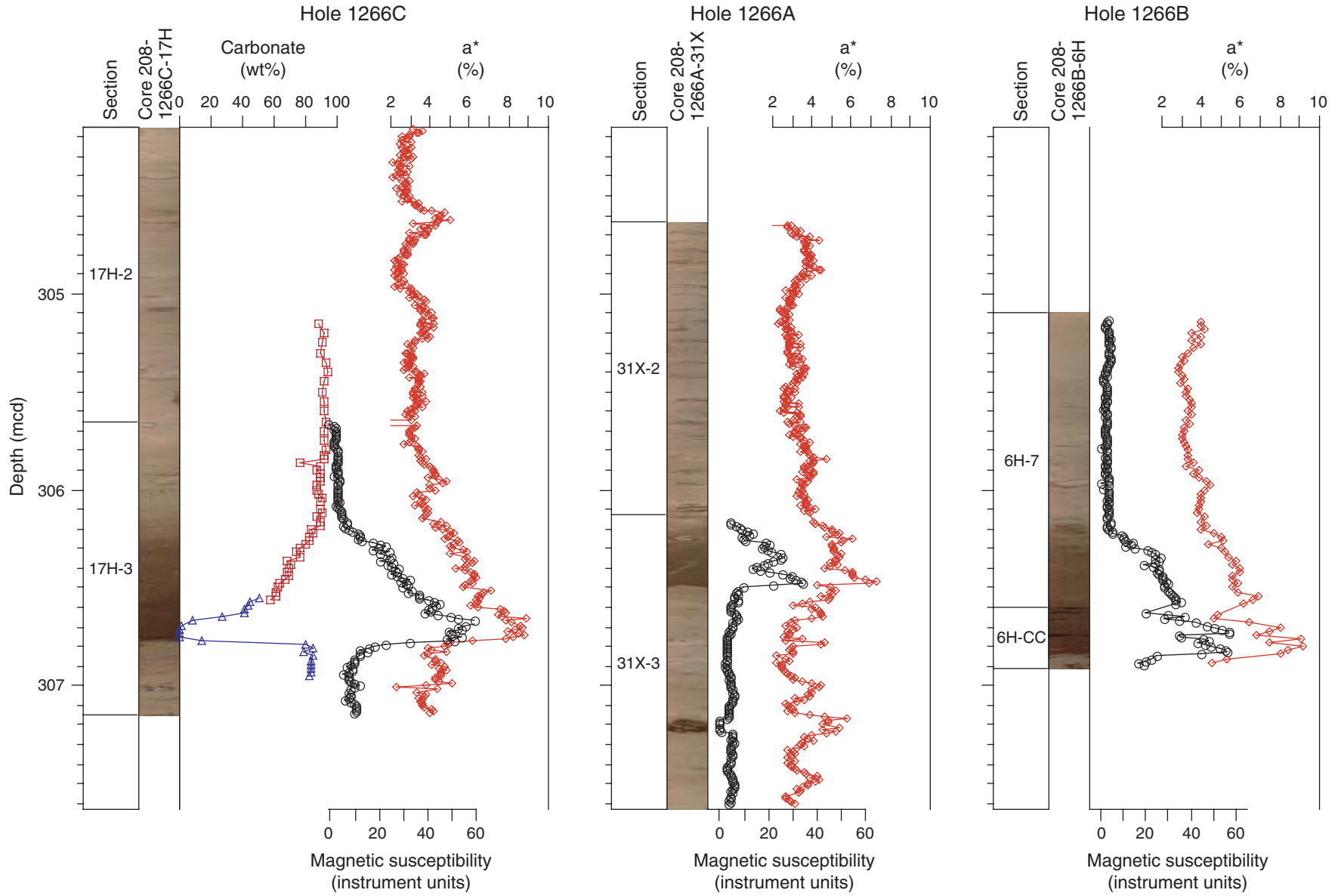
Figure F19. Composite digital images, carbonate content (blue), magnetic susceptibility (black), and red-green chromaticity (a*; red) for sections spanning the early Eocene (Chron C24n) red clay layer.
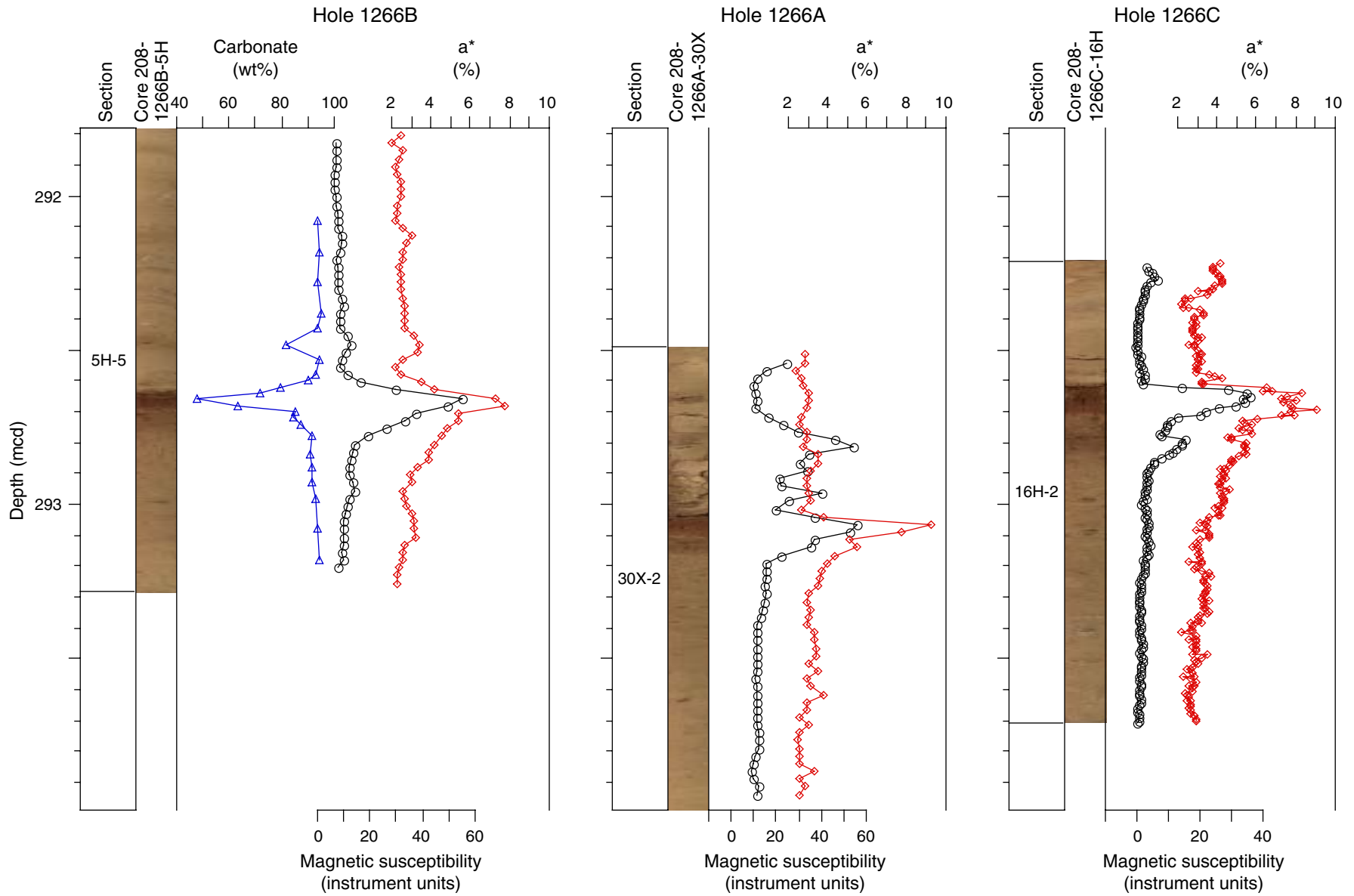
Figure F20. Summary of composite planktonic foraminiferal and calcareous nannofossil biozonation constructed for Site 1266. The paleobathymetric history of Site 1266 is inferred from benthic foraminifers shown on the right. Shading indicates an interval of reworking. Nanno = nannofossils. B = bottom. P/E = Paleocene/Eocene.
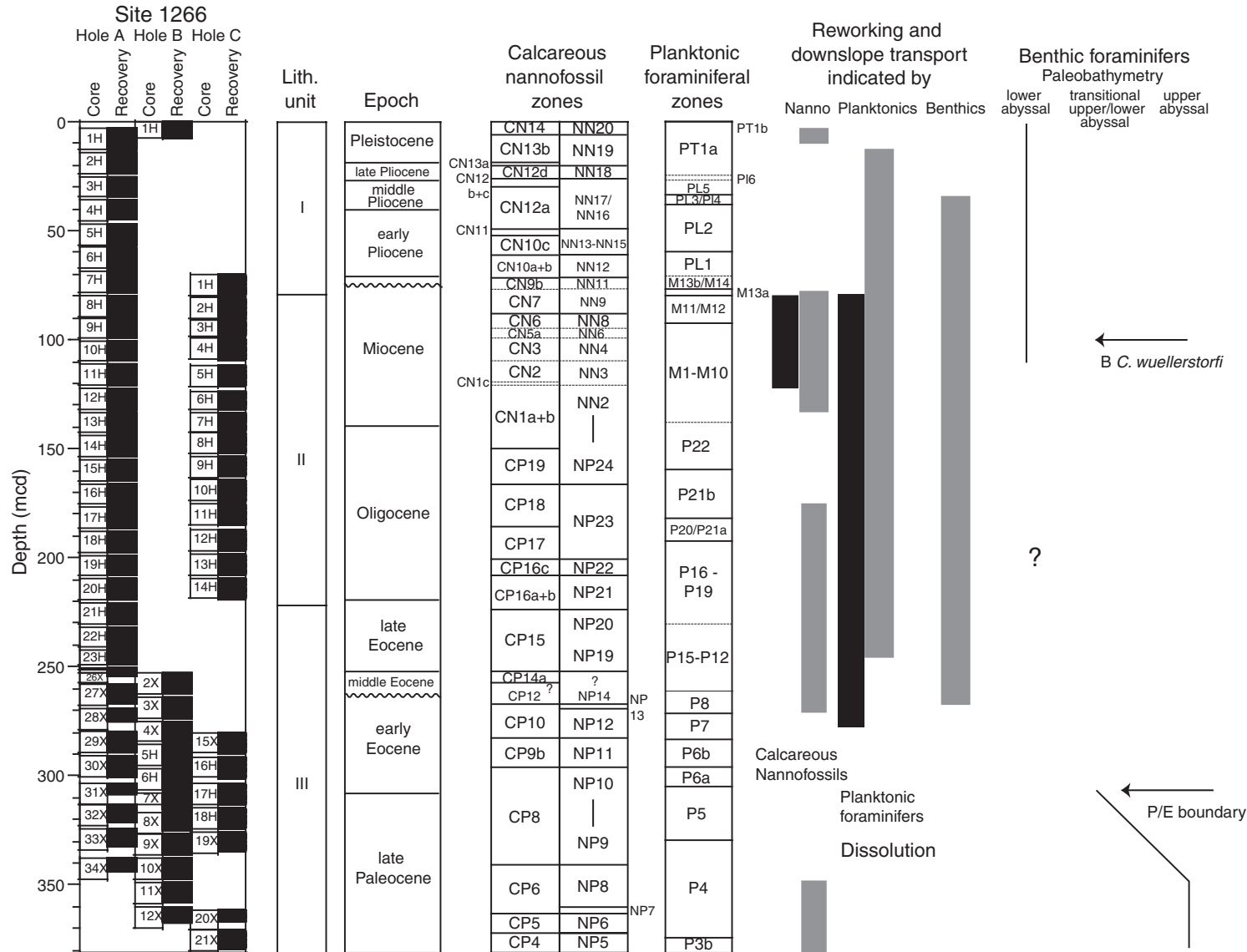
Figure F21. Summary of sedimentation rates at Site 1266 constructed using datum levels of calcareous nannofossils and planktonic and benthic foraminifers.
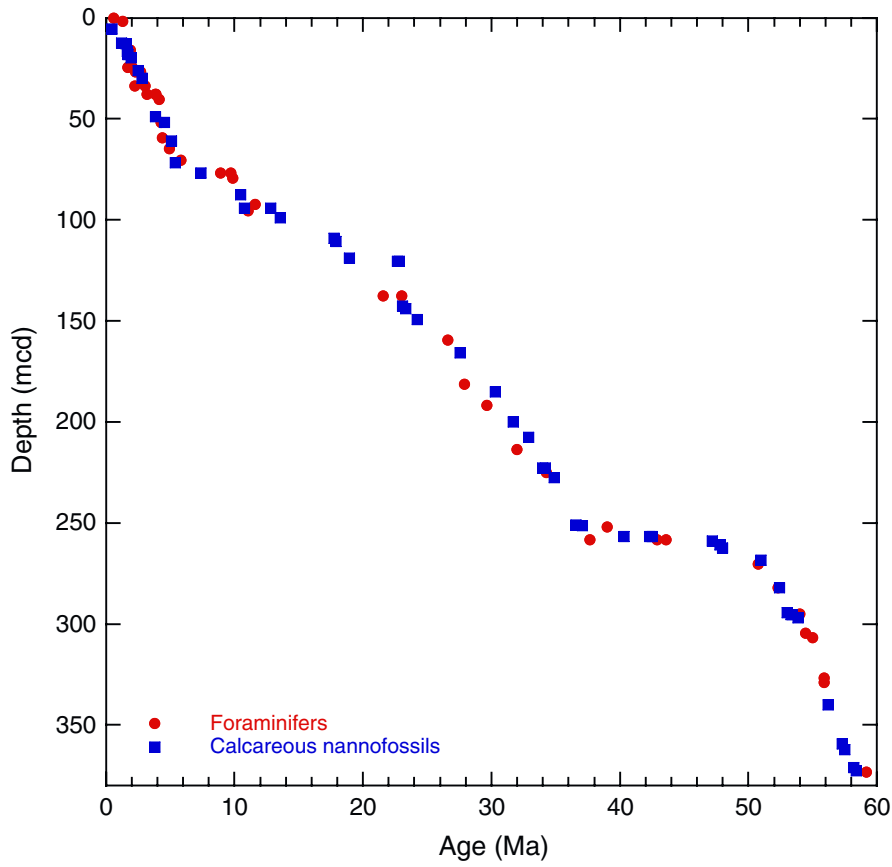
Figure F22. Inclination and intensity data from test sections before and after splitting. **A.** Section 208-1266C-2H-3. All data shown after maximum demagnetization to 10 mT. **B.** Section 208-1266C-18H-3 shown after maximum demagnetization to 15 mT. **C.** Section 208-1266C-10H-3 shown after maximum demagnetization to 15 mT.
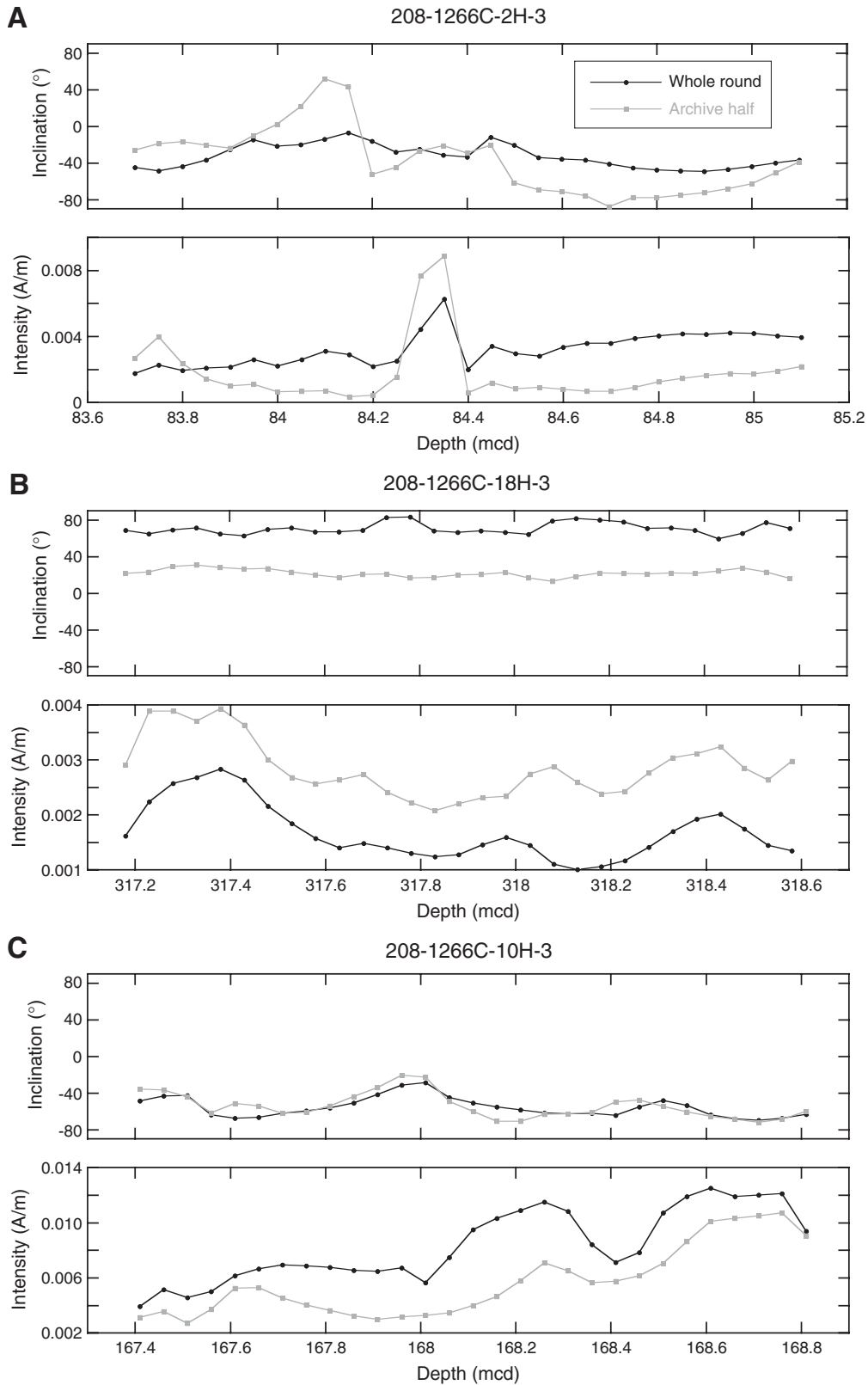
Figure F23. Downhole variation in intensities of remanent magnetization before (gray) and after (black) demagnetization to 15 mT in Holes 1266A, 1266B, and 1266C.
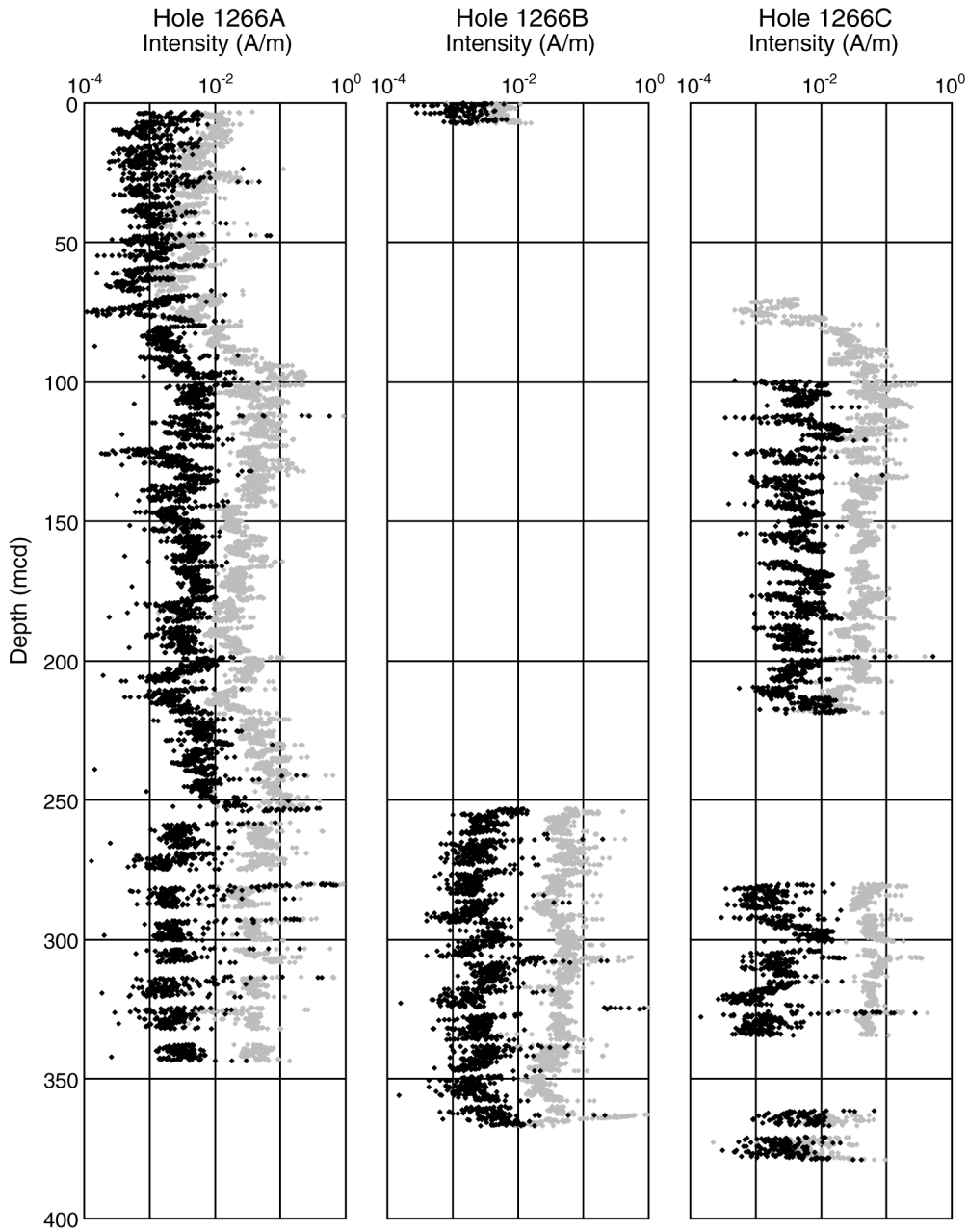
Figure F24. Downhole variation in initial magnetic susceptibility in Holes 1266A, 1266B, and 1266C.
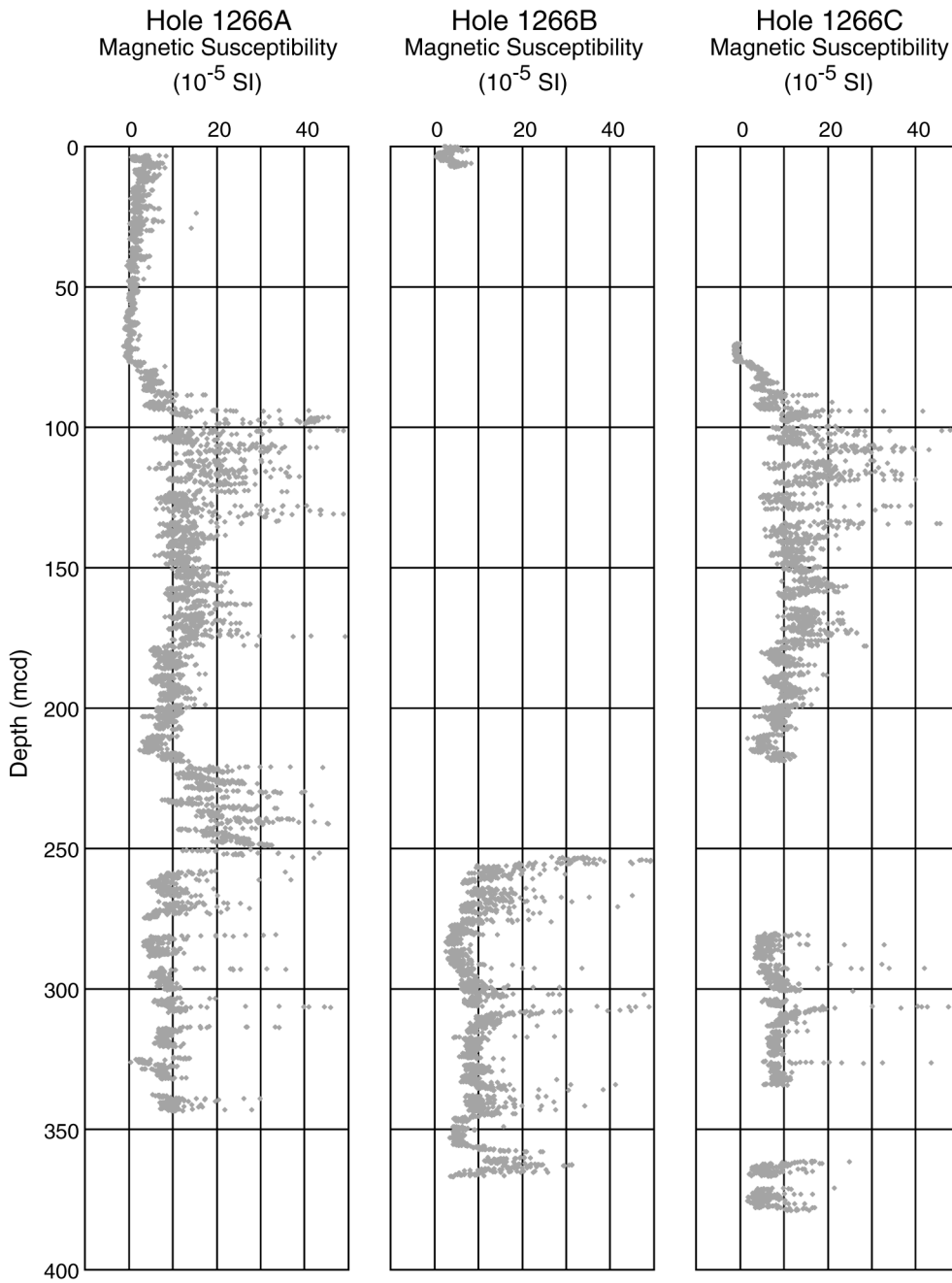
Figure F25. Downhole variation in depositional remanent magnetization after demagnetization to 15 mT and normalized by magnetic susceptibility (nDRM$_{15 mT}$) in Holes 1266A, 1266B, and 1266C.
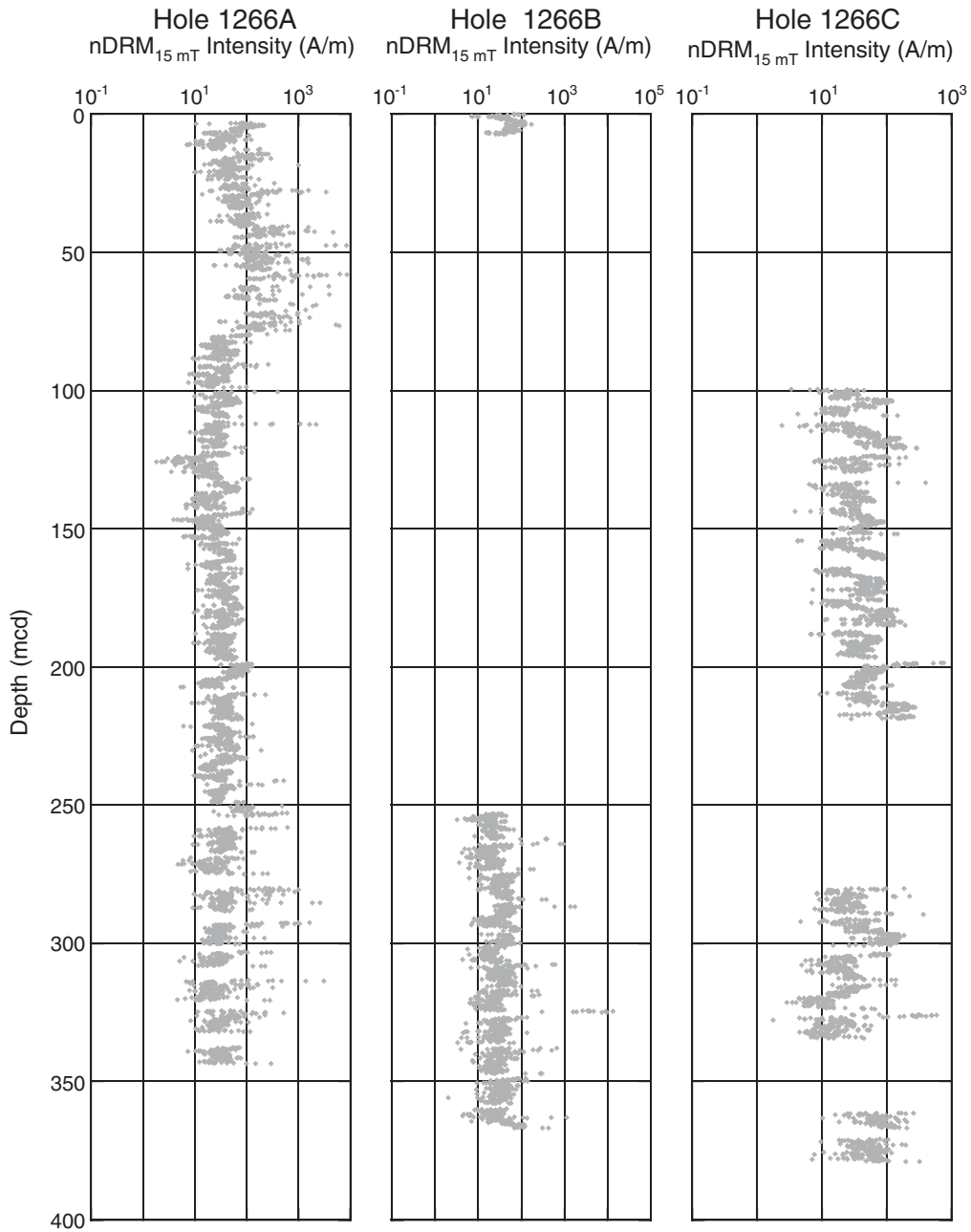
Figure F26. Preliminary magnetostratigraphic interpretation. Inclination data are shown for Holes 1266A, 1266B, and 1266C. Hole 1266A and 1266B data are from archive halves demagnetized to 15 mT. Hole 1266C data are from whole rounds. Cores 208-1266C-1H through 3H (data above 100 mcd) were demagnetized only to 10 mT. Cores from the remainder of the hole were demagnetized to 15 mT. Data within 50 cm of a core top and 5 cm of section ends are not shown. Core breaks are denoted by green squares. Black rectangle = normal polarity, white = reversed polarity, and shaded = uncertain polarity. X = intervals with no core recovery. **A.** 0–75 mcd. (Continued on next four pages.)
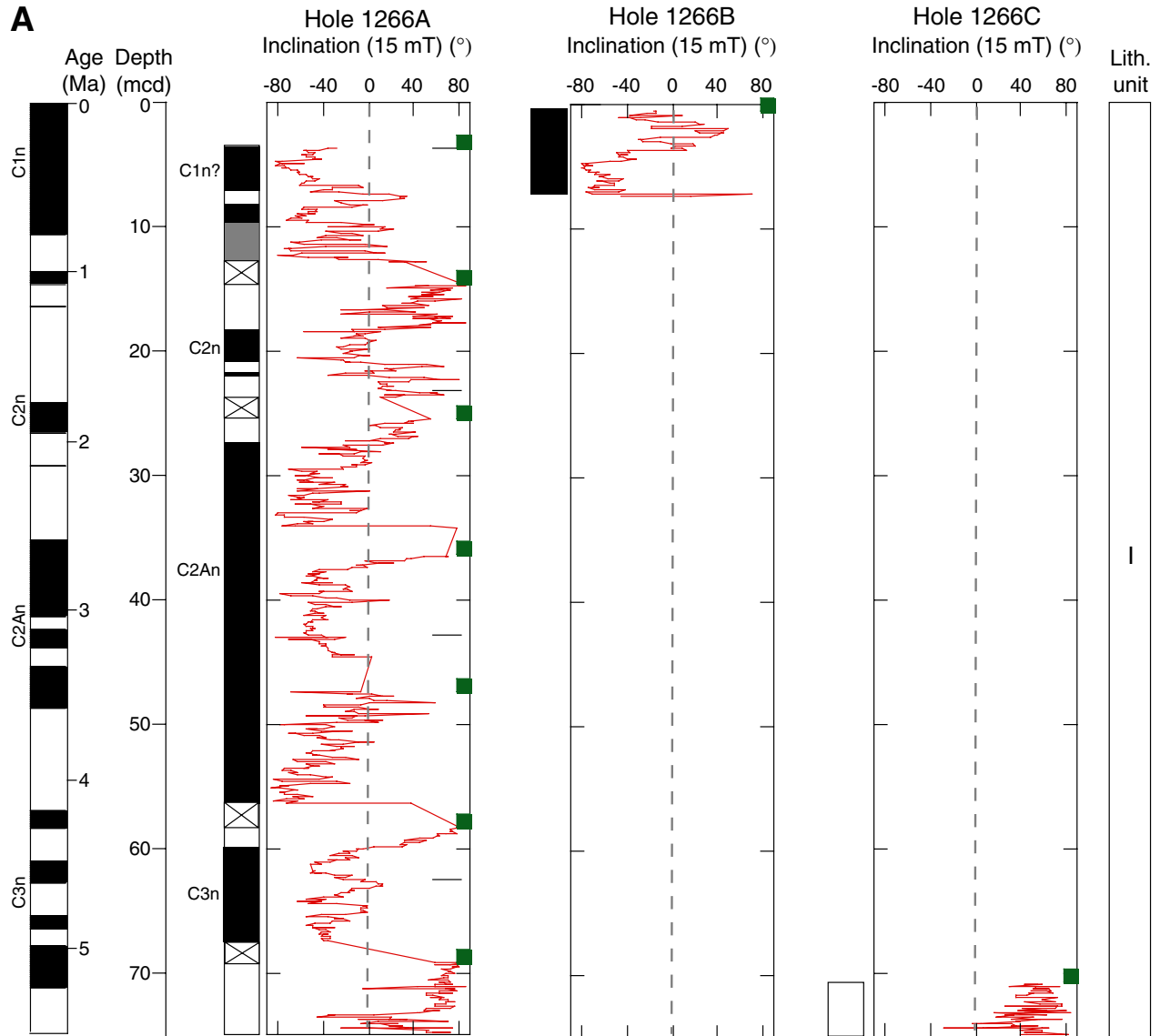
Figure F26 (continued). B. 65–150 mcd.
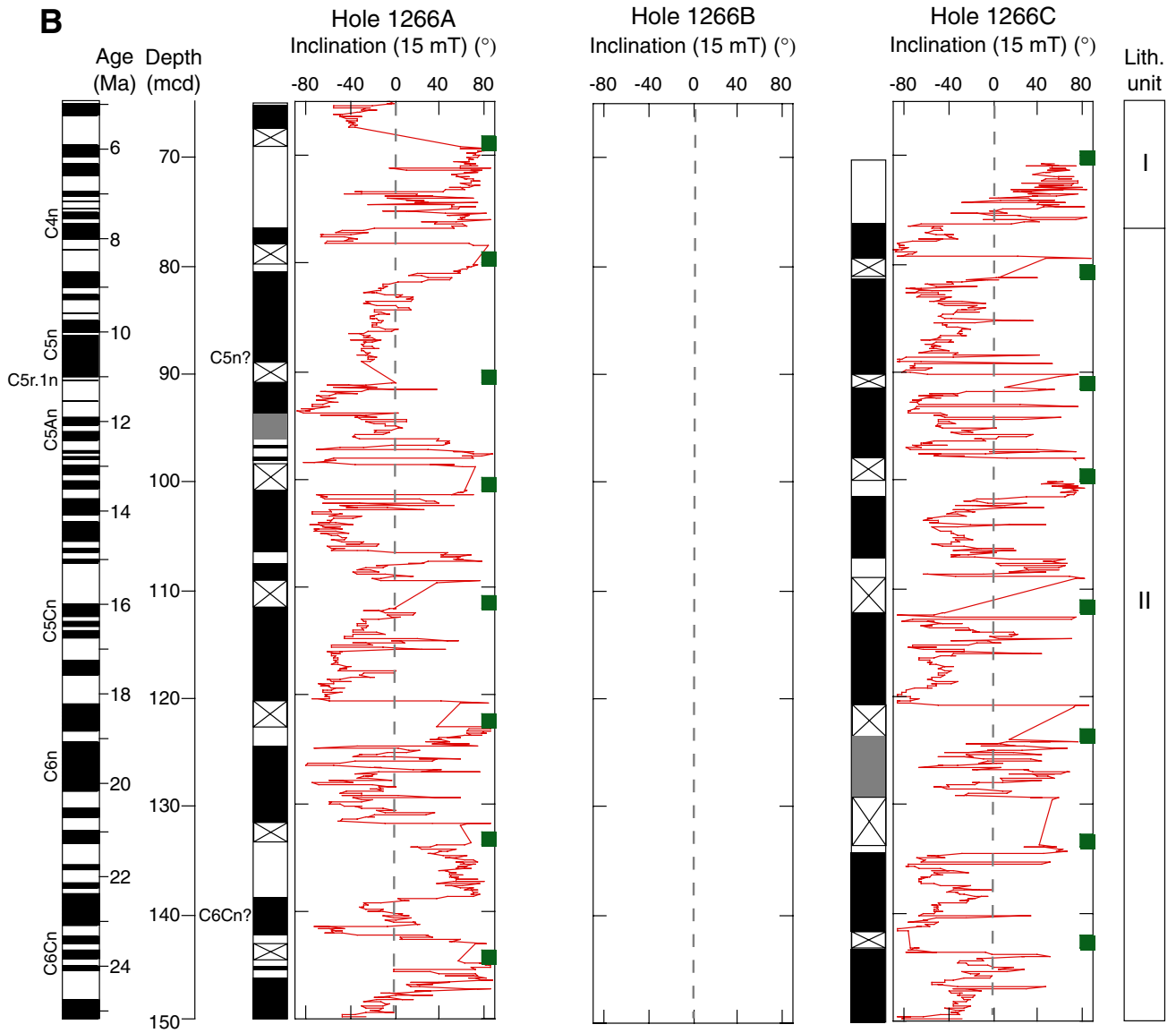
Figure F26 (continued). C. 140–225 mcd.
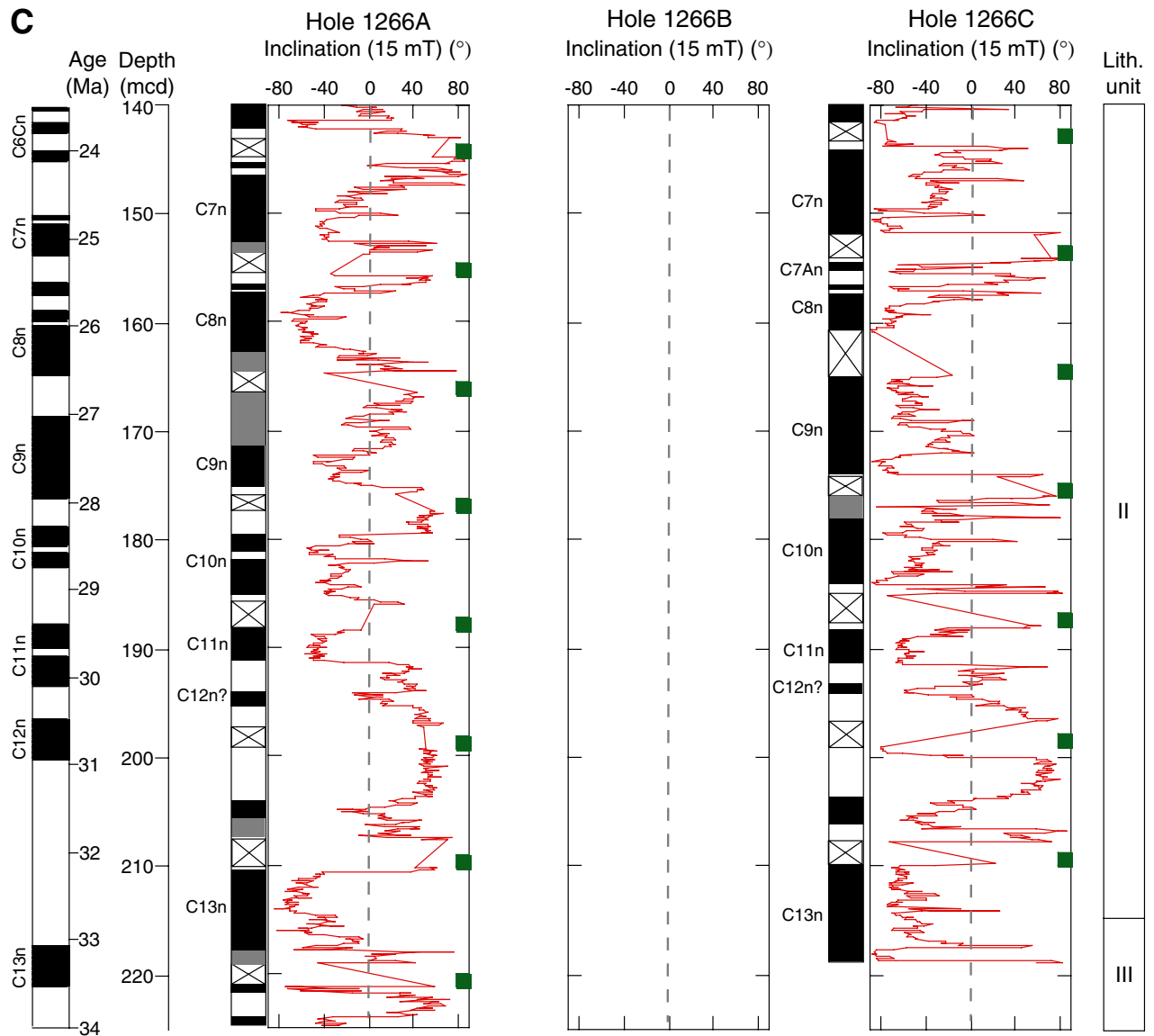
Figure F26 (continued). D. 215–300 mcd.
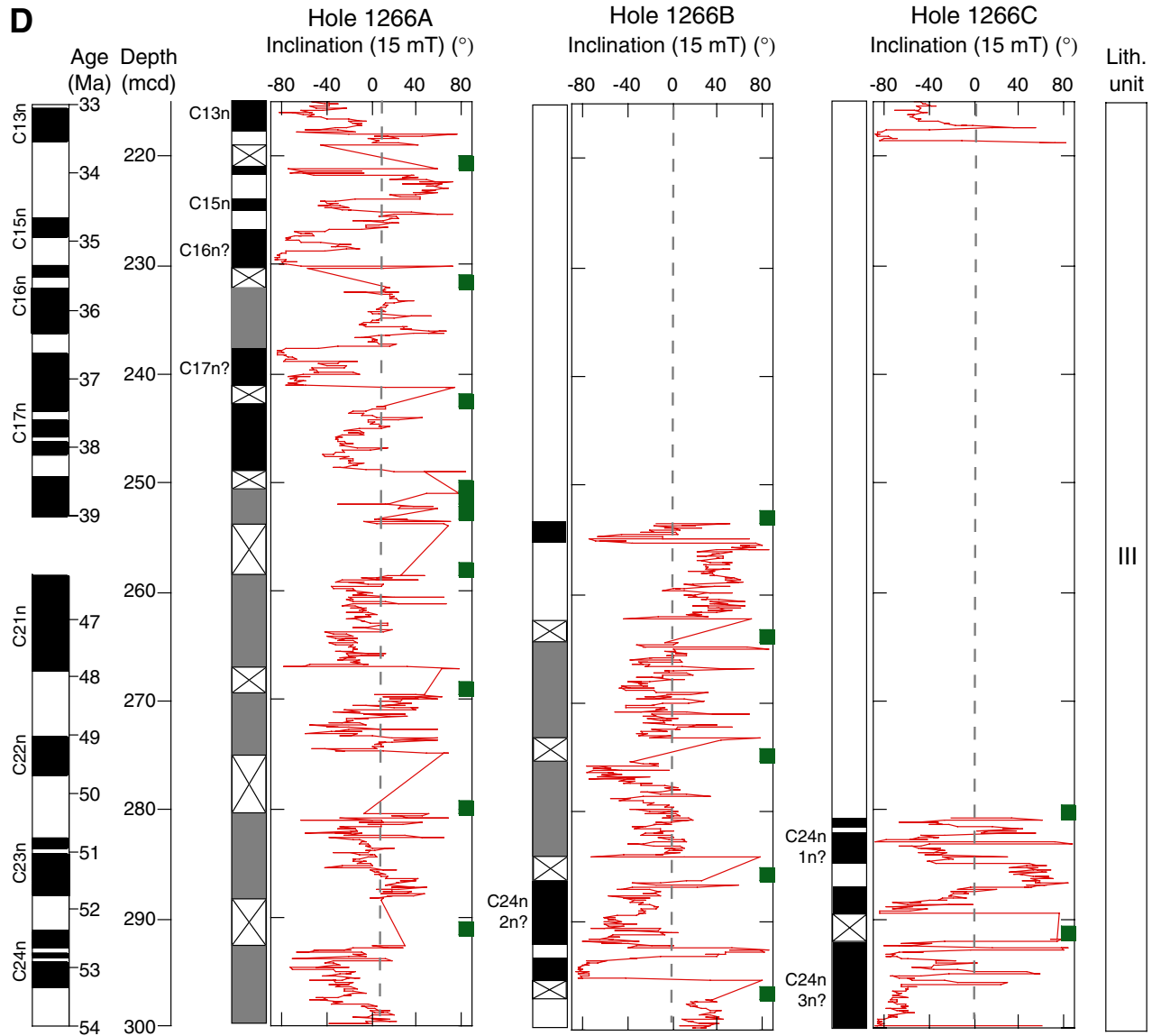
Figure F26 (continued). E. 290–380 mcd.
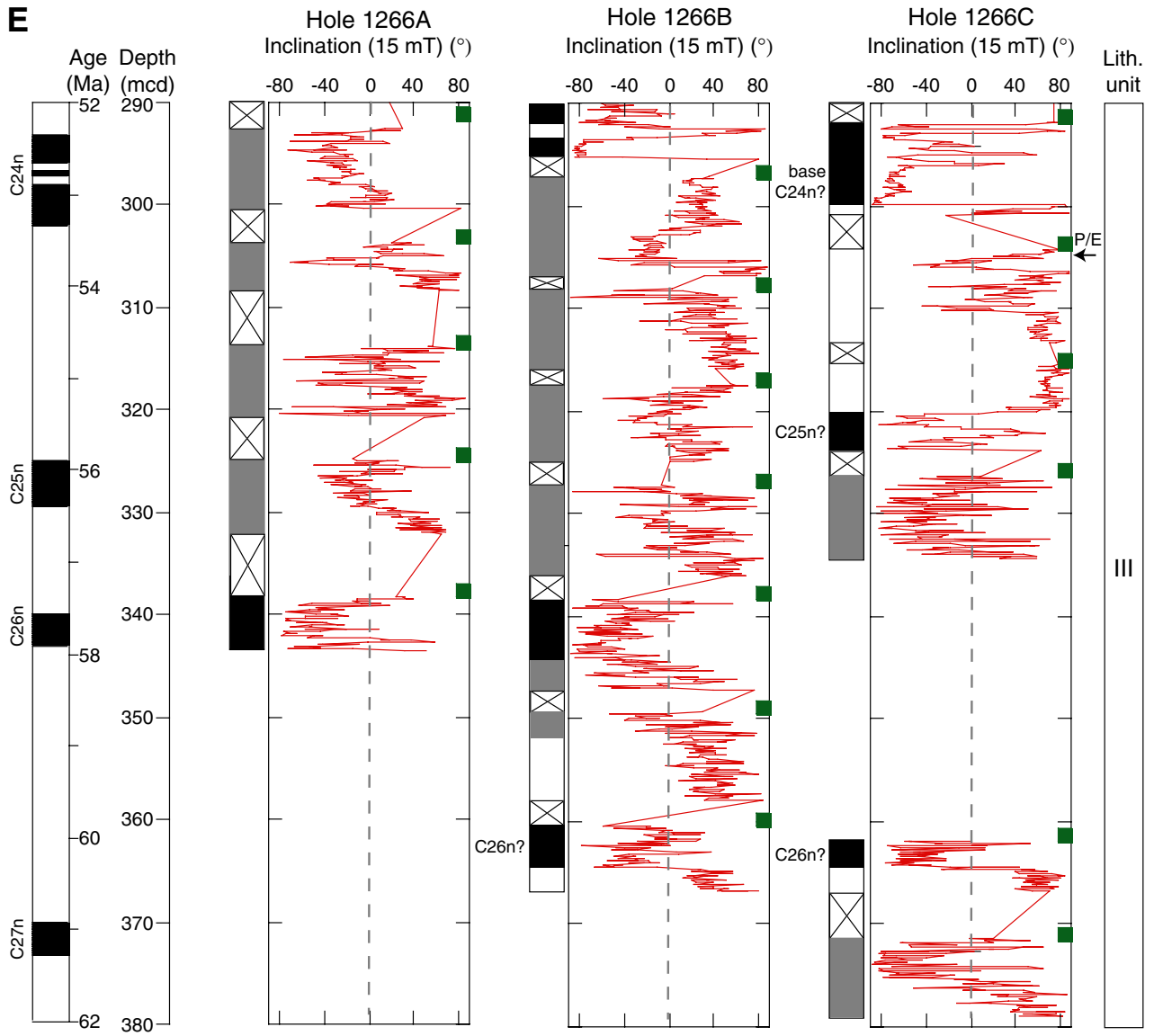
Figure F27. Profiles of chemical constituents in interstitial waters. **A.** Alkalinity. **B.** Chloride. **C.** Sodium. **D.** Potassium. **E.** Calcium. **F.** Magnesium. **G.** Strontium. **H.** Lithium. **I.** Boron. **J.** Barium. **K.** Sulfate. **L.** Manganese. **M.** Iron. **N.** Silicon.
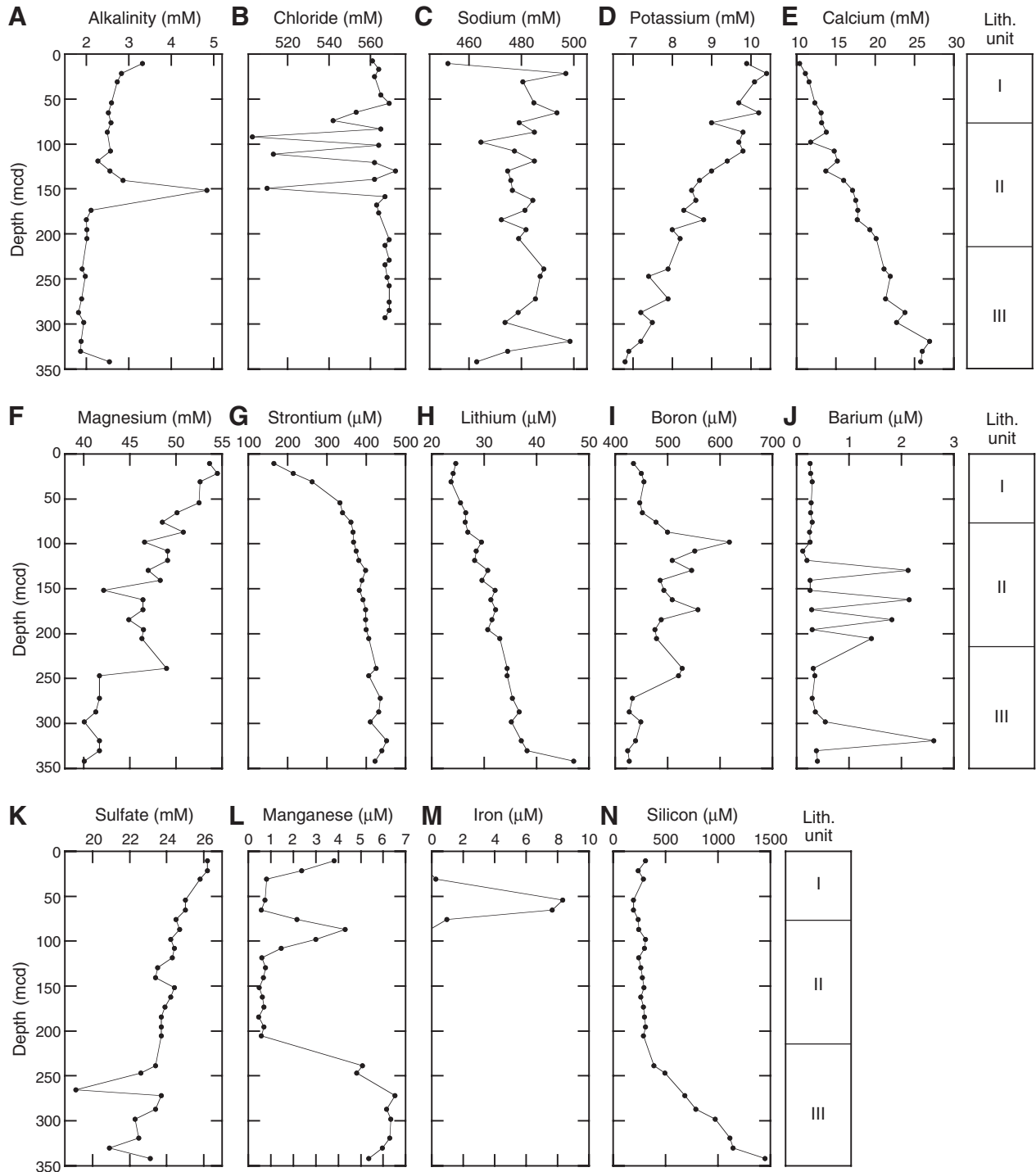
Figure F28. Sedimentary carbonate contents vs. composite depth for (**A**) the entire Site 1266 section, (**B**) the P/E boundary section at high resolution, and (**C**) the Chron C24n clay-rich horizon.
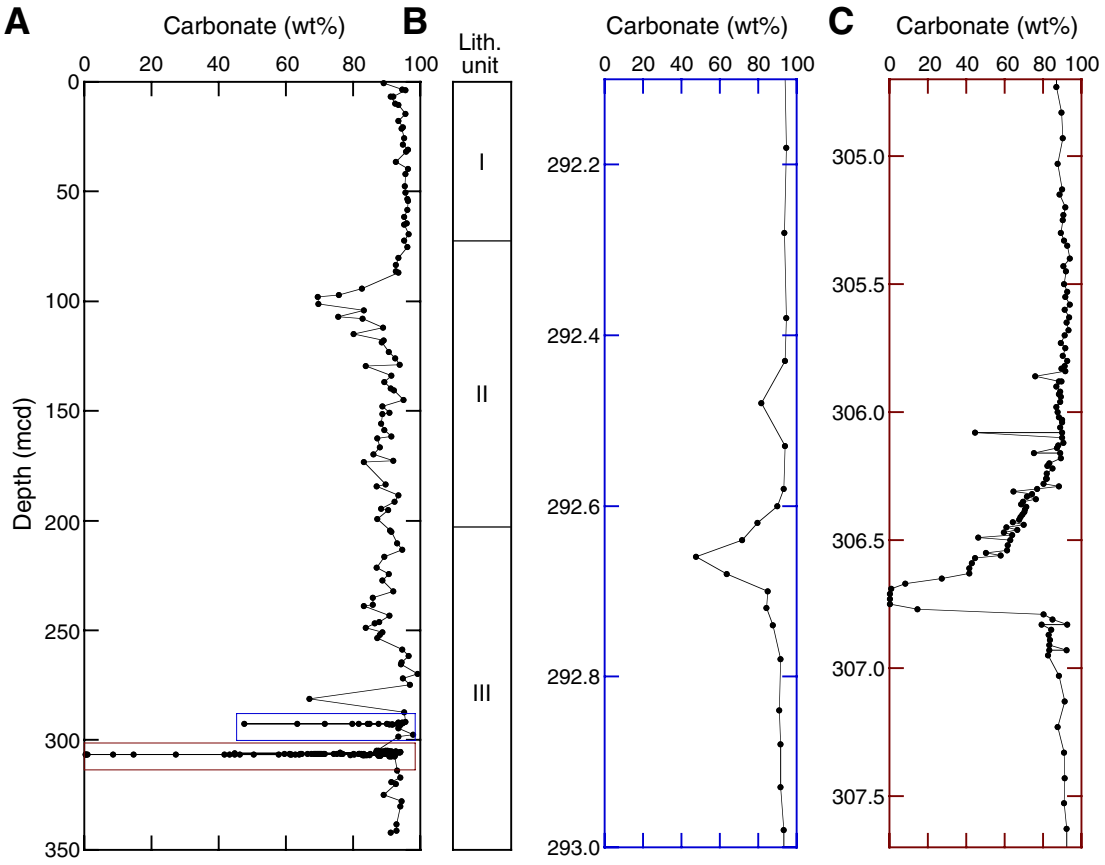
Figure F29. Mass chromatograms (*m/z* 85) of aliphatic hydrocarbon extracted from Samples 208-1266A-2H-5, 140–150 cm, and 208-1266C-11H-CC, 0–1 cm. Results from Sites 1263 and 1264 are also shown for comparison. Note the remarkable similarity in relative abundance of *n*-alkanes (*n*-C$_{14-18}$) pristane and phytane in samples from the Oligocene and above.
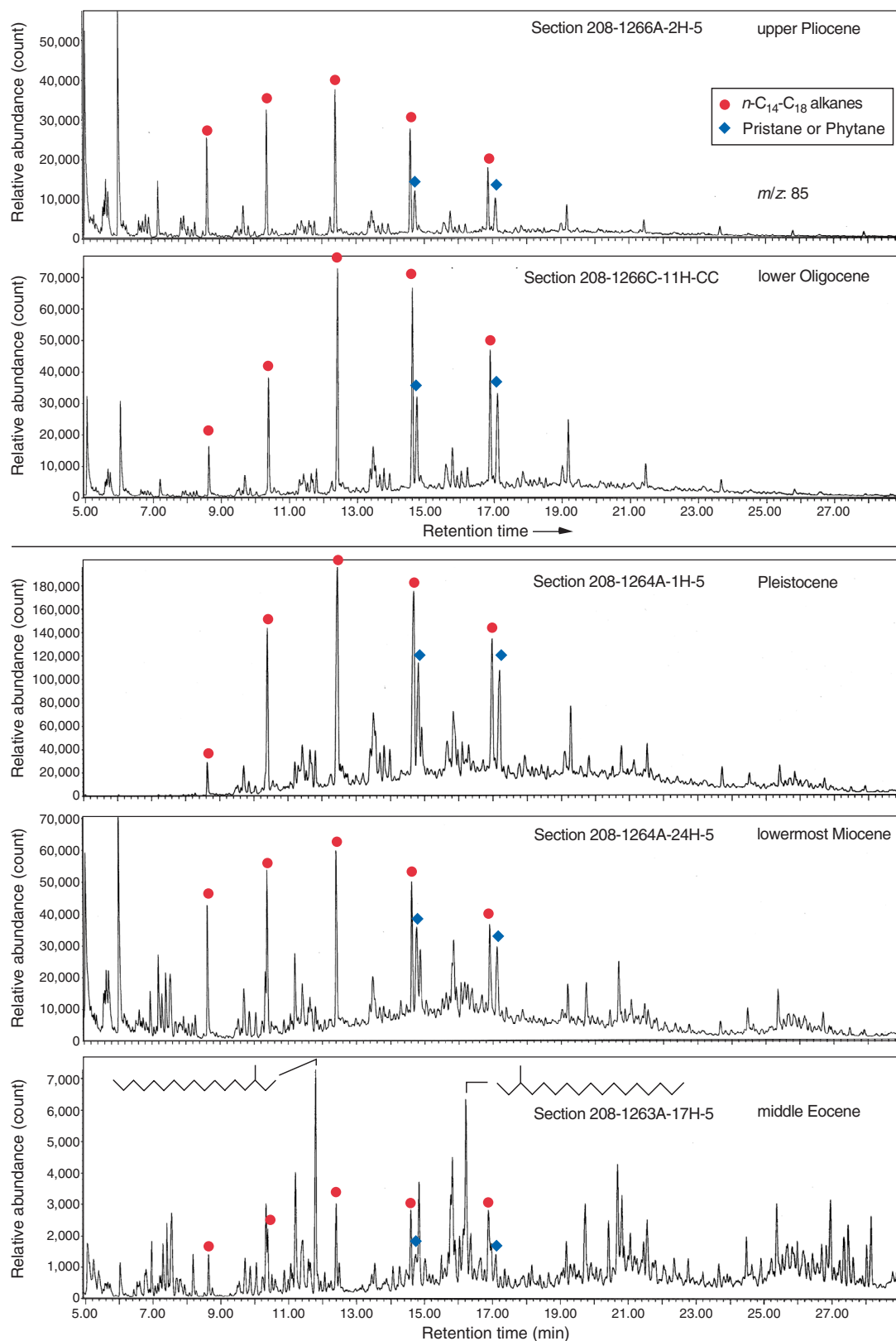
Figure F30. Examples of mass chromatograms (m/z 85). A series of long-chain n-alkanes (n-C$_{27-33}$) is present in Sample 208-1266A-2H-5, 140–150 cm, but not in other samples. Note that n-C$_{31}$ has the highest abundance among the n-C$_{27-33}$.
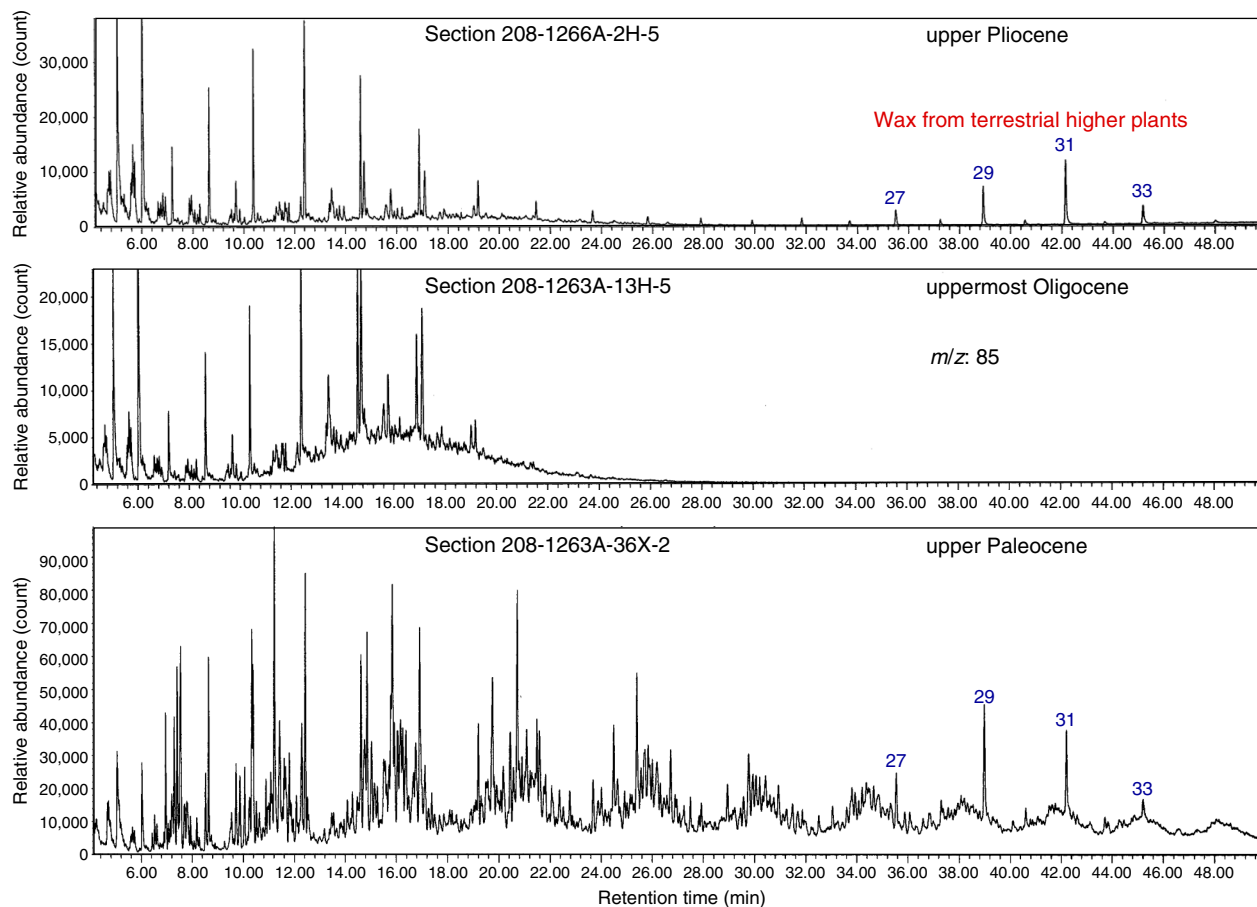
Figure F31. A. Core recovery plot. **B.** Shipboard biostratigraphic and magnetostratigraphic datums and the interpreted age-depth model. **C.** Corrected linear sedimentation rate (LSR), total, carbonate, and noncarbonate mass accumulation rates (MARs), calculated from the age model sampled at 1-m.y. intervals, and dry density and calcium carbonate concentrations averaged over the same 1-m.y. intervals. B = bottom, T = top.

Table T1. Coring summary, Site 1266. (**See table notes.** Continued on next page.)

Core	Date (Apr 2003)	Local time (hr)	Depth (mbsf) Top	Depth (mbsf) Bottom	Length (m) Cored	Length (m) Recovered	Recovery (%)	Tool deployment
208-1266A-								
1H	15	2215	0.0	9.5	9.5	10.04	105.7	
2H	15	2305	9.5	19.0	9.5	9.93	104.5	NMCB
3H	16	15	19.0	28.5	9.5	9.40	99.0	Tensor
4H	16	125	28.5	38.0	9.5	8.95	94.2	Tensor, NMCB
5H	16	225	38.0	47.5	9.5	9.95	104.7	Tensor
6H	16	325	47.5	57.0	9.5	9.88	104.0	Tensor, NMCB
7H	16	445	57.0	66.5	9.5	9.94	104.6	APCT, Tensor
8H	16	545	66.5	76.0	9.5	9.73	102.4	Tensor, NMCB
9H	16	720	76.0	84.6	8.6	8.66	100.7	DO, Tensor
10H	16	900	84.6	94.1	9.5	9.38	98.7	DO, Tensor
11H	16	1000	94.1	103.6	9.5	9.71	102.2	Tensor
12H	16	1055	103.6	113.1	9.5	10.16	107.0	Tensor
13H	16	1240	113.1	122.6	9.5	10.12	106.5	DO, APCT, Tensor
14H	16	1350	122.6	132.1	9.5	9.88	104.0	Tensor, NMCB
15H	16	1445	132.1	141.6	9.5	9.88	104.0	Tensor
16H	16	1625	141.6	151.1	9.5	10.13	106.6	DO, APCT, Tensor
17H	16	1735	151.1	160.6	9.5	9.38	98.7	Tensor
18H	16	1855	160.6	170.1	9.5	9.79	103.1	DO, Tensor, NMCB
19H	16	1955	170.1	179.6	9.5	9.12	96.0	Tensor
20H	16	2115	179.6	189.1	9.5	9.63	101.4	DO, Tensor
21H	16	2305	189.1	198.6	9.5	10.05	105.8	DO, Tensor
22H	17	108	198.6	208.1	9.5	10.12	106.5	DO, Tensor
23H	17	300	208.1	215.0	6.9	6.97	101.0	DO, Tensor
24H	17	410	215.0	215.9	0.9	0.93	103.3	Tensor
25H	17	520	215.9	217.1	1.2	1.28	106.7	Tensor
26X	17	700	217.1	221.6	4.5	1.61	35.8	
27X	17	800	221.6	231.1	9.5	9.39	98.8	
28X	17	900	231.1	240.7	9.6	6.33	65.9	
29X	17	1005	240.7	250.3	9.6	9.41	98.0	
30X	17	1130	250.3	260.0	9.7	9.68	99.8	
31X	17	1235	260.0	269.7	9.7	5.29	54.5	
32X	17	1345	269.7	279.3	9.6	7.82	81.5	
33X	17	1500	279.3	288.9	9.6	8.19	85.3	
34X	17	1630	288.9	298.6	9.7	6.31	65.1	
				Cored totals:	298.6	287.04	96.1	
208-1266B-								
1H	17	2020	0.0	7.6	7.6	7.65	100.7	APCT
			*****Drilled from 7.6 to 220.0 mbsf*****					
2X	18	505	220.0	229.5	9.5	9.61	101.2	
3X	18	600	229.5	239.0	9.5	9.77	102.8	
4X	18	740	239.0	248.5	9.5	9.68	101.9	
5H	18	915	248.5	258.0	9.5	9.99	105.2	DO
6H	18	1100	258.0	267.5	9.5	10.21	107.5	DO
7X	18	1220	267.5	273.0	5.5	8.39	152.6	
8X	18	1330	273.0	282.6	9.6	8.51	88.7	
9X	18	1450	282.6	292.2	9.6	9.77	101.8	
10X	18	1610	292.2	301.8	9.6	9.93	103.4	
11X	18	1725	301.8	311.4	9.6	9.48	98.8	
12X	18	1900	311.4	321.0	9.6	7.45	77.6	
				Cored totals:	108.6	110.44	101.7	
208-1266C-								
			*****Drilled from 0.0 to 62.0 mbsf*****					
1H	19	255	62.0	71.5	9.5	9.61	101.2	Tensor
2H	19	350	71.5	81.0	9.5	10.00	105.3	Tensor
3H	19	505	81.0	88.4	7.4	7.45	100.7	DO, Tensor
4H	19	615	88.4	97.9	9.5	9.83	103.5	Tensor
5H	19	900	97.9	107.4	9.5	9.50	100.0	DO, Tensor
6H	19	1315	107.4	116.0	8.6	8.60	100.0	Tensor
7H	19	1435	116.0	125.5	9.5	9.04	95.2	Tensor
8H	19	1530	125.5	135.0	9.5	9.53	100.3	Tensor
9H	19	1635	135.0	144.5	9.5	9.07	95.5	Tensor
10H	19	1745	144.5	154.0	9.5	10.04	105.7	Tensor
11H	19	1845	154.0	163.5	9.5	9.89	104.1	Tensor
12H	19	1950	163.5	173.0	9.5	9.53	100.3	Tensor
13H	19	2125	173.0	182.5	9.5	9.54	100.4	DO, Tensor
14H	19	2255	182.5	192.0	9.5	9.82	103.4	DO, Tensor
			*****Drilled from 192.0 to 245.0 mbsf*****					

Table T1 (continued).

Core	Date (Apr 2003)	Local time (hr)	Depth (mbsf)		Length (m)		Recovery (%)	Tool deployment
			Top	Bottom	Cored	Recovered		
15X	20	520	245.0	254.5	9.5	9.65	101.6	
16H	20	715	254.5	264.0	9.5	10.08	106.1	DO
17H	20	915	264.0	273.5	9.5	9.93	104.5	DO
18H	20	1110	273.5	282.7	9.2	9.28	100.9	DO
19X	20	1240	282.7	292.2	9.5	9.07	95.5	
			*****Drilled from 292.2 to 315.0 mbsf*****					
20X	20	1635	315.0	324.6	9.6	5.98	62.3	
21X	20	1845	324.6	334.2	9.6	8.53	88.9	
				Cored totals:	196.4	193.97	98.8	
				Total:	603.6	591.45	98.0	

Notes: NMCB = nonmagnetic core barrel, including cutting shoe (made from Monel). Tensor = brand name for core barrel orientation tool. APCT = Advanced Piston Corer Temperature tool (stainless steel housing is cutting shoe). DO = drillover. See Table T1, p. 106, in the "Leg 208 Summary" chapter.

Table T2. Composite depth scale, Site 1266.

Core	Offset (m)	Depth (mbsf)	Depth (mcd)
208-1266A-			
1H	3.14	0.00	3.14
2H	4.57	9.50	14.07
3H	5.99	19.00	24.99
4H	7.41	28.50	35.91
5H	8.84	38.00	46.84
6H	10.27	47.50	57.77
7H	11.69	57.00	68.69
8H	13.11	66.50	79.61
9H	14.54	76.00	90.54
10H	15.83	84.60	100.43
11H	17.25	94.10	111.35
12H	18.68	103.60	122.28
13H	20.10	113.10	133.20
14H	21.53	122.60	144.13
15H	22.95	132.10	155.05
16H	24.38	141.60	165.98
17H	25.81	151.10	176.91
18H	27.23	160.60	187.83
19H	28.66	170.10	198.76
20H	30.08	179.60	209.68
21H	31.50	189.10	220.60
22H	32.93	198.60	231.53
23H	34.35	208.10	242.45
24H	35.39	215.00	250.39
25H	35.53	215.90	251.43
26X	35.71	217.10	252.81
27X	36.38	221.60	257.98
28X	37.81	231.10	268.91
29X	39.24	240.70	279.94
30X	40.69	250.30	290.99
31X	43.13	260.00	303.13
32X	43.60	269.70	313.30
33X	45.03	279.30	324.33
34X	48.78	288.90	337.68
208-1266B-			
1H	0.00	0.00	0.00
2X	33.00	220.00	253.00
3X	34.42	229.50	263.92
4X	35.85	239.00	274.85
5H	37.28	248.50	285.78
6H	38.70	258.00	296.70
7X	40.12	267.50	307.62
8X	43.86	273.00	316.86
9X	44.17	282.60	326.77
10X	45.61	292.20	337.81
11X	47.05	301.80	348.85
12X	48.49	311.40	359.89
208-1266C-			
1H	8.17	62.00	70.17
2H	9.15	71.50	80.65
3H	9.95	81.00	90.95
4H	11.12	88.40	99.52
5H	13.85	97.90	111.75
6H	16.12	107.40	123.52
7H	17.26	116.00	133.26
8H	17.19	125.50	142.69
9H	18.48	135.00	153.48
10H	19.86	144.50	164.36
11H	21.36	154.00	175.36
12H	23.73	163.50	187.23
13H	25.47	173.00	198.47
14H	26.75	182.50	209.25
15X	35.13	245.00	280.13
16H	36.71	254.50	291.21
17H	39.66	264.00	303.66
18H	41.43	273.50	314.93
19X	43.03	282.70	325.73
20X	46.28	315.00	361.28
21X	46.28	324.60	370.88

Table T3. Splice tie points, Site 1266.

Hole, core, section, interval (cm)	Depth (mbsf)	Depth (mcd)		Hole, core, section, interval (cm)	Depth (mbsf)	Depth (mcd)
208-				208-		
1266B-1H-4, 142.5	5.93	5.93	Tie to	1266A-1H-2, 128.5	2.79	5.93
1266A-1H-C, 15	9.95	13.09	Append to	1266A-2H-1, 0	9.49	14.06
1266A-2H-C, 12.5	19.33	23.90	Append to	1266A-3H-1, 0	18.99	24.98
1266A-3H-C, 5	28.31	34.30	Append to	1266A-4H-1, 0	28.50	35.91
1266A-4H-C, 5	37.36	44.77	Append to	1266A-5H-1, 0	38.00	46.84
1266A-5H-7, 77.5	47.78	56.62	Append to	1266A-6H-1, 0	47.50	57.77
1266A-6H-7, 67.5	57.17	67.44	Append to	1266A-7H-1, 0	57.00	68.69
1266A-7H-6, 52.5	65.02	76.71	Tie to	1266C-1H-5, 53.5	68.54	76.71
1266C-1H-C, 7.5	71.54	79.71	Append to	1266A-8H-1, 0	66.50	79.61
1266A-8H-6, 120	75.20	88.31	Tie to	1266C-2H-6, 14.5	79.16	88.31
1266C-2H-C, 15	81.43	90.58	Append to	1266A-9H-1, 0	76.00	90.54
1266A-9H-C, 15	84.59	99.13	Append to	1266C-4H-1, 0	88.40	99.52
1266C-4H-4, 107.5	93.98	105.10	Tie to	1266A-10H-4, 16	89.27	105.10
1266A-10H-C, 10	93.87	109.70	Append to	1266A-11H-1, 0	94.10	111.35
1266A-11H-7, 92.5	103.53	120.78	Append to	1266A-12H-1, 0	103.60	122.28
1266A-12H-C, 22.5	113.64	132.32	Append to	1266A-13H-1, 0	113.10	133.20
1266A-13H-7, 82.5	122.92	143.02	Tie to	1266C-8H-1, 32	125.83	143.02
1266C-8H-6, 25	133.25	150.44	Tie to	1266A-14H-5, 31	128.91	150.44
1266A-14H-7, 47.5	132.08	153.61	Tie to	1266C-9H-1, 12	135.13	153.61
1266C-9H-4, 60	140.10	158.58	Tie to	1266A-15H-3, 52	135.63	158.58
1266A-15H-7, 55	141.65	164.60	Tie to	1266C-10H-1, 23.5	144.74	164.60
1266C-10H-6, 122.5	153.22	173.08	Tie to	1266A-16H-5, 110	148.70	173.08
1266A-16H-7, 47.5	151.08	175.46	Tie to	1266C-11H-1, 10	154.10	175.46
1266C-11H-7, 5	163.05	184.41	Tie to	1266A-17H-5, 150	158.60	184.41
1266A-17H-C, 10	160.38	186.19	Append to	1266C-12H-1, 0	163.50	187.23
1266C-12H-7, 35	172.85	196.58	Tie to	1266A-18H-6, 125	169.35	196.58
1266A-18H-C, 10	170.28	197.51	Append to	1266A-19H-1, 0	170.10	198.76
1266A-19H-7, 77.5	178.98	207.64	Append to	1266C-14H-1, 0	182.50	209.25
1266C-14H-5, 65	189.15	215.90	Tie to	1266A-20H-5, 22.5	185.82	215.90
1266A-20H-7, 45	189.05	219.13	Append to	1266A-21H-1, 0	189.10	220.60
1266A-21H-C, 12.5	199.01	230.51	Append to	1266A-22H-1, 0	198.60	231.53
1266A-22H-C, 17.5	208.63	241.56	Append to	1266A-23H-1, 0	208.10	242.45
1266A-23H-C, 20	215.01	249.36	Append to	1266A-24H-1, 0	215.00	250.39
1266A-24H-C, 12.5	215.82	251.21	Append to	1266A-25H-1, 0	215.90	251.43
1266A-25H-C, 20	217.10	252.63	Append to	1266A-26X-1, 0	217.10	252.81
1266A-26X-1, 107.5	218.18	253.89	Tie to	1266B-2X-1, 88.5	220.89	253.89
1266B-2X-6, 52.5	228.02	261.02	Tie to	1266A-27X-3, 3.5	224.64	261.02
1266A-27X-7, 25	230.35	266.73	Tie to	1266B-3X-2, 131	232.31	266.73
1266B-3X-5, 137.5	236.88	271.30	Tie to	1266A-28X-2, 88.5	233.49	271.30
1266A-28X-5, 50	237.10	274.91	Tie to	1266A-4X-1, 4.5	239.06	274.91
1266B-4X-7, 30	248.30	284.15	Tie to	1266C-15X-3, 102.5	249.02	284.15
1266C-15X-7, 12.5	254.12	289.25	Tie to	1266B-5H-3, 46	251.97	289.25
1266B-5H-5, 107.5	255.58	292.86	Tie to	1266C-16H-2, 65	256.15	292.86
1266C-16H-8, 60	264.09	300.80	Tie to	1266B-6H-4, 20	262.10	300.80
1266B-6H-6, 77.5	265.68	304.38	Tie to	1266C-17H-2, 22.5	264.72	304.38
1266C-17H-7, 40	272.39	312.05	Tie to	1266B-7X-3, 143	271.93	312.05
1266B-7X-6, 50	275.50	315.62	Tie to	1266B-32X-2, 87.5	272.02	315.62
1266A-32X-5, 117.5	276.82	320.42	Tie to	1266B-8X-3, 54.5	276.56	320.42
1266B-8X-6, 12.5	280.62	324.48	Tie to	1266A-33X-1, 15	279.45	324.48
1266A-33X-6, 57.5	286.88	331.91	Tie to	1266B-9X-4, 63.5	287.74	331.91
1266B-9X-C, 22.5	292.23	336.40	Append to	1266B-10X-1, 0	292.20	337.81
1266B-10X-C, 37.5	302.02	347.63	Append to	1266B-11X-1, 0	301.80	348.85
1266B-11X-C, 17.5	311.18	358.23	Append to	1266B-12X-1, 0	311.40	359.89
1266B-12X-C, 30	318.74	367.23	Append to	1266C-21X-1, 0	324.60	370.88
1266C-21X-7, 32.5	333.08	379.36				

Note: This table is also available in **ASCII.**

Table T4. Lithostratigraphic subdivisions, Site 1266.

Unit	Unit boundary depth (mcd)	Hole 1266A						Hole 1265B						Hole 1266C					
		Core, section, interval (cm)		Depth (mbsf)		Depth (mcd)		Core, section, interval (cm)		Depth (mbsf)		Depth (mcd)		Core, section, interval (cm)		Depth (mbsf)		Depth (mcd)	
		Top	Base	Top	Base	Top	Base	Top	Base	Top	Base	Top	Base	Top	Base	Top	Base	Top	Base
I		1H-1	7H-6, 55	0.0	65.1	3.1	76.8	1H-1	1H-CC	0.0	7.7	0.0	7.7	1H-1	1H-5, 57	62.0	68.6	70.2	76.8
	76.8																		
II		7H-6, 55	20H-4, 50	65.1	184.6	76.8	214.7	—	—	—	—	—	—	2H-1	14H-4, 95	71.5	188.0	80.7	214.7
	214.7																		
III	(379.4)*	20H-4, 50	34X-CC, 4	184.6	294.9	214.7	343.7	2X-1	12X-CC	220.0	318.9	253.0	367.3	14H-4, 95	21X-CC	188.0	333.1	214.7	379.4

Notes: Bold intervals and depths define the unit boundaries; other intervals are recognized as part of units but do not contain the unit boundaries. — = lithostratigraphic unit not recovered. * = bottom of deepest hole.

Unit	Unit boundary depth (mcd)	Description
I		Foraminifer-bearing nannofossil ooze and nannofossil ooze
	76.8	
II		Clay-bearing nannofossil ooze and nannofossil ooze
	214.7	
III	(379.4)*	Clay-bearing nannofossil ooze, nannofossil ooze, and nannofossil chalk

Table T5. Stratigraphic positions of selected calcareous nannofossil datums, Site 1266. (**See table note.** Continued on next page.)

| | | Age (Ma) | | Top of sample interval | | | Base of sample interval | | |
	Datum	Youngest	Oldest	Core, section, interval (cm)	Depth (mbsf)	(mcd)	Core, section, interval (cm)	Depth (mbsf)	(mcd)
				208-1266A-			208-1266A-		
T	*Pseudoemiliania lacunosa*	0.46	0.46	1H-1, 110	1.10	4.24	1H-3, 110	4.10	7.24
T	Large *Gephyrocapsa* spp.	1.22	1.22	1H-5, 110	7.10	10.24	1H-7, 35	9.35	14.49
B	Large *Gephyrocapsa* spp.	1.58	1.58	1H-7, 35	9.35	12.49	1H-CC	9.99	13.13
T	*Calcidiscus macintyrei*	1.67	1.67	2H-2, 40	11.40	15.97	2H-3, 40	12.90	17.47
B	Medium *Gephyrocapsa* spp.	1.69	1.69	2H-3, 40	12.90	17.47	2H-4, 40	14.40	18.97
T	*Discoaster brouweri* and *D. triradiatus*	1.95	1.95	2H-4, 40	14.40	18.97	2H-5, 40	15.90	20.47
T	*Discoaster pentaradiatus*	2.52	2.52	3H-1, 40	19.40	25.39	3H-2, 40	20.90	26.89
T	*Discoaster tamalis*	2.83	2.83	3H-3, 110	23.10	29.09	3H-4, 110	24.60	30.59
T	*Reticulofenestra pseudoumbilicus*	3.82	3.82	5H-1, 130	39.30	48.14	5H-2, 130	40.80	49.64
T	*Amaurolithus* spp.	4.56	4.56	5H-3, 130	42.30	51.14	5H-4, 130	43.80	52.64
B	*Ceratolithus rugosus*	5.1	5.1	6H-2, 30	49.30	59.57	6H-3, 130	51.80	62.07
B	*Ceratolithus acutus*	5.37	5.37	7H-2, 130	59.80	71.49	7H-3, 30	60.30	71.99
B	*Amaurolithus primus*	7.39	7.39	7H-6, 30	64.80	76.49	7H-6, 70	65.20	76.89
B	*Discoaster bellus* gr. (*D. hamatus*)	10.48	10.48	8H-5, 120	73.70	86.81	8H-6, 140	75.40	88.51
B	*Catinaster coalitus*	10.79	10.79	9H-2, 130	78.80	93.34	9H-3, 130	80.30	94.84
B	*Triquetrorhabdulus rugosus*	12.81	12.81	9H-2, 130	78.80	93.34	9H-3, 130	80.30	94.84
T	*Sphenolithus heteromorphus*	13.55	13.55	9H-6, 70	84.20	98.74	9H-CC	84.61	99.15
B	*Sphenolithus heteromorphus*	17.76	17.76	10H-6, 80	92.90	108.73	10H-7, 55	93.65	109.48
T	*Sphenolithus belemnos*	17.89	17.89	10H-CC	93.93	109.76	11H-1, 30	94.40	111.65
B	*Sphenolithus belemnos*	18.92	18.92	11H-5, 120	101.30	118.55	11H-6, 60	102.20	119.45
B	*Sphenolithus disbelemnos*	22.67	22.67	13H-3, 130	117.40	137.50	13H-4, 130	118.90	139.00
B	*Discoaster druggii*	22.82	22.82	11H-7, 20	102.80	120.05	11H-7, 90	103.50	120.75
T	*Sphenolithus delphix*	23.07	23.07	13H-7, 20	122.30	142.40	13H-7, 80	122.90	143.00
B	*Sphenolithus delphix*	23.33	23.33	13H-CC	123.12	143.22	14H-1, 40	123.00	144.53
T	*Sphenolithus ciperoensis*	24.23	24.23	14H-5, 40	129.00	150.53	14H-6, 45	130.55	152.08
B	*Sphenolithus ciperoensis*	27.55	27.55	15H-CC	141.88	164.83	16H-1, 50	142.10	166.48
T	*Sphenolithus distentus*	25.98	25.98	16H-3, 50	145.10	169.48	16H-5, 50	148.10	172.48
T	*Sphenolithus pseudoradians*	29.1	29.1	17H-2, 120	153.80	179.61	17H-3, 120	155.30	181.11
B	*Sphenolithus distentus*	30.32	30.32	17H-5, 120	158.30	184.11	17H-CC	160.43	186.24
T	*Reticulofenestra umbilicus* >14 µm	31.7	31.7	19H-2, 30	171.00	199.66	19H-2, 130	172.00	200.66
T	*Ericsonia formosa*	32.9	32.9	19H-7, 75	178.95	207.61	19H-CC	179.12	207.78
T	*Discoaster saipanensis*	34.0	34.0	21H-1, 40	189.50	221.00	21H-1, 120	190.30	221.80
T	*Discoaster barbadiensis*	34.2	34.2	21H-2, 30	190.90	222.40	21H-2, 120	191.80	223.30
T	*Calcidiscus protoannulus*	34.9	34.9	21H-5, 30	195.40	226.90	21H-6, 30	196.90	228.40
B	*Isthmolithus recurvus*	36.6	36.6	24H-1, 45	215.45	250.84	24H-CC	215.88	251.27
T	*Chiasmolithus grandis*	37.1	37.1	24H-CC	215.88	251.27	25H-1, 15	216.05	251.58
B	*Dictyococcites scrippsae*	40.3	40.3	26X-CC	218.66	254.37	27X-1, 128	222.88	259.26
T	*Nannotetrina* spp.	42.3	42.3	26X-CC	218.66	254.37	27X-1, 128	222.88	259.26
B	*Reticulofenestra umbilicus* >14 µm	42.5	42.5	26X-CC	218.66	254.37	27X-1, 128	222.88	259.26
T	*Discoaster sublodoensis*	47.2	47.2	27X-1, 28	221.88	258.26	27X-2, 30	223.40	259.78
B	*Nannotetrina* spp.	47.8	47.8	27X-2, 118	224.28	260.66	27X-3, 30	224.90	261.28
T	*Discoaster lodoensis*	48.0	48.0	27X-3, 120	225.80	262.18	27X-4, 30	226.40	262.78
B	*Discoaster sublodoensis*	49.3	49.3	27X-6, 85	229.95	266.33	27X-7, 30	230.40	266.78
T	*Tribrachiatus orthostylus*	51.0	51.0	27X-CC	230.94	267.32	28X-1, 60	231.70	269.51
B	*Discoaster lodoensis*	52.4	52.4	29X-2, 40	242.60	281.84	29X-2, 112	243.32	282.56
T	*Discoaster multiradiatus*	53.0	53.0	30X-3, 18	253.48	294.17	30X-3, 99	254.29	294.98
B	*Sphenolithus radians*	53.3	53.3	30X-3, 99	254.29	294.98	30X-4, 40	255.20	295.89
B	*Tribrachiatus orthostylus*	53.4	53.4	30X-3, 99	254.29	294.98	30X-4, 40	255.20	295.89
B	*Discoaster diastypus*	53.9	53.9	30X-4, 102	255.82	296.51	30X-5, 50	256.80	297.49
T	*Fasciculithus* spp.			30X-CC	259.93	300.62	31X-1, 10	260.10	303.23
	Decrease *Fasciculithus* spp.			31X-3, 3	263.03	306.16	31X-3, 13	263.13	306.26
	Increase *Zygrhablithus bijugatus*			31X-3, 13	263.13	306.26	31X-3, 23	263.23	306.36
B	*Rhomboaster* spp.			31X-3, 36	263.36	306.49	31X-3, 38	263.38	306.51
B	*Discoaster multiradiatus*	56.2	56.2	34X-2, 30	290.70	339.48	34X-2, 120	291.60	340.38
				208-1266B-			208-1266B-		
T	*Chiasmolithus grandis*	37.1	37.1	1H-CC	7.60	7.60	2H-CC	229.56	262.56
B	*Nannotetrina* spp.	47.8	47.8	1H-CC	7.60	7.60	2H-CC	229.56	262.56
T	*Discoaster lodoensis*	48.0	48.0	2H-CC	229.56	262.56	3H-CC	239.17	273.59
T	*Tribrachiatus orthostylus*	51.0	51.0	2H-CC	229.56	262.56	3H-CC	239.17	273.59
B	*Discoaster lodoensis*	52.4	52.4	4H-CC	248.63	284.48	5H-CC	258.44	295.72
T	*Discoaster multiradiatus*	53.0	53.0	4H-CC	248.63	284.48	5H-CC	258.44	295.72
B	*Sphenolithus radians*	53.3	53.3	4H-CC	248.63	284.48	5H-CC	258.44	295.72
B	*Tribrachiatus orthostylus*	53.4	53.4	4H-CC	248.63	284.48	5H-CC	258.44	295.72
B	*Discoaster diastypus*	53.9	53.9	4H-CC	248.63	284.48	5H-CC	258.44	295.72
T	*Fasciculithus* spp.			5H-CC	258.44	295.72	6H-7, 114	267.54	306.24

Table T5 (continued).

	Datum	Age (Ma)		Top of sample interval			Base of sample interval		
		Youngest	Oldest	Core, section, interval (cm)	(mbsf)	(mcd)	Core, section, interval (cm)	(mbsf)	(mcd)
	Increase *Zygrhablithus bijugatus*			6H-7, 114	267.54	306.24	6H-7, 128	267.68	306.38
B	*Rhomboaster* spp.			6H-7, 148	267.88	306.58	6H-CC	268.16	306.86
B	*Discoaster multiradiatus*	56.2	56.2	9X-CC	292.32	336.49	10X-CC	302.08	347.69
B	*Heliolithus riedelii*	57.3	57.3	11X-CC	311.23	358.28	12X-1, 30	311.70	360.19
B	*Discoaster mohleri*	57.5	57.5	12X-2, 12	313.02	361.51	12X-2, 115	314.05	362.54
				208-1266C-			208-1266C-		
B	*Catinaster coalitus*	10.79	10.79	1H-CC	71.56	79.73	2H-CC	81.45	90.60
T	*Sphenolithus heteromorphus*	13.55	13.55	3H-CC	88.4	98.35	4H-CC	98.18	109.30
B	*Sphenolithus heteromorphus*	17.76	17.76	4H-CC	98.18	109.3	5H-CC	107.35	121.20
B	*Sphenolithus disbelemnos*	22.67	22.67	5H-CC	107.35	121.2	6H-CC	115.95	132.07
B	*Discoaster druggii*	22.82	22.82	5H-CC	116.52	133.1	6H-CC	115.95	132.07
T	*Sphenolithus ciperoensis*	24.23	24.23	9H-CC	144.02	162.5	10H-CC	154.49	174.35
T	*Sphenolithus distentus*	25.98	25.98	9H-CC	144.02	162.5	10H-CC	154.49	174.35
B	*Sphenolithus ciperoensis*	27.55	27.55	11H-CC	163.79	185.15	12H-CC	172.98	196.71
T	*Sphenolithus pseudoradians*	29.1	29.1	11H-CC	163.79	185.15	12H-CC	172.98	196.71
T	*Reticulofenestra umbilicus* >14 µm	31.7	31.7	12H-CC	172.98	196.71	13H-CC	182.49	207.96
T	*Ericsonia formosa*	32.9	32.9	13H-CC	182.49	207.96	14H-CC	192.27	219.02
B	*Reticulofenestra umbilicus* >14 µm	42.5	42.5	14H-CC	192.27	219.02	15X-CC	254.60	289.73
T	*Tribrachiatus orthostylus*	51.0	51.0	14H-CC	192.27	219.02	15X-CC	254.60	289.73
T	*Discoaster multiradiatus*	53.0	53.0	15X-CC	254.6	289.73	16H-7, 22	262.21	298.92
B	*Sphenolithus radians*	53.3	53.3	15X-CC	254.6	289.73	16H-7, 22	262.21	298.92
B	*Tribrachiatus orthostylus*	53.4	53.4	15X-CC	254.6	289.73	16H-7, 22	262.21	298.92
	Increase *Zygrhablithus bijugatus*			16H-CC	264.53	301.24	17H-CC	273.88	313.54
B	*Rhomboaster* spp.			16H-CC	264.53	301.24	17H-CC	273.88	313.54
B	*Discoaster multiradiatus*	56.2	56.2	19X-CC	291.72	334.75	20X-1, 125	316.25	362.53
B	*Discoaster mohleri*	57.5	57.5	19X-CC	291.72	334.75	20X-1, 125	316.25	362.53
B	*Heliolithus kleinpellii*	58.2	58.2	21X-1, 19	324.79	371.07	21X-1, 25	324.85	371.13
B	*Sphenolithus anarrhopus*	58.4	58.4	21X-2, 20	326.30	372.58	21X-3, 28	327.88	374.16

Note: T = top, B = bottom.

Table T6. Stratigraphic ranges and relative abundances of selected calcareous nannofossil taxa, Site 1266. (This table is available in an **oversized format.**)

Table T7. Stratigraphic positions of selected planktonic foraminiferal datums, Site 1266.

	Datum	Age (Ma) Youngest	Oldest	Hole, core, section, interval (cm)	Depth (mbsf)	(mcd)	Hole, core, section, interval (cm)	Depth (mbsf)	(mcd)	Average (mcd)
				208-			208-			
T	*Globorotalia tosaensis*	0.61	0.61	1266B-1H-1, 0–2	0.00	0.00	1266B-1H-1, 32–34	0.32	0.32	0.16
T	*Globigerinoides obliquus*	1.30	1.30	1266B-1H-1, 32–34	0.32	0.32	1266B-1H-3, 32–34	3.32	3.32	1.82
T	*Globigerina apertura*	1.68	1.68	1266A-2H-CC	19.38	23.95	1266A-3H-1, 32–34	19.32	25.31	24.63
T	*Globigerinoides extremus*	1.91	1.91	1266A-2H-1, 32–34	9.82	14.39	1266A-2H-3, 32–34	12.82	17.39	15.89
B	*Globorotalia truncatulinoides*	2.03	2.03	1266A-2H-CC	19.38	23.95	1266A-3H-1, 32–34	19.32	25.31	24.63
	Pulleniatina reappearance	2.28	2.28	1266A-3H-6, 49–50	26.99	32.98	1266A-3H-CC	28.35	34.34	33.66
T	*Globoturborotalia woodi*	2.30	2.30	1266A-3H-1, 32–34	19.32	25.31	1266A-3H-3, 32–34	22.32	28.31	26.81
T	*Globigerina decoraperta*	2.70	2.70	1266A-3H-1, 32–34	19.32	25.31	1266A-3H-3, 32–34	22.32	28.31	26.81
T	*Dentoglobigerina altispira*	3.02	3.02	1266A-3H-6, 49–50	26.99	32.98	1266A-3H-CC	28.35	34.34	33.66
T	*Sphaeroidinellopsis seminulina*	3.18	3.18	1266A-4H-1, 32–34	28.82	36.23	1266A-4H-3, 32–34	31.82	39.23	37.73
T	*Neogloboquadrina acostaensis*	3.83	3.83	1266A-4H-1, 32–34	28.82	36.23	1266A-4H-3, 32–34	31.82	39.23	37.73
T	*Hirsutella margaritae*	3.88	3.88	1266A-4H-1, 32–34	28.82	36.23	1266A-4H-3, 32–34	31.82	39.23	37.73
T	*Globorotalia plesiotumida*	4.15	4.15	1266A-4H-3, 32–34	31.82	39.23	1266A-4H-5, 32–34	34.32	41.73	40.48
T	*Hirsutella cibaoensis*	4.16	4.16	1266A-4H-3, 32–34	31.82	39.23	1266A-4H-5, 32–34	34.32	41.73	40.48
B	*Globorotalia crassaformis* s.l.	4.31	4.31	1266A-5H-3, 32–34	41.32	50.16	1266A-5H-5, 32–34	44.32	53.16	51.66
T	*Globoturborotalita nepenthes*	4.37	4.37	1266A-6H-1, 32–34	47.82	58.09	1266A-6H-3, 32–34	50.82	61.09	59.59
B	*Sphaeroidinella dehiscens* (s.l.)	4.94	4.94	1266A-6H-5, 32–34	53.82	64.09	1266A-6H-6, 22–23	55.22	65.49	64.79
B	*Globigerinoides conglobatus*	5.84	5.84	1266A-7H-1, 32–34	57.32	69.01	1266A-7H-3, 32–34	60.32	72.01	70.51
B	*Globorotalia plesiotumida*	8.91	8.91	1266A-7H-5, 32–34	63.32	75.01	1266A-7H-CC	66.89	78.58	76.80
B	*Hirsutella juanai*	9.75	9.75	1266A-7H-5, 32–34	63.32	75.01	1266A-7H-CC	66.89	78.58	76.80
B	*Neogloboquadrina acostaensis*	9.89	9.89	1266A-7H-CC	66.89	78.58	1266A-8H-1, 32–34	66.82	79.93	79.26
B	*Globigerina apertura*	11.06	11.06	1266A-9H-3, 32–34	79.32	93.86	1266A-9H-5, 32–34	82.32	96.86	95.36
B	*Globoturborotalita nepenthes*	11.64	11.64	1266A-9H-1, 32–34	76.32	90.86	1266A-9H-3, 32–34	79.32	93.86	92.36
T	*Globigerina angulisuturalis*	21.60	21.60	1266A-12H-CC	113.66	132.34	1266A-13H-CC	123.12	143.22	137.78
T	*Globigerina euapertura*	23.03	23.03	1266A-12H-CC	113.66	132.34	1266A-13H-CC	123.12	143.22	137.78
T	*Paragloborotalia opima*	26.64	26.64	1266A-14H-CC	132.43	153.96	1266A-15H-CC	141.88	164.83	159.40
T	*Chiloguembelina cubensis* (common)	27.92	27.92	1266A-16H-CC	151.63	176.01	1266A-17H-CC	160.43	186.24	181.13
T	*Subbotina angioporoides*	29.67	29.67	1266A-17H-CC	160.43	186.24	1266A-18H-CC	170.34	197.57	191.91
T	*Pseudohastigerina* spp.	32.00	32.00	1266A-19H-CC	179.12	207.78	1266A-20H-CC	189.18	219.26	191.91
T	*Globigerinatheka index*	34.30	34.30	1266A-20H-CC	189.18	219.26	1266A-21H-CC	199.10	230.60	224.93
T	*Subbotina linaperta*	37.70	37.70	1266A-26X-CC	218.66	254.37	1266B-2X-CC	229.56	262.56	258.47
T	*Acarinina coalingensis* (= *primitiva*)	39.00	39.00	1266A-24X-CC	215.88	251.27	1266A-25X-CC	217.13	252.66	251.97
B	*Globigerinatheka index*	42.90	42.90	1266A-26X-CC	218.66	254.37	1266B-2X-CC	229.56	262.56	258.47
T	*Morozovella aragonensis*	43.60	43.60	1266A-26X-CC	218.66	254.37	1266B-2X-CC	229.56	262.56	258.47
T	*Morozovella formosa*	50.80	50.80	1266A-27X-CC	230.94	267.32	1266B-3X-CC	239.17	273.59	270.46
B	*Morozovella aragonensis*	52.30	52.30	1266A-28X-CC	237.33	275.14	1266A-29X-CC	250.06	289.30	282.22
B	*Morozovella lensiformis*	54.00	54.00	1266A-29X-CC	250.06	289.30	1266A-30X-CC	259.93	300.62	294.96
B	*Morozovella gracilis*	54.46	54.46	1266A-29X-CC	250.06	289.30	1266A-30X-CC	259.93	300.62	304.51
T	*Stensioeina beccariiformis**	55.00	55.00	1266B-6H-CC, 22–23	268.12	306.82	1266B-6H-CC, 26–27	268.16	306.86	306.84
B	*Morozovella subbotinae*	55.90	55.90	1266A-32X-CC	277.47	321.07	1266A-33X-CC	287.44	332.47	326.77
T	*Globanomalina pseudomenardii*	55.90	55.90	1266B-8X-CC	281.46	325.32	1266A-33X-CC	287.44	332.47	328.90
B	*Globanomalina pseudomenardii*	59.20	59.20	1266C-20X-CC	320.93	367.21	1266C-21X-CC	333.08	379.36	373.29

Notes: T = top, B = bottom. * = benthic foraminifer datum level.

Table T8. Stratigraphic ranges and relative abundances for selected planktonic foraminifer taxa, Site 1266. (This table is available in an **oversized format.**)

Table T9. Occurrence of selected benthic foraminifer taxa, Site 1266. (This table is available in an **oversized format.**)

Table T10. Magnetostratigraphic age-depth tie points, Site 1266.

Chron	Age (Ma) 1	Age (Ma) 2	Top Hole, core, section, interval (cm)	Depth (mbsf)	Depth (mcd)	Bottom Hole, core, section, interval (cm)	Depth (mbsf)	Depth (mcd)
			208-			208-		
C1n (o)	0.781	0.780	1266A-1H-3, 50	3.50	6.64	1266A-1H-4, 10	4.60	7.74
C1r.1n (y)	0.988	0.990	1266A-1H-4, 20	4.70	7.84	1266A-1H-4, 90	5.40	8.54
C1r.1n (o)	1.072	1.070	1266A-1H-5, 45	6.45	9.59	1266A-1H-5, 110	7.10	10.24
C2n (y)	1.785	1.770	1266A-2H-3, 85	13.35	17.92	1266A-2H-3, 130	13.80	18.37
C2n (o)	1.942	1.950	1266A-2H-5, 80	16.30	20.87	1266A-2H-5, 105	16.55	21.12
C2An (y)	2.582	2.581	1266A-3H-2, 40	20.90	26.89	1266A-3H-4, 5	23.55	29.54
C3n (o)	5.236	5.230	1266A-6H-7, 65	57.15	67.42	1266A-7H-1, 70	57.70	69.39
C5n (o)	11.043	10.949	1266A-9H-3, 30	79.30	93.84	1266A-9H-4, 20	80.70	95.24
C6Cn (y)	22.564	23.353	1266A-13H-4, 95	118.55	138.65	1266A-13H-5, 10	119.20	139.30
C7n (y)	24.001	24.730	1266A-14H-1, 125	123.85	145.38	1266A-14H-3, 45	126.05	147.58
C7An (y)	24.781	25.496	1266C-9H-1, 95	135.95	154.43	1266C-9H-1, 115	136.15	154.63
C7An (o)	24.942	25.648	1266C-9H-2, 45	136.95	155.43	1266C-9H-2, 85	137.35	155.83
C8n (y)	25.053	25.823	1266C-9H-2, 145	137.95	156.43	1266C-9H-4, 25	139.75	158.23
C10n (y)	27.760	28.283	1266A-17H-2, 110	153.70	179.51	1266A-17H-2, 120	153.80	179.61
C10n (o)	28.053	28.745	1266C-11H-6, 120	162.70	184.06	1266A-17H-7, 55	160.15	185.96
C11n (o)	29.828	30.098	1266A-18H-3, 45	164.05	191.28	1266C-12H-3, 140	167.90	191.63
C12n (y)		30.479	1266C-12H-4, 110	169.10	192.83	1266A-18H-5, 40	167.00	194.23
C12n (o)		30.939	1266C-12H-5, 95	170.45	194.18	1266A-18H-6, 10	168.20	195.43
C13n (o)		33.058	1266C-13H-7, 20	182.20	207.67	1266A-20H-1, 100	180.60	210.68
C15n (y)		34.655	1266A-21H-3, 30	192.40	223.90	1266A-21H-3, 50	192.60	224.10
C15n (o)		34.940	1266A-21H-3, 145	193.55	225.05	1266A-21H-4, 20	193.80	225.30
C16n (y)		35.343	1266A-21H-4, 105	194.65	226.15	1266A-21H-5, 40	195.50	227.00
C24n (o)		53.347	1266B-5H-7, 50	258.00	295.28	1266C-16H-7, 120	263.19	299.90
C25n (y)		55.904	1266C-18H-4, 100	278.2	319.63	1266C-18H-5, 30	279.00	320.43
C26n (o)		57.911	1266C-20X-3, 5	318.05	364.33	1266B-12X-4, 45	316.35	364.84

Notes: o = old end of chron, y = young end of chron. 1 = ages as in Lourens et al. (in press), and H. Pälike (pers. comm., 2003), 2 = ages as in Cande and Kent (1995).

Table T11. Interstitial water analyses, Hole 1266A.

Core, section, interval (cm)	Depth (mcd)	pH	Alkalinity (mM)	Salinity	Cl (mM)	SO$_4$ (mM)	ND (mM)	Mg (mM)	Ca (mM)	K (mM)	B (µM)	Fe (µM)	Mn (µM)	Li (µM)	Ba (µM)	Sr (µM)	Si (µM)
208-1266A-																	
1H-5, 140–150	10.5	7.46	3.32	35.0	561	26.2	452	53.6	10.4	9.9	435	0.00	3.82	24.6	0.26	165	307
2H-5, 140–150	21.5	7.43	2.82	35.0	564	26.2	497	54.5	11.1	10.4	449	0.00	2.38	24.0	0.27	214	238
3H-4, 140–150	30.9	7.37	2.73	35.0	562	25.8	481	52.6	11.6	10.1	455	0.00	0.80	23.7	0.30	263	287
5H-5, 140–150	54.2	7.34	2.59	35.5	565	25.0	485	52.5	12.3	9.7	446	8.34	0.75	25.5	0.28	333	194
6H-5, 140–150	65.2	7.33	2.52	35.5	569	25.0	494	50.1	13.1	10.2	452	7.66	0.58	26.5	0.27	340	195
7H-5, 140–150	76.1	7.42	2.58	35.5	553	24.5	479	48.5	13.2	9.0	477	0.95	2.17	26.4	0.29	360	239
8H-5, 140–150	87.0	7.39	2.49	35.0	542	24.7	485	50.8	13.8	9.8	500	0.00	4.32	26.9	0.25	367	243
9H-5, 140–150	97.9	7.42	ND	35.0	565	24.2	465	46.6	11.8	9.7	618	0.00	3.01	29.4	0.26	367	308
10H-4, 140–150	107.8	7.39	2.57	35.0	503	24.4	477	49.1	14.8	9.8	552	0.00	1.47	28.5	0.12	374	300
11H-5, 140–150	118.8	7.31	2.28	35.0	564	24.3	485	49.1	15.2	9.4	509	0.00	0.61	28.2	0.20	380	245
12H-5, 140–150	129.7	7.33	2.56	35.0	513	23.5	475	47.0	13.7	9.0	546	0.00	0.77	30.7	2.12	399	266
13H-5, 140–150	140.6	7.42	2.86	35.5	562	23.4	476	48.3	16.0	8.7	486	0.00	0.68	29.5	0.26	389	279
14H-5, 140–150	151.5	7.40	4.84	35.5	572	24.4	477	42.2	17.1	8.5	493	0.00	0.47	32.1	0.26	382	292
15H-5, 140–150	162.5	7.41	ND	35.0	562	24.2	484	46.4	17.5	8.6	508	0.00	0.61	31.2	2.15	392	263
16H-5, 140–150	173.4	7.40	2.11	35.0	510	23.9	481	46.4	17.8	8.3	558	0.00	0.69	32.2	0.28	398	290
17H-5, 140–150	184.3	7.39	2.00	35.5	567	23.7	472	44.9	17.7	8.8	488	0.00	0.45	31.5	1.82	399	301
18H-5, 140–150	195.2	7.37	2.02	35.0	563	23.7	482	46.5	19.3	8.0	476	0.00	0.69	30.6	0.29	400	306
19H-5, 140–150	205.3	7.33	2.01	35.5	564	23.7	479	46.3	20.1	8.2	479	0.00	0.57	32.9	1.43	407	289
22H-5, 140–150	238.9	7.35	1.91	35.5	569	23.4	489	49.0	21.1	7.9	527	0.00	5.09	34.4	0.32	425	387
23H-3, 140–150	246.9	7.27	1.97	35.5	567	22.6	487	41.7	21.9	7.4	521	0.00	4.83	34.4	0.35	406	491
27X-5, 140–150	265.4	7.32	ND	35.0	569	19.1	457	41.4	21.7	6.89	465	0.00	7.28	35.0	0.34	427	619
28X-2, 140–150	271.8	7.28	1.89	35.0	567	23.7	485	41.7	21.3	7.9	432	0.00	6.53	35.4	0.30	436	686
29X-5, 140–150	287.3	7.29	1.81	35.0	568	23.4	479	41.3	23.8	7.2	426	0.00	6.16	36.7	0.36	432	790
30X-5, 140–150	298.4	7.18	1.94	35.0	569	22.3	474	40.1	22.7	7.5	449	0.00	6.35	35.2	0.55	411	975
32X-4, 140–150	319.2	7.32	1.88	35.0	569	22.5	499	41.7	26.9	7.2	439	0.00	6.28	37.1	2.62	452	1114
33X-4, 140–150	330.2	7.34	1.87	35.5	569	20.9	475	41.7	26.0	6.9	423	0.00	5.96	38.2	0.37	440	1142
34X-3, 140–150	342.1	7.12	2.55	35.5	567	23.1	463	40.1	25.8	6.8	426	0.00	5.37	47.0	0.40	422	1446

Note: ND = not determined.

Table T12. Sedimentary calcium carbonate, total carbon, and organic carbon concentrations, Site 1266. (Continued on next page.)

Hole, core, section, interval (cm)	Depth (mcd)	Inorganic carbon (wt%)	CaCO$_3$ (wt%)
208-			
1266B-1H-1, 72–73	0.72	10.7	89.1
1266B-1H-3, 72–73	3.72	11.4	94.6
1266A-1H-1, 72–73	3.86	11.5	95.6
1266B-1H-5, 72–73	6.72	11.1	92.1
1266A-1H-3, 72–73	6.86	11.0	91.3
1266A-1H-5, 72–73	9.86	11.1	92.6
1266A-1H-5, 140–150	10.54	11.2	93.6
1266A-2H-1, 72–73	14.79	11.5	95.6
1266A-2H-3, 72–73	17.79	11.2	93.6
1266A-2H-5, 72–73	20.79	11.4	94.8
1266A-2H-5, 140–150	21.47	11.4	94.6
1266A-3H-1, 72–73	25.71	11.4	95.3
1266A-3H-3, 72–73	28.71	11.4	94.8
1266A-3H-4, 140–150	30.89	11.6	96.4
1266A-3H-5, 72–73	31.71	11.5	95.8
1266A-4H-1, 72–73	36.63	11.1	92.7
1266A-4H-3, 72–73	39.63	11.6	96.5
1266A-4H-5, 72–73	42.13	11.5	95.7
1266A-5H-1, 72–73	47.56	11.5	95.5
1266A-5H-3, 72–73	50.56	11.5	95.7
1266A-5H-5, 72–73	53.56	11.5	96.1
1266A-5H-5, 140–150	54.24	11.6	96.5
1266A-6H-1, 72–73	58.49	11.6	96.2
1266A-6H-3, 72–73	61.49	11.4	95.2
1266A-6H-5, 72–73	64.49	11.5	96.0
1266A-6H-5, 140–150	65.17	11.4	95.3
1266A-7H-1, 72–73	69.41	11.6	96.5
1266A-7H-3, 72–73	72.41	11.4	95.3
1266A-7H-5, 72–73	75.41	11.5	96.1
1266A-7H-5, 140–150	76.09	7.3	60.8
1266A-8H-1, 72–73	80.33	11.2	93.6
1266A-8H-3, 72–73	83.33	11.1	92.7
1266A-8H-5, 72–73	86.33	11.1	92.8
1266A-8H-5, 140–150	87.01	11.2	93.6
1266A-9H-3, 72–73	94.26	9.9	82.6
1266A-9H-5, 72–73	97.26	9.1	75.9
1266A-9H-5, 140–150	97.94	8.4	69.6
1266A-10H-1, 72–73	101.15	8.4	69.7
1266A-10H-3, 72–73	104.15	10.0	83.1
1266A-10H-5, 72–73	107.15	9.1	75.6
1266A-10H-5, 140–150	107.83	10.0	82.9
1266A-11H-1, 72–73	112.07	10.7	89.0
1266A-11H-3, 72–73	115.07	9.6	80.1
1266A-11H-5, 72–73	118.07	10.7	89.2
1266A-11H-5, 140–150	118.75	10.6	88.6
1266A-12H-1, 72–73	123.00	10.9	90.6
1266A-12H-3, 72–73	126.00	11.1	92.6
1266A-12H-5, 72–73	129.00	11.3	93.9
1266A-12H-5, 140–150	129.68	10.1	83.8
1266A-13H-1, 72–73	133.92	11.0	91.5
1266A-13H-3, 72–73	136.92	10.7	89.4
1266A-13H-5, 72–73	139.92	11.0	91.3
1266A-13H-5, 140–150	140.60	11.1	92.1
1266A-14H-1, 72–73	144.85	11.4	95.1
1266A-14H-3, 72–73	147.85	10.7	88.9
1266A-14H-5, 72–73	150.85	10.9	91.0
1266A-14H-5, 140–150	151.53	10.7	88.9
1266A-15H-1, 72–73	155.77	10.6	88.4
1266A-15H-3, 72–73	158.77	10.7	89.4
1266A-15H-5, 72–73	161.77	11.0	91.6
1266A-15H-5, 140–150	162.45	10.5	87.3
1266A-16H-1, 72–73	166.70	10.6	88.1
1266A-16H-3, 72–73	169.70	10.3	86.1
1266A-16H-5, 72–73	172.70	11.0	92.0
1266A-16H-5, 140–150	173.38	10.0	83.1
1266A-17H-5, 72–73	183.63	10.8	89.8
1266A-17H-5, 140–150	184.31	10.4	87.0
1266A-18H-1, 72–73	188.55	11.2	93.5
1266A-18H-3, 72–73	191.55	11.1	92.4
1266A-18H-5, 72–73	194.55	10.6	88.4
1266A-18H-5, 140–150	195.23	10.9	90.5
1266A-19H-1, 54–55	199.30	10.5	87.2
1266A-19H-5, 72–73	204.58	10.9	91.1
1266A-19H-5, 140–150	205.26	11.0	91.4
1266A-20H-1, 72–73	210.40	11.2	93.2
1266A-20H-3, 72–73	213.40	11.4	94.7
1266A-20H-5, 72–73	216.40	10.7	89.5
1266A-21H-1, 72–73	221.32	10.5	87.1
1266A-21H-3, 72–73	224.32	10.9	90.7
1266A-21H-5, 72–73	227.32	10.7	88.9
1266A-22H-1, 72–73	232.25	11.0	92.0
1266A-22H-3, 72–73	235.25	10.3	85.8
1266A-22H-5, 72–73	238.25	10.3	85.8
1266A-22H-5, 140–150	238.93	10.0	83.1
1266A-23H-1, 72–73	243.17	10.9	91.0
1266A-23H-3, 72–73	246.17	10.5	87.8
1266A-23H-3, 140–150	246.85	10.4	86.6
1266A-23H-5, 56–57	249.01	10.1	83.9
1266A-24H-1, 56–57	250.95	10.7	88.8
1266A-25H-1, 72–73	252.15	10.6	88.1
1266A-26X-1, 72–73	253.53	10.5	87.2
1266A-27X-1, 72–73	258.70	11.4	94.7
1266A-27X-3, 72–73	261.70	11.6	96.5
1266A-27X-5, 72–73	264.70	11.4	94.6
1266A-27X-5, 140–150	265.38	11.3	94.3
1266A-28X-1, 86–87	269.77	11.9	99.3
1266A-28X-2, 140–150	271.81	11.4	94.9
1266A-28X-5, 46–47	274.87	11.6	97.0
1266A-29X-1, 123–124	281.17	8.1	67.1
1266A-29X-5, 140–150	287.34	11.4	95.3
1266A-30X-1, 72–73	291.71	11.5	95.6
1266B-5H-5, 30–30	292.08	11.2	93.6
1266B-5H-5, 40–40	292.18	11.4	94.6
1266B-5H-5, 50–50	292.28	11.2	93.6
1266B-5H-5, 60–60	292.38	11.4	94.8
1266B-5H-5, 65–65	292.43	11.3	94.0
1266B-5H-5, 70–70	292.48	9.8	81.6
1266B-5H-5, 75–75	292.53	11.3	94.1
1266B-5H-5, 80–80	292.58	11.2	93.3
1266B-5H-5, 82–82	292.60	10.8	90.1
1266B-5H-5, 84–84	292.62	9.6	79.8
1266B-5H-5, 86–86	292.64	8.6	71.6
1266B-5H-5, 88–88	292.66	5.7	47.7
1266B-5H-5, 90–90	292.68	7.6	63.5
1266B-5H-5, 92–92	292.70	10.2	85.0
1266B-5H-5, 94–94	292.72	10.1	84.5
1266B-5H-5, 96–96	292.74	10.5	87.6
1266B-5H-5, 100–100	292.78	11.0	91.9
1266B-5H-5, 106–106	292.84	10.9	91.0
1266B-5H-5, 110–110	292.88	11.0	91.6
1266B-5H-5, 115–115	292.93	11.0	91.6
1266B-5H-5, 120–120	292.98	11.2	93.3
1266B-5H-5, 130–130	293.08	11.2	93.4
1266B-5H-5, 140–140	293.18	11.3	94.2
1266A-30X-3, 72–73	294.71	11.2	93.6
1266A-30X-5, 72–73	297.71	11.8	97.9
1266A-30X-5, 140–150	298.39	11.2	93.6
1266A-31X-2, 10–10	304.73	10.4	87.0
1266A-31X-2, 20–20	304.83	10.8	89.6
1266A-31X-2, 30–30	304.93	10.9	90.4
1266A-31X-2, 40–40	305.03	10.5	87.7
1266A-31X-2, 50–50	305.13	10.8	89.9
1266B-6H-7, 5–5	305.15	10.6	88.6

Table T12 (continued).

Hole, core, section, interval (cm)	Depth (mcd)	Inorganic carbon (wt%)	CaCO$_3$ (wt%)
1266B-6H-7, 10–10	305.20	11.0	91.6
1266A-31X-2, 60–60	305.23	10.9	90.7
1266B-6H-7, 15–15	305.25	10.8	90.2
1266B-6H-7, 20–20	305.30	10.7	89.5
1266A-31X-2, 70–70	305.33	10.9	91.0
1266B-6H-7, 25–25	305.35	11.1	92.7
1266B-6H-7, 30–30	305.40	11.3	94.1
1266A-31X-2, 80–80	305.43	10.9	90.8
1266B-6H-7, 35–35	305.45	11.0	92.0
1266B-6H-7, 40–40	305.50	10.9	91.0
1266A-31X-2, 90–90	305.53	11.1	92.8
1266B-6H-7, 45–45	305.55	11.0	91.7
1266A-31X-2, 95–95	305.58	11.3	94.1
1266B-6H-7, 50–50	305.60	11.0	91.3
1266A-31X-2, 100–100	305.63	11.3	93.8
1266B-6H-7, 55–55	305.65	11.1	92.5
1266A-31X-2, 105–105	305.68	11.2	93.2
1266B-6H-7, 60–60	305.70	11.0	91.4
1266A-31X-2, 110–110	305.73	10.7	89.5
1266B-6H-7, 65–65	305.75	11.0	91.7
1266A-31X-2, 115–115	305.78	10.9	90.5
1266B-6H-7, 70–70	305.80	11.1	92.8
1266B-6H-7, 72–72	305.82	11.0	91.4
1266A-31X-2, 120–120	305.83	10.8	89.8
1266B-6H-7, 74–74	305.84	11.0	91.6
1266B-6H-7, 76–76	305.86	9.1	76.1
1266A-31X-2, 125–125	305.88	10.6	88.5
1266B-6H-7, 78–78	305.88	10.8	89.6
1266B-6H-7, 80–80	305.90	10.4	86.9
1266B-6H-7, 82–82	305.92	10.7	89.1
1266A-31X-2, 130–130	305.93	10.6	88.5
1266B-6H-7, 84–84	305.94	10.7	89.4
1266B-6H-7, 86–86	305.96	10.7	88.9
1266A-31X-2, 135–135	305.98	10.8	89.7
1266B-6H-7, 88–88	305.98	10.4	86.9
1266B-6H-7, 90–90	306.00	10.5	87.6
1266B-6H-7, 92–92	306.02	10.6	88.3
1266A-31X-2, 140–140	306.03	10.8	90.0
1266B-6H-7, 94–94	306.04	10.8	90.1
1266B-6H-7, 96–96	306.06	10.7	88.9
1266A-31X-2, 145–145	306.08	10.8	90.0
1266B-6H-7, 98–98	306.08	10.9	90.5
1266B-6H-7, 100–100	306.10	10.8	90.0
1266B-6H-7, 102–102	306.12	10.9	90.7
1266A-31X-2, 150–150	306.13	10.5	87.9
1266B-6H-7, 104–104	306.14	10.5	87.2
1266A-31X-3, 3–3	306.16	9.0	75.2
1266B-6H-7, 106–106	306.16	10.7	88.9
1266B-6H-7, 108–108	306.18	10.7	89.3
1266B-6H-7, 110–110	306.20	10.0	83.1
1266A-31X-3, 8–8	306.21	10.0	82.5
1266B-6H-7, 112–112	306.22	10.2	85.1
1266B-6H-7, 114–114	306.24	9.8	81.9
1266A-31X-3, 13–13	306.26	9.8	81.6
1266B-6H-7, 116–116	306.26	9.8	81.9
1266B-6H-7, 118–118	306.28	9.6	80.3
1266A-31X-3, 16–16	306.29	10.6	88.4
1266B-6H-7, 120–120	306.30	9.2	77.0
1266A-31X-3, 18–18	306.31	7.8	64.7
1266B-6H-7, 122–122	306.32	8.9	74.2
1266A-31X-3, 20–20	306.33	8.6	71.6
1266B-6H-7, 124–124	306.34	9.2	76.3
1266A-31X-3, 22–22	306.35	8.4	69.6
1266B-6H-7, 126–126	306.36	8.3	68.7
1266A-31X-3, 24–24	306.37	8.6	71.2
1266B-6H-7, 128–128	306.38	8.5	70.7
1266A-31X-3, 26–26	306.39	8.4	70.3
1266B-6H-7, 130–130	306.40	8.3	69.1
1266A-31X-3, 28–28	306.41	8.2	68.3
1266B-6H-7, 132–132	306.42	8.1	67.7
1266A-31X-3, 30–30	306.43	7.7	64.3
1266B-6H-7, 134–134	306.44	8.4	70.0
1266A-31X-3, 32–32	306.45	7.3	61.1
1266B-6H-7, 136–136	306.46	8.0	66.6
1266A-31X-3, 34–34	306.47	7.2	59.6
1266B-6H-7, 138–138	306.48	7.7	64.0
1266A-31X-3, 36–36	306.49	5.6	46.3
1266B-6H-7, 140–140	306.50	7.6	63.0
1266B-6H-7, 142–142	306.52	7.4	61.6
1266A-31X-3, 40–40	306.53	10.1	83.9
1266B-6H-7, 144–144	306.54	7.4	61.4
1266C-17H-3, 90–90	306.55	6.1	50.5
1266B-6H-7, 146–146	306.56	7.0	58.0
1266C-17H-3, 92–92	306.57	5.4	44.8
1266C-17H-3, 94–94	306.59	5.2	43.2
1266C-17H-3, 96–96	306.61	5.0	41.7
1266A-31X-3, 50–50	306.63	10.0	83.6
1266C-17H-3, 98–98	306.63	5.0	41.8
1266C-17H-3, 100–100	306.65	3.3	27.3
1266C-17H-3, 102–102	306.67	1.0	8.5
1266C-17H-3, 104–104	306.69	0.1	1.0
1266C-17H-3, 106–106	306.71	0.1	0.4
1266A-31X-3, 60–60	306.73	11.0	92.0
1266C-17H-3, 108–108	306.73	0.1	0.5
1266C-17H-3, 110–110	306.75	0.1	0.5
1266C-17H-3, 112–112	306.77	1.8	14.6
1266C-17H-3, 114–114	306.79	9.7	80.4
1266C-17H-3, 116–116	306.81	10.2	85.0
1266A-31X-3, 70–70	306.83	11.1	92.6
1266C-17H-3, 118–118	306.83	9.5	79.2
1266C-17H-3, 120–120	306.85	10.1	84.2
1266C-17H-3, 122–122	306.87	10.0	83.0
1266C-17H-3, 124–124	306.89	10.1	83.8
1266C-17H-3, 126–126	306.91	10.0	83.4
1266A-31X-3, 80–80	306.93	11.1	92.2
1266C-17H-3, 128–128	306.93	10.0	83.3
1266C-17H-3, 130–130	306.95	9.9	82.8
1266A-31X-3, 90–90	307.03	10.6	88.2
1266A-31X-3, 100–100	307.13	11.0	91.4
1266A-31X-3, 110–110	307.23	10.5	87.6
1266A-31X-3, 120–120	307.33	10.9	90.9
1266A-31X-3, 130–130	307.43	11.0	91.4
1266A-31X-3, 140–140	307.53	10.9	90.9
1266A-31X-3, 150–150	307.63	11.1	92.5
1266A-32X-1, 72–73	314.02	11.2	93.1
1266A-32X-3, 72–73	316.97	11.3	94.1
1266A-32X-4, 140–150	319.15	11.0	91.5
1266A-32X-5, 72–73	319.97	11.1	92.7
1266A-33X-1, 72–73	325.05	10.7	89.1
1266A-33X-3, 72–73	328.05	11.4	94.6
1266A-33X-4, 140–150	330.23	11.3	94.2
1266A-34X-1, 72–73	338.40	11.2	92.9
1266A-34X-3, 72–73	341.40	11.2	93.1
1266A-34X-3, 140–150	342.08	11.0	91.2

Table T13. Age-depth control points, Site 1266. (**See table notes.** Continued on next page.)

	Datum	Type	Upper depth (mcd)	Lower depth (mcd)	Minimum age (Ma)	Maximum age (Ma)
T	*Globorotalia tosaensis*	PF	0.02	0.32	0.61	0.61
T	*Globigerinoides obliquus*	PF	0.32	3.32	1.30	1.30
T	*Pseudoemiliania lacunosa*	CN	4.24	7.24	0.46	0.46
	C1n (o)	PMAG	6.64	7.74	0.781	0.781
	C1r.1n (y)	PMAG	7.84	8.54	0.988	0.988
	C1r.1n (o)	PMAG	9.59	10.24	1.072	1.072
T	Large *Gephyrocapsa* spp.	CN	10.24	14.49	1.22	1.22
B	Large *Gephyrocapsa* spp.	CN	12.49	13.13	1.58	1.58
T	*Globigerinoides extremus*	PF	14.39	17.39	1.91	1.91
T	*Calcidiscus macintyrei*	CN	15.97	17.47	1.67	1.67
B	Medium *Gephyrocapsa* spp.	CN	17.47	18.97	1.69	1.69
	C2n (y)	PMAG	17.92	18.37	1.785	1.785
T	*Discoaster brouweri* and *D. triradiatus*	CN	18.97	20.47	1.95	1.95
	C2n (o)	PMAG	20.87	21.12	1.942	1.942
T	*Globigerina apertura*	PF	23.95	25.31	1.68	1.68
B	*Globorotalia truncatulinoides*	PF	23.95	25.31	2.03	2.03
T	*Globoturborotalia woodi*	PF	25.31	28.31	2.30	2.30
T	*Globigerina decoraperta*	PF	25.31	28.31	2.70	2.70
T	*Discoaster pentaradiatus*	CN	25.39	26.89	2.52	2.52
	C2An (y)	PMAG	26.89	29.54	2.582	2.582
T	*Discoaster tamalis*	CN	29.09	30.59	2.83	2.83
	Pulleniatina reappearance	PF	32.98	34.34	2.28	2.28
T	*Dentoglobigerina altispira*	PF	32.98	34.34	3.02	3.02
T	*Sphaeroidinellopsis seminulina*	PF	36.23	39.23	3.18	3.18
T	*Neogloboquadrina acostaensis*	PF	36.23	39.23	3.83	3.83
T	*Hirsutella margaritae*	PF	36.23	39.23	3.88	3.88
T	*Globorotalia plesiotumida*	PF	39.23	41.73	4.15	4.15
T	*Hirsutella cibaoensis*	PF	39.23	41.73	4.16	4.16
T	*Reticulofenestra pseudoumbilicus*	CN	48.14	49.64	3.82	3.82
B	*Globorotalia crassaformis* s.l.	PF	50.16	53.16	4.31	4.31
T	*Amaurolithus* spp.	CN	51.14	52.64	4.56	4.56
T	*Globoturborotalita nepenthes*	PF	58.09	61.09	4.37	4.37
B	*Ceratolithus rugosus*	CN	59.57	62.07	5.1	5.1
B	*Sphaeroidinella dehiscens* (s.l.)	PF	64.09	65.49	4.94	4.94
	C3n (o)	PMAG	67.42	69.39	5.236	5.236
B	*Globigerinoides conglobatus*	PF	69.01	72.01	5.84	5.84
B	*Ceratolithus acutus*	CN	71.49	71.99	5.37	5.37
B	*Globorotalia plesiotumida*	PF	75.01	78.58	8.91	8.91
B	*Hirsutella juanai*	PF	75.01	78.58	9.75	9.75
B	*Amaurolithus primus*	CN	76.49	76.89	7.39	7.39
B	*Neogloboquadrina acostaensis*	PF	78.58	79.93	9.89	9.89
B	*Discoaster bellus* gr. (*D. hamatus*)	CN	86.81	88.51	10.48	10.48
B	*Globoturborotalita nepenthes*	PF	90.86	93.86	11.64	11.64
B	*Catinaster coalitus*	CN	93.34	94.84	10.79	10.79
B	*Triquetrorhabdulus rugosus*	CN	93.34	94.84	12.81	12.81
	C5n (o)	PMAG	93.84	95.24	11.043	11.043
B	*Globigerina apertura*	PF	93.86	96.86	11.06	11.06
T	*Sphenolithus heteromorphus*	CN	98.74	99.15	13.55	13.55
	Sphenolithus heteromorphus	CN	108.73	109.48	17.76	17.76
T	*Sphenolithus belemnos*	CN	109.76	111.65	17.89	17.89
B	*Sphenolithus belemnos*	CN	118.55	119.45	18.92	18.92
B	*Discoaster druggii*	CN	120.05	120.75	22.82	22.82
T	"*Globigerina*" "*angulisuturalis*"	PF	132.34	143.22	21.60	21.60
T	*Globigerina euapertura*	PF	132.34	143.22	23.03	23.03
B	*Sphenolithus disbelemnos*	CN	134.20	139.00	22.67	22.67
	C6Cn (y)	PMAG	138.65	139.30	22.564	22.564
T	*Sphenolithus delphix*	CN	142.40	143.00	23.07	23.07
B	*Sphenolithus delphix*	CN	143.22	144.53	23.33	23.33
	C7n (y)	PMAG	145.38	147.58	24.001	24.001
T	*Sphenolithus ciperoensis*	CN	150.53	152.08	24.23	24.23
T	*Paragloborotalia opima*	PF	153.96	164.83	26.64	26.64
	C7An (y)	PMAG	154.43	154.63	24.781	24.781
	C7An (o)	PMAG	155.43	155.83	24.942	24.942
	C8n (y)	PMAG	156.50	158.23	25.053	25.053
B	*Sphenolithus ciperoensis*	CN	164.83	166.48	27.55	27.55
T	*Chiloguembelina cubensis* (common)	PF	176.01	186.24	27.92	27.92
	C10n (y)	PMAG	179.51	179.61	27.760	27.760
	C10n (o)	PMAG	184.06	185.96	28.053	28.053

Table T13 (continued).

	Datum	Type	Upper depth (mcd)	Lower depth (mcd)	Minimum age (Ma)	Maximum age (Ma)
B	*Sphenolithus distentus*	CN	184.11	186.24	30.32	30.32
T	*Subbotina angioporoides*	PF	186.24	197.57	29.67	29.67
	C11n (o)	PMAG	191.28	191.63	29.828	29.828
	C12n (y)	PMAG	192.83	194.23	30.479	30.479
	C12n (o)	PMAG	194.18	195.43	30.939	30.939
T	*Reticulofenestra umbilicus* >14 µm	CN	199.66	200.66	31.7	31.7
T	*Ericsonia formosa*	CN	207.61	207.78	32.9	32.9
	C13n (y)	PMAG	207.67	210.68	33.058	33.058
T	*Pseudohastigerina* spp.	PF	207.78	219.26	32.00	32.00
T	*Globigerinatheka index*	PF	219.26	230.60	34.30	34.30
T	*Discoaster saipanensis*	CN	221.00	221.80	34.0	34.0
T	*Discoaster barbadiensis*	CN	222.40	223.30	34.2	34.2
	C15n (y)	PMAG	223.90	224.10	34.655	34.655
	C15n (o)	PMAG	225.05	225.30	34.940	34.940
	C16n (y)	PMAG	226.15	227.00	35.343	35.343
T	*Calcidiscus protoannulus*	CN	226.90	228.40	34.9	34.9
B	*Isthmolithus recurvus*	CN	250.84	251.27	36.6	36.6
T	*Acarinina coalingensis* (= *primitiva*)	PF	251.27	252.66	39.00	39.00
T	*Chiasmolithus grandis*	CN	251.27	251.58	37.1	37.1
T	*Subbotina linaperta*	PF	254.37	262.56	37.70	37.70
B	*Globigerinatheka index*	PF	254.37	262.56	42.90	42.90
T	*Morozovella aragonensis*	PF	254.37	262.56	43.60	43.60
B	*Dictyococcites scrippsae*	CN	254.37	259.26	40.3	40.3
T	*Nannotetrina* spp.	CN	254.37	259.26	42.3	42.3
B	*Reticulofenestra umbilicus* >14 µm	CN	254.37	259.26	42.5	42.5
T	*Discoaster sublodoensis*	CN	258.26	259.78	47.2	47.2
B	*Nannotetrina* spp.	CN	260.66	261.28	47.8	47.8
T	*Discoaster lodoensis*	CN	262.18	262.78	48.0	48.0
T	*Morozovella formosa*	PF	267.32	273.59	50.80	50.80
T	*Tribrachiatus orthostylus*	CN	267.32	269.51	51.0	51.0
B	*Morozovella aragonensis*	PF	275.14	289.30	52.30	52.30
B	*Discoaster lodoensis*	CN	281.84	282.56	52.4	52.4
B	*Morozovella lensiformis*	PF	289.30	300.62	54.00	54.00
T	*Discoaster multiradiatus*	CN	294.17	294.98	53.0	53.0
B	*Sphenolithus radians*	CN	294.98	295.89	53.3	53.3
B	*Tribrachiatus orthostylus*	CN	294.98	295.89	53.4	53.4
	C24n (o)	PMAG	295.28	299.90	53.347	53.347
B	*Discoaster diastypus*	CN	296.51	297.49	53.9	53.9
T	*Stensioeina beccariiformis*	BF	306.82	306.86	55.00	55.00
B	*Morozovella gracilis*	PF	389.30	300.62	54.46	54.46
	C25n (y)	PMAG	319.63	320.43	55.904	55.904
	Morozovella subbotinae	PF	321.07	332.47	55.90	55.90
T	*Globanomalina pseudomenardii*	PF	325.32	332.47	55.90	55.90
B	*Discoaster multiradiatus*	CN	339.48	340.38	56.2	56.2
B	*Heliolithus riedelii*	CN	358.28	360.19	57.3	57.3
B	*Discoaster mohleri*	CN	361.50	362.54	57.5	57.5
	C26n (o)	PMAG	364.33	364.84	57.911	57.911
B	*Globanomalina pseudomenardii*	PF	367.21	379.36	59.20	59.20
B	*Heliolithus kleinpellii*	CN	371.07	371.13	58.2	58.2
B	*Sphenolithus anarrhopus*	CN	372.58	372.71	58.4	58.4

Notes: T = top, B = bottom. o = oldest, y = youngest. PF = planktonic foraminifers, CN = calcareous nannoplankton, PMAG = paleomagnetic reversals, BF = benthic foraminifers. This table is also available in **ASCII.**

Table T14. Age model, linear sedimentation rates, and mass accumulation rates, Site 1266.

Age (Ma)	Depth (mcd)	LSR	Growth factor	Corrected LSR	Dry density (g/cm³)	CaCO₃ (wt%)	Total MAR (g/cm²/k.y.)	CaCO₃ MAR (g/cm²/k.y.)	Noncarbonate MAR (g/cm²/k.y.)
1	8.47	8.47	1.15	7.36	1.04	92.5	0.77	0.711	0.058
2	21.62	13.16	1.15	11.44	1.13	94.1	1.30	1.220	0.077
3	33.13	11.50	1.15	10.00	1.18	95.6	1.18	1.128	0.052
4	49.40	16.27	1.15	14.15	1.20	95.1	1.69	1.612	0.083
5	59.20	9.80	1.15	8.53	1.20	96.1	1.03	0.987	0.040
6	74.26	15.06	1.15	13.10	1.21	95.7	1.59	1.520	0.069
7	76.21	1.95	1.15	1.70	1.27	78.5	0.21	0.168	0.046
8	77.24	1.03	1.15	0.89					
9	78.12	0.88	1.15	0.76					
10	80.56	2.44	1.15	2.12	1.25	93.6	0.32	0.301	0.020
11	93.94	13.38	1.15	11.64	1.16	93.0	1.33	1.235	0.093
12	94.19	0.25	1.15	0.22					
13	95.37	1.18	1.15	1.03	1.40	82.6	0.14	0.118	0.025
14	100.16	4.79	1.15	4.17	1.25	72.7	0.52	0.378	0.142
15	102.72	2.56	1.15	2.23	1.33	69.7	0.30	0.206	0.090
16	105.27	2.55	1.15	2.21	1.28	83.1	0.28	0.236	0.048
17	107.75	2.48	1.15	2.16	1.22	75.6	0.26	0.200	0.064
18	110.63	2.88	1.15	2.50		82.9			
19	119.53	8.90	1.15	7.74	1.33	86.7	1.03	0.891	0.137
20	125.23	5.71	1.15	4.96	1.34	90.6	0.67	0.603	0.063
21	130.71	5.47	1.15	4.76	1.34	90.1	0.64	0.573	0.063
22	135.90	5.19	1.15	4.51	1.40	91.5	0.63	0.577	0.054
23	141.78	5.88	1.15	5.11	1.37	90.9	0.70	0.635	0.063
24	147.19	5.42	1.15	4.71	1.32	95.1	0.62	0.590	0.030
25	156.24	9.05	1.15	7.87	1.31	89.3	1.03	0.921	0.111
26	160.17	3.93	1.15	3.41	1.31	89.4	0.45	0.401	0.048
27	163.62	3.45	1.15	3.00	1.33	89.4	0.40	0.357	0.042
28	168.82	5.19	1.15	4.52	1.30	88.1	0.59	0.516	0.070
29	175.04	6.22	1.15	5.41	1.36	87.1	0.73	0.638	0.095
30	182.51	7.47	1.15	6.49	1.26		0.82		
31	192.47	9.96	1.15	8.66	1.24	90.7	1.07	0.974	0.100
32	202.03	9.56	1.15	8.31	1.22	88.7	1.01	0.900	0.115
33	208.53	6.50	1.15	5.65	1.26	91.2	0.71	0.650	0.063
34	218.49	9.96	1.15	8.66	1.27	92.5	1.10	1.018	0.083
35	228.67	10.18	1.15	8.85	1.38	88.9	1.22	1.084	0.136
36	239.00	10.33	1.15	8.98	1.43	86.7	1.29	1.115	0.172
37	251.35	12.35	1.15	10.74	1.42	87.6	1.52	1.334	0.189
38	252.27	0.92	1.15	0.80	1.42	88.1	0.11	0.100	0.014
39	253.33	1.06	1.15	0.92					
40	254.33	1.00	1.15	0.87	1.53	87.2	0.13	0.116	0.017
41	255.20	0.87	1.15	0.76					
42	256.00	0.80	1.15	0.70					
43	256.76	0.76	1.15	0.66					
44	257.49	0.73	1.15	0.63					
45	258.15	0.67	1.15	0.58					
46	258.76	0.61	1.15	0.53	1.35	94.7	0.07	0.067	0.004
47	259.38	0.63	1.15	0.54					
48	262.20	2.82	1.15	2.45	1.24	96.5	0.30	0.293	0.011
49	265.00	2.80	1.15	2.43	1.32	94.6	0.32	0.304	0.018
50	267.00	2.00	1.15	1.74		94.3			
51	269.00	2.00	1.15	1.74	1.41		0.25		
52	277.21	8.21	1.15	7.14	1.46	97.0	1.04	1.013	0.031
53	294.57	17.36	1.15	15.10	1.40	86.7	2.11	1.828	0.280
54	297.46	2.88	1.15	2.51	1.37	93.6	0.34	0.322	0.022
55	306.84	9.38	1.15	8.16	1.40	76.1	1.15	0.872	0.274
56	325.49	18.65	1.15	16.22	1.32	88.7	2.15	1.903	0.242
57	354.84	29.35	1.15	25.52	1.33	92.5	3.40	3.146	0.255

Note: LSR = linear sedimentation rate, MAR = mass accumulation rate. This table is also available in ASCII.